DOCTORAL THESIS

Relay Selection and User Scheduling in Reconfigurable Intelligent Surface Assisted Millimeter-wave D2D Communication

by

Mr. Lakshmikanta Sau

A thesis submitted in partial fulfillment of the requirements
for the degree of

Doctor of Philosophy in Computer Science

Under the supervision of

Prof. Sasthi Charan Ghosh

Advanced Computing and Microelectronics Unit
Indian Statistical Institute
203 B. T. Road, Kolkata-700108

June 2026

Abstract

Reconfigurable intelligent surface (RIS) assisted millimeter wave (mmWave) device to device (D2D) communication has recently been proposed as a viable solution to support the overwhelming data traffic in fifth-generation (5G) and beyond wireless networks. However, due to the substantial propagation and penetration losses of mmWave, a direct line of sight (LoS) link between a pair of proximity devices is required for effective communication. Static obstacles like trees and buildings can easily obstruct the direct LoS connectivity between a device pair. In such cases, RISs help to establish an indirect LoS link between an obstructed device pair by reflecting the signals in the desired direction.

In Chapter 2, we propose a set cover-based RIS deployment strategy to serve the maximum number of obstructed device pairs with the minimum number of RISs. In particular, we have demonstrated that double reflections via two consecutive RISs can greatly lower the RIS density in the environment, preventing resource waste and enabling the service of more obstructed device pairs. After the RIS deployment, for information transfer, we also propose an energy-efficient RIS group selection criteria. Moreover, we prove that under some conditions, double reflections are more beneficial than single reflection, which is counter-intuitive. Numerical results show that our approach outperforms a random and a recent deployment strategy.

In Chapter 3, assuming that the RISs are already deployed and the positions of the nearby users are known, we propose a double-RIS assisted multihop routing scheme for a device pair. Besides the RISs, the emphasis of this work is to make more use of the existing intermediate users (IUs), which can act as relays. Hence, the density of RIS deployment in the surroundings can be reduced, which leads to the avoidance of resource wastage. However, we cannot solely depend on the IUs because this implies complete dependence on their availability for relaying and as a result, the aspect of reliability in terms of delay-constrained information transfer may not be guaranteed. Moreover, the IUs are considered capable of energy harvesting, and as a result, they do not waste their own energy in the process of volunteering to act as a relay for other users. Numerical results demonstrate the advantage of the proposed scheme over some existing approaches, and lastly, useful insights related to the scheme design are also drawn, where we characterize the maximum acceptable delay at each hop under different set-ups.

The previous chapter presented a routing scheme for a particular device pair. For multiple device pairs, a single RIS may be simultaneously requested by several devices to act as a relay for their seamless communications. To deal with such cases, in Chapter 4, we propose a priority-aware, user traffic–dependent, grouping-based multihop user scheduling scheme for RIS-assisted mmWave D2D communication under spatially correlated channels. Specifically, the proposed scheme exploits the priority of the users (based on their respective delay-constrained applications) and the aspect of spatial correlation in the narrowly spaced reflecting elements of the RISs. Here, based on the other users in the neighborhood, their respective traffic characteristics, and the already deployed RISs in the surroundings, we establish a multihop connection for energy-efficient information transfer from one of the users to its intended receiver. In this context, we take into account the impact of considering practical discrete phase shifts at the RIS patches instead of its ideal continuous counterpart. Moreover, we also claim and demonstrate that the existing classic least remaining distance based approach is not always the optimal solution. Finally, the numerical results demonstrate the advantages of the proposed strategy over the existing benchmark schemes in terms of data throughput, energy consumption, and energy efficiency.

In the previous chapter, each device pair selects the best energy-efficient group, and in case of multiple pairs selecting the same best group, they are scheduled as per their priorities. However, the best group may lead to a large delay for some of the pairs. Moreover, the energy harvesting aspect is not considered there. In Chapter 5, we investigate various group selection strategies which select the k-th best group by considering self-sustainable RIS with spatially correlated channels. Specifically, we consider both power splitting and time switching configurations of the self-sustainable RIS to analyze the system performance and propose appropriate bounds on the choice of system parameters. The analysis takes into account both linear and non-linear energy harvesting models. Based on the application requirements, we propose various group selection strategies, which schedule the k-th best available group based on the end-to-end signal-to-noise ratio and also the energy harvested at a particular group. Accordingly, by using tools from high-order statistics, we derive analytical expressions for the outage probability of each selection strategy. Moreover, using extreme value theory, we investigate an asymptotic scenario where the number of groups available for selection at an RIS approaches infinity. The nontrivial insights obtained from this approach are especially beneficial in applications like large intelligent surface-aided wireless communication. Finally, the numerical results demonstrate the importance and benefits of the proposed approaches in terms of throughput and outage performance.

Dedicated

to

my beloved parents and elder brothers

DECLARATION

Thesis Title	**Relay Selection and User Scheduling in Reconfigurable Intelligent Surface Assisted millimeter-wave D2D Communication.**
Author	*Mr. Lakshmikanta Sau*
Supervisor	Prof. Sasthi Charan Ghosh

I declare that this thesis entitled **"Relay Selection and User Scheduling in Reconfigurable Intelligent Surface Assisted millimeter-wave D2D Communication".** is the result of my own work except as cited in the references. The thesis has not been accepted for any degree and is not concurrently submitted in candidature of any other degree.

Lakshmikanta Sau

Advanced Computing and Microelectronics Unit
Indian Statistical Institute, Kolkata

Date: 09/06/2026

ACKNOWLEDGEMENTS

First and foremost, I would like to express my sincere and heartfelt gratitude to my supervisor, Prof. Sasthi C. Ghosh, for his invaluable guidance, encouragement, and support throughout the course of my doctoral research. His insightful suggestions, constructive feedback, and continuous motivation have been instrumental in the successful completion of this thesis. I deeply appreciate his patience, understanding, and commitment to nurturing his students' academic and personal growth. Without his mentorship and unwavering support, this work would not have been possible.

I would like to sincerely thank Dr. Priyadarshi Mukherjee for his inspirational leadership, which has changed my life. During our collaborations, I have had the privilege of taking part in insightful discoveries and internalizing the core concepts that define our field. I am incredibly grateful to him for his contributions to problem formulation and modeling, which produced important insights and noteworthy results.

I am sincerely grateful to the Indian Statistical Institute (ISI), Kolkata, for granting me the opportunity to pursue research and for their generous financial support throughout this wonderful journey. I am appreciative of the cozy research environment provided by the Advanced Computing and Microelectronics Unit (ACMU) at ISI, Kolkata, and all of its members. They would frequently share with us anecdotes and fascinating facts about academics and, of course, other subjects. I also want to express my sincere gratitude to all of my professors who helped me with my PhD coursework and constantly encouraged me to push myself. I am also thankful to our proficient ACMU office staff for their support. I am also appreciative of the welcoming atmosphere provided by all of the research scholars, students, and project staff at ACMU.

I would like to express my sincere gratitude to Manas Da, Rajib Da, Susmita, Aritri Di, and Mamata Di for their invaluable encouragement and support throughout this journey. They have been more like my own family, who always stand with me during the toughest situations of my life and continue to do so. I would also like to sincere gratitude to Dr. Raju Maiti, Mr. Manik Jana, and Mr. Subrata Burai for their cooperation, constant support, and motivation. I would like to express my heartfelt gratitude to the members of the "9-6 Mess" for welcoming me into their group with such warmth and generosity. It was there that I had the privilege of meeting some of the finest seniors one could wish for - Papu Da, Bidyut Da,

Amit Da, Swarnendu Da, and Sandip Da - whose guidance and camaraderie enriched my time immensely. I also feel fortunate to have shared memorable moments with my juniors - Pabitra, Bappa, and Tapas - whose companionship made my stay at the mess truly enjoyable. I remain sincerely thankful to all my mess members for their friendship and support.

I am very much indebted to my labmates Souvik, Siddhanta, Saikat, Abid, Shawon, Subhadip, and Anupam, as well as my seniors Rathin Da, Subhojit Da, Durgesh Da, Subhasis Da, and Shankar Da, for their unwavering passion and logical, creative contributions. I am especially thankful to Siddhanta and Souvik for their constant support and help.

I wish to express my profound gratitude to my family for their unwavering support, encouragement, and sacrifices throughout my academic journey. Their constant faith in me has been a source of strength and motivation, without which the pursuit of higher education would not have been possible. Above all, I am deeply thankful to Almighty God for blessing me with the intellect, perseverance, and good health required to complete this work.

Finally, I dedicate this thesis to my beloved parents and my esteemed elder brothers, Srikanta and Nilkanta, whose dreams and aspirations have always guided and inspired me. This achievement stands as a tribute to their love, faith, and unending encouragement.

Lakshmikanta Sau

Publications and preprints from the content of the thesis

1. **L. Sau**, P. Mukherjee, and S. C. Ghosh, "Generalized group selection strategies for self-sustainable RIS-aided communication", **IEEE Transactions on Communications**, Vol. 74, pp. 6584-6598, 2026,, DOI: 10.1109/TCOMM.2026.3675555.

2. **L. Sau** and S. C. Ghosh, "RIS deployment and group selection strategy in double-RIS assisted mmWave D2D communication", **IEEE Transactions on Green Communications and Networking**, Vol. 10, pp. 723-736, 2026, DOI: 10.1109/TGCN.2025.3597412.

3. **L. Sau**, P. Mukherjee, and S. C. Ghosh, "Priority-aware grouping-based multihop routing scheme for RIS-assisted wireless networks", **IEEE Transactions on Network Science and Engineering**, Vol. 12, No. 2, pp. 1172–1185, March-April 2025, DOI: 10.1109/TNSE.2024.3524619.

4. **L. Sau**, P. Mukherjee, and S. C. Ghosh, "DRAMS: Double-RIS assisted multihop routing scheme for device-to-device communication", **Computer Communication (Elsvier)**, Vol. 220, pp.52-63, April 2024, https://doi.org/10.1016/j.comcom.2024.03.020.

Publications and preprints completed during the Ph.D period but are not part of the thesis

1. Sk. Hassan, **L. Sau**, and S. C. Ghosh, "Geometry based UAV trajectory planning for mixed user traffic in mmWave communication", **The 5th IEEE International Mediterranean Conference on Communications and Networking (IEEE MediterCom 2025)**, Nice, France, pp. 1–6, July 2025.

2. **L. Sau**, P. Mukherjee, and S. C. Ghosh, "A Graph-Based Strategic Sensor Deployment Approach for k-Coverage in WSN", **The 39th International Conference on Advanced Information Networking and Applications (AINA 2025)**, Barcelona, Spain, pp. 11–23, April 2025.

3. **L. Sau**, and S. C. Ghosh, "A Geometry-Based Strategic Placement of RISs in Millimeter Wave Device-to-Device Communication", **The 3rd International Conference on Computer and Communication Engineering (CCCE 2023)**, Stockholm, Sweden, pp. 41-53, April 2023.

Contents

List of Figures

List of Tables

Table 1: List of Abbreviations

Acronym	Full Form
AF	Amplify and Forward
AWGN	Additive White Gaussian Noise
BER	Bit Error Rate
CSI	Channel State Information
CDF	Cumulative Distribution Function
D2D	Device-to-Device
DF	Decode and Forward
EBGS	Energy-Based Group Selection
eMBB	Enhanced Mobile Broadband
EC	Energy Consumption
EE	Energy-efficiency
EH	Energy Harvesting
EVT	Extreme Value Theory
GBS	Grouping-based Scenario
IoT	Internet of Things
IT	Information Transmission
IUs	Intermediate Users
LIS	Large Intelligent Surface
LRD	Least Remaining Distance
LoS	Line of Sight
MIMO	Multiple-Input Multiple-Output
mMTC	Massive Machine-Type Communications
mmWave	millimeter-wave
M-QAM	M-ary Quadrature Amplitude Modulation
nGBS	Non Grouping-based Scenario
nLoS	non Line of Sight
OFDM	Orthogonal Frequency-Division Multiplexing
PDF	Probability Distribution Function
PIN	P-type/Intrinsic/N-type
PS	Power Splitting
QoS	Quality of Service
RIS	Reconfigurable Intelligent Surface
RF	Radio Frequency
RGS	Random Group Selection
SBGS	SNR-Based Group Selection
SNR	Signal-to-Noise Ratio
SINR	Signal-to-Interference-plus-Noise Ratio
TS	Time Splitting
URLLC	Ultra-Reliable Low-Latency Communications
WSN	Wireless Sensor Network

Table 2: Summary of Notations.

Notation	Description	Notation	Description
N_R, N_I	Number of RISs and IUs, respectively	T_s	Slot duration
M	Number of elements in i-th RIS	R_i	i-th RIS
K_g	Number of group of R_i	M_g	Number of elements in a group
θ_n	Phase shift at n-th RIS element	λ	Wave length
l	Euclidean distance from S to D	Φ	Phase shift matrix
t_i	Actual waiting time at U_i	m_q	Modulation scheme
M_h	Maximum harvested power	U_i	i-th IU
τ_{req}	Required slots for information transfer	λ_k	ON period length
$\nu_I(\nu_B)$	Duration of idleness (busyness)	α_k	Number of packets
K_b	Number of code bits	$\Omega_I(\Omega_B)$	Set of idle (busy) IUs
τ_{req}	Required slots for information transfer	E_{req}	Required energy
η_w	Waiting time (in slots) at a busy IU	P_b	Bit error rate
ψ	Minimum number of hops for information transfer	T_d	Total delay
T_{d_i}	Maximum waiting time at i-th IU	γ	SINR
P_{th}	Acceptable threshold probability	$T(\gamma)$	Achievable data rate
$R_{r,b}$	b-th subgroup of r-th RIS	T_c	Channel coherent time
χ	Number of hops between S and D	$\mathcal{D}_{\mathcal{T}}$	Data throughput
σ^2	Variance of the AWGN	$\mathcal{E}_{\text{eff}}$	Energy efficiency
δ_e	Acceptable error threshold	r	Coverage area
ρ_L	Path-loss at one meter distance	α	Path-loss exponent
$d_{m,n}$	Distance between nodes m and n	h_i, g_i	Complex channel gain
P_{tx}, P_{ph} and P_t	Transmit , phase shift, and processing power respectively	h_c, g_c	Composite channels
$E_{\text{req,PS/TS}}$	Required energy for PS/TS configuration	γ_{th}	Required SNR
$\mathcal{O}$, $\mathbb{O}$	Data and energy Outage probability, respectively.	$E_{l/nl}$	Harvested energy
R_{req}	Required data rate	E_{req}	Required energy
$\gamma_{PS/TS}$	Signal to noise ratio in PS/TS configuration	K	Rician fading factor
δ, β	Scaling and shape parameter	$T_{\text{PS/TS}}$	Achievable data rate
ρ, ζ	Power splitting and time switching factors	σ_0^2	Variance of the AWGN
a, b, c	Circuit specific constant	$\mathbf{R}$	Correlation matrix
$W_{k,i}$	Waiting time of k-th source at U_i	m_r	Modulation scheme
β	A function of delay constraint and, channel condition	$\phi_{r,b}$	phase shift for $R_{r,b}$
$T_{k,i}$	Information transfer time for k-th $S-D$ pair at i-th IU	α_k	Number of packets
$\tau_{k,i}$	Processing time of k-th source at i-th IU	λ	Wave length
$\eta_{w,i}$	Waiting time (in slots) at a busy i-th IU	P_b	Bit error rate
N_κ	Number of sources which satisfied $T_{d_{n,i}} \leq \kappa_{I,i}$	μ_s	Service rate
$T_{d_{n,i}}$	Maximum waiting time at i-th IU of n-th source	$\gamma_{j,k}^{r,b}$	signal-to-noise ratio
$\mu_{1,n}$	Spatial correlation between 1st and n-th element of $R_{r,b}$	$T_{j,k}^{r,b}$	Achievable data rate
$\kappa_{I,i}$	Estimated idle time of i-th IU	$\mathrm{D_T}$	Data throughput
p_j	Priority of the j-th source	δ_p	Phase shift error
$\mathrm{E_C}$	Energy consumption	γ_{sr} (γ_{dr})	SINR for single (double) reflection
$\mathcal{B}$	Set of all blind pairs	R_l^p	p-th group of l-th RIS
$E_{\mathrm{C}}^{i,j}$	Energy consumption of i-th and j-th groups	B_{rem}^r	Set of remaining blind pairs
$E_{\text{eff}}^{p^*,q^*}(l^*, m^*)$	Energy efficiency of p-th and q-th groups of l-th and m-th RIS	$M_r \times M_c$	Number of grid points

Chapter 1

Introduction

In recent years, most of the Internet of Things (IoT) devices are connected to the Internet, and due to their smart applications, they need a high data rate. As a result, the wireless traffic has been increasing at an explosive rate; it is expected to increase more than five times in between 2023 and 2028 [1]. Even if two devices are within the communication range of each other, all communications in a conventional cellular network must pass through the base station (BS). This architecture works well with traditional low data rate mobile services like text messaging and voice calls, where users are typically too far apart to communicate directly. To support the overwhelming data rate and reduce the traffic of the BS, device to device (D2D) communication has been introduced [2, 3]. In D2D communication, the exchange of information between two proximity mobile users can take place directly without going via the BS.

Furthermore, millimeter wave (mmWave) in D2D communication has emerged as the main technology in 5th generation (5G) [4, 5] wireless communication networks to support the increased data traffic [6, 7]. The mmWave bands roughly correspond to frequencies from 30 GHz to 300 GHz [7], and the available spectrum at these higher frequencies can be easily 200 times greater than all cellular allocations today. Note that, although mmWaves solve the problem of enhanced data rate, it has its own set of shortcomings such as significant propagation and high penetration losses. As a result, in order to achieve successful communication in mmWave bands, a direct line-of-sight (LoS) link is required. Furthermore, due to the unique propagation characteristics of mmWaves, it needs to transmit in beams with much greater directionality than in cellular systems.

Additionally, to support the enhanced data traffic, technologies such as beamforming and adaptive modulation have been developed over the last few decades. However, irrespective of the technicalities, the unifying motivation behind all of them is to intelligently adapt to

the randomly varying wireless channel instead of having a control over it. In this context, a new technology that promises to address this issue is the so-called reconfigurable intelligent surfaces (RISs) [8, 9, 10, 11]. RISs help to establish an indirect LoS link between an obstructed device pair by reflecting the signals in the desired direction. A RIS consists of an array of reconfigurable passive elements embedded on a flat metasurface and is able to 'control' the wireless channel instead of adapting to it [12]. This is practically done by tuning the parameters of its passive elements [13]. Furthermore, as a RIS simply reflects the incident signal in a desired direction, it does not need any radio frequency (RF) chains. As a result, this reduces the hardware cost, thereby enhancing the energy efficiency of the future wireless networks. In 5G and beyond mmWave wireless networks, RIS helps to improve the spectral efficiency as well as the coverage area.

We further note that the RIS is essentially a passive device that simply reflects the incoming signal as well as the noise to its desired direction by tuning its parameters. However, a few works also consider active RIS configurations in addition to the passive types. As a result, in multi-RIS scenarios, secondary reflection can be used in addition to single reflection to greatly enhance the communication range through appropriate RIS tuning. For reliable signal reflection and propagation in mmWave communication, a LoS between the devices and the RIS is essential. Optimal RIS placement can significantly extend the coverage of such networks with a minimum number of RISs, which effectively reduces both the hardware and installation expenditure. Furthermore, once RISs are deployed, they don't move with the mobile users; they stay fixed. Therefore, the strategic placement of RISs employing both single and double reflections is one of the most significant operational challenges to overcome the signal obstruction.

Furthermore, any given user pair will communicate with one another for only a limited period of time. Therefore, adding a lot of RISs to the environment could lead to the wastage of resources. A cooperative multihop communication is one possible way to prevent this waste [14, 15, 16]. In other words, in addition to using the RISs, other idle intermediate users (IUs) in the vicinity can also be used as relays for a successful communication between a pair of devices. Here, IUs can relay the signal by amplifying-and-forwarding (AF) or decoding-and-forwarding (DF) [17, 18]. AF relays increase the effective noise at the intended user while also enabling low-cost processing. However, because DF relays only send the information that has been received and not the complete information-plus-noise mixture to the subsequent hop, they ensure high reliability. Therefore, it would seem that choosing to serve as a DF relay is a good option for the idle IUs. Note that we cannot totally rule out the

use of RISs and rely solely on the IUs. Reliability in terms of delay-constrained information transfer cannot be ensured if a pair of users' communication is entirely dependent on the availability of the idle IUs. In that scenario, the traffic characteristics of these IUs will determine the duration of the entire communication process. Therefore, selection of appropriate IUs and RISs for the communication between a pair of devices in a cooperative framework is a challenging issue.

The conventional RIS fundamentally reflects the incident signal in a desired direction by adjusting its phase shift parameters. It is evident that training time increases in direct proportion to the number of elements in the RIS [19, 20, 21], which can result in a significant feedback overhead and jeopardize anticipated performance improvements. Moreover, any given D2D pair always communicates with each other for a limited period of time. As a result, using the entire RIS is not energy efficient and may result in unnecessary resource waste. Therefore, the works in [22, 19] suggest grouping strategies where the nearby RIS elements are grouped together into smaller non-overlapping surfaces with identical phase shifts in order to avoid the massive channel estimation overhead in RIS-based systems [23]. Additionally, the arrays of the reconfigurable elements are very narrowly spaced. Hence, we cannot overlook the impact of spatial correlation in RIS-assisted communication. Furthermore, a lot of current research assumes that the phase shifts provided by a RIS are continuous, but in real-world systems, they are actually discrete in nature [24]. Hence, these limited phase shifts do have a significant impact on the system performance. Moreover, a single RIS may be concurrently requested by multiple device pairs to serve as a relay for their seamless communications in a multihop D2D communication scenario. Consequently, designing a user-traffic-aware, grouping-based multihop scheduling scheme under spatially correlated channels becomes particularly challenging.

Besides, an RIS is a 'nearly' passive device, meaning it reflects the incident signal through adjustable phase shifts without any amplification, relying solely on passive meta-materials that consume minimal power. To support this energy requirement, a self-sustainable RIS is required. Additionally, the aspect of choosing an appropriate group at the RIS is important because there is always a chance that the best group, which serves our objective, is preoccupied or currently serving another user pair. Moreover, as the arrays of the reconfigurable elements are very narrowly spaced, we cannot ignore the impact of spatial correlation. Therefore, the k-th best group selection strategies are more crucial in a self-sustainable RIS-assisted communication.

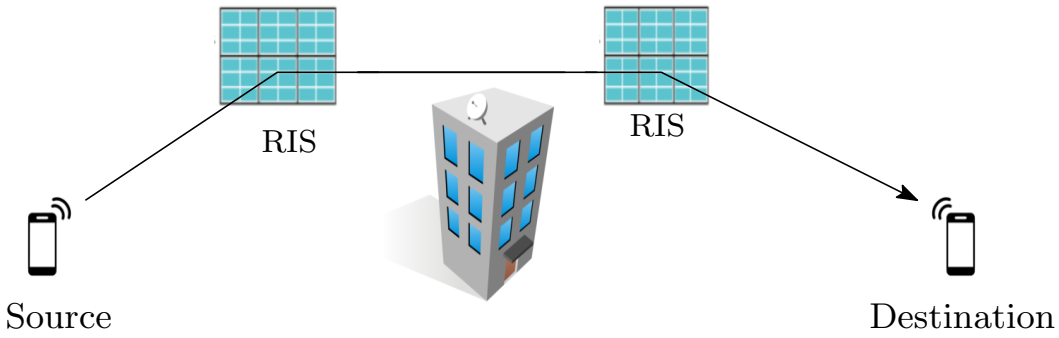

Figure 1.1: RIS-assisted communication environment.

This thesis deals with developing algorithms for 1) strategically positioning the RISs, 2) appropriately selecting the RISs and IUs for a multihop cooperative framework, 3) scheduling multiple requests according to their traffic characteristics, and 4) selecting the k-th best group in a self-sustainable RIS-assisted communication.

1.1 Background: RIS architecture and its key uses

A RIS is a flat metasurface made up of numerous inexpensive, quasi-passive reconfigurable reflecting elements, each of which has the ability to reflect incoming electromagnetic signals in a desired direction by controlling its phase shifts [25]. Every passive element contains a series of embedded PIN diodes that may be switched between the ON and OFF states by adjusting the biased voltage using a direct current (DC) input line. Therefore, RIS can directly reshape the wireless propagation channel in favor of signal transmission, which differs from traditional wireless communication techniques used in transceivers. Note that this depends on the channel conditions and must be adjusted when the channel conditions change. Moreover, there is a popular self-sustainable RIS architecture, where RIS elements can perform both energy harvesting (EH) and information transfer (IT) simultaneously. Note that the required phase shift and the circuit processing power are harvested from the incoming signals, and the EH process is done according to the linear or nonlinear EH model [26, 27]. Additionally, reflective components based on RF switches, varactor diodes, liquid crystal (LC) metamaterials, and other technologies are used in some RISs. However, in our work, we only look at the variation that is most frequently used in the literature, which is RIS elements that are implemented using P-type/Intrinsic/N-type (PIN) diodes. Specifically, we use self-sustainable RIS in RIS-assisted D2D communication scenarios. The performance of D2D communication in a 5G network can be significantly enhanced by integrating RIS.

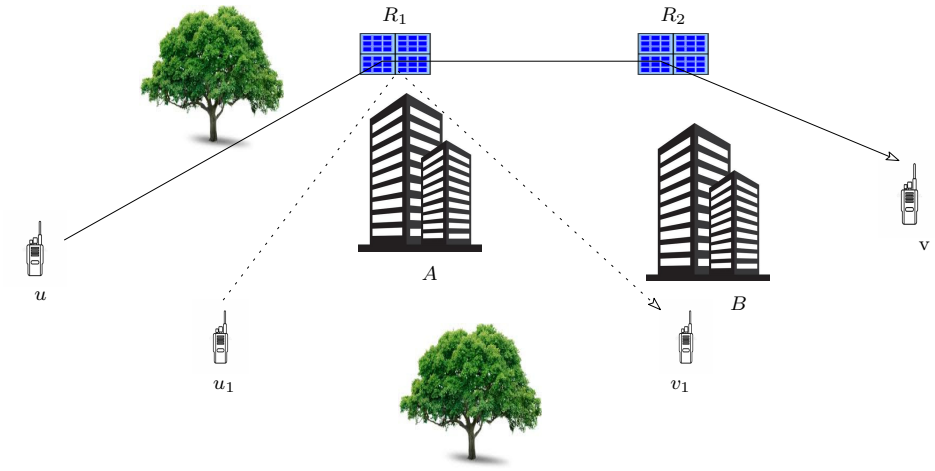

Figure 1.2: Coverage enhancement by RIS.

1.1.1 Data rate enhancement

In a RIS-assisted mmWave wireless communication setup, due to the presence of obstacles, a device cannot communicate to its desired counterpart when the direct LoS link between them is blocked (as shown in Fig. 1.1). As a result, the achievable data rate at the receiver end is not adequate to ensure successful communication. In this context, when a direct LoS link is blocked, we use a RIS between the transceivers to improve the channel gain at the receiver end. In order to increase the signal strength, the reflective components of RISs are arranged so that the reflected signal constructively complements the direct signal, and this process is called the phase shift optimization technique.

The reflective components of the RIS are set up to produce passive beamforming because the RIS itself does not contain any active RF chains. The signal-to-interference-plus-noise ratio (SINR) at the user equipments (UEs) can be significantly improved by simultaneously optimizing the active beamforming at the transmitter and the passive beamforming at the RIS [28, 29]. Consequently, the transmit power and RIS phase shifts can be optimized together to maximize the total throughput of all UEs. An RIS can also be set up to maximize the sum data rate while strictly adhering to the power budget of each transmitter and the acceptable outage probability of each UE in order to guarantee equity among all UEs.

1.1.2 Coverage area enhancement

The mmWave suffers from high propagation and penetration losses from obstacles such as trees and buildings and has a great impact on wireless communication scenarios. For

example, the penetration loss due to concrete is more than 120 dB, while moving obstacles such as cars cause a loss of more than 17 dB [30]. Specifically, for mmWave communication, a LoS link is required between the transcievers to ensure successful data communication. As shown in Fig. 1.2, due to the presence of obstacles, the direct LoS link is blocked. To support the communication, a RIS is placed between them in order to provide a indirect LoS link. Therefore, the coverage area in terms of the number of pairs of serving devices can be significantly increased.

In addition to the RIS, an intermediate user (IU) can also act as relay to support seamless connection when the direct LoS link is blocked. Thus a strategic cooperative communication model that uses both the IUs and RISs can enhance system coverage by providing an indirect LoS link between an obstructed device pair.

1.1.3 Performance Enhancement

The loss of spectral efficiency caused by severe interference in dense multi-user networks with constantly expanding UE populations is one of the primary obstacles to achieving the necessary data rate for mixed user traffic. The orthogonal frequency division multiplexing (OFDM) [31] in combination with multiple input multiple output (MIMO) is a promising technology to improve spectral efficiency for mmWave D2D communication. The entire channel in OFDM is split up into numerous narrow-band subchannels, which are sent in tandem to sustain high data rate transmission while simultaneously lengthening the symbol duration to counteract inter-symbol interference. Note that OFDM allocates each frequency to a particular user to avoid interference. Therefore, by appropriately grouping the RIS configuration and using OFDM, it is possible to intelligently redesign the propagation environment and control the UE's channel conditions. Moreover, by tunning the phase shifts of the elements of the RIS, we can reduce interference between the device pairs that share the common RIS, which in turn enhances the SINR and throughput.

1.1.4 Improvement of reliability

Numerous low-latency services are anticipated by 5G and beyond wireless networks, including industrial automation, remote surgery, virtual reality, tactile internet, and connected and autonomous cars, among many others. According to the 3GPP standard for the 5G new radio, a 32-byte URLLC packet must have a URLLC latency (delay tolerance time) of less than 1 ms and a reliability of more than 0.99999. The authors [32, 33] have shown

a significant rise in the bit error rate (BER), which reduces the transmission reliability, if the direct link between the transceivers is blocked. When the direct link is blocked, we can provide an indirect LoS link by integrating RIS into 5G and beyond networks. The RIS-assisted cooperative D2D network maximizes the possible data rate by optimizing the combined phase shift matrix and power allocation [34], which significantly improves the reliability.

1.2 Challenges in RIS-assisted D2D Communication

RIS is a game-changing technology in mmWave D2D communication environments. Although RIS helps to enhance data rate, coverage area, and improve reliability, there are several challenges of using RISs. Due to the presence of obstacles, a direct LoS link between transceivers may not be available. A proper placement of RISs can help to get indirect LoS in such cases. Thus, RIS placement is a very challenging issue. Moreover, in a multi-hop scenario, a source can send its data packets to its desired destination by using a cooperative framework of IUs and RISs. The routing aspect of a cooperative framework is not well investigated. Additionally, multiple sources may request a particular RIS to forward their data packets to their intended destinations. In such a case, the users must be scheduled appropriately to use the concerned RIS. Furthermore, at a particular moment in time, if the best RIS for a given requesting pair is not available, the k-th best RIS may need to be selected to facilitate communication. These motivations and challenges are discussed in detail below.

1.2.1 Strategic RIS placement

In the mmWave D2D communication scenario, RIS plays a key role in 5G and beyond to provide a high data rate. In this setup, a LoS link is essential for successful data communication. However, in the urban and highly obstructed scenario, most of the direct LoS links between a device pair are blocked. In this context, RISs are used to provide an indirect LoS link between them. Note that the RIS is only usable if the LoS link between the devices and the RIS is unobstructed and falls within the devices' communication distance threshold. It should be noted that although the RIS used less power than active antenna arrays, power is still needed for it to function. Thus, reducing the number of RISs installed in the network environment is also crucial for increasing energy efficiency. Furthermore,

augmenting the environment with a large number of RISs may result in unnecessary wastage of resources. Note that, in the RIS-aided D2D communication setup, the transceivers are mobile while the RISs are static in nature. Therefore, optimal RIS placement can significantly extend the coverage of such networks with a minimum number of RISs, which effectively reduces both the hardware and installation expenditure.

1.2.2 Cooperative routing scheme

The optimal placement of RISs [35, 36, 37] can significantly extend the coverage with a minimum number of RISs. However, augmenting the environment with a large number of RISs may result in unnecessary wastage of resources. In addition to utilizing the RISs, other nearby idle users could serve as a relay to help a particular pair of users for successful communication. Note that we cannot totally rule out the use of RISs. On the other hand, reliability in terms of delay-constrained information transfer cannot be ensured if the communication between two users depends only on the IUs. This is because, only idle IUs can act as a relay node. Therefore, a cooperative multi-hop routing scheme that uses both the IUs and RISs can improve the system performance significantly.

1.2.3 User scheduling

In mmWave D2D communication scenarios, the RIS-assisted cooperative framework is a potent technique that can increase D2D communication coverage. In a cooperative framework, a source wants to send its data packets to its intended counterpart by using idle IUs and RISs. However, in practice, multiple sources can request a particular RIS or IU to forward their data packets to their desired counterpart. Note that a particular RIS or IU can serve a single request at a time. Additionally, energy efficiency is also a very important factor in low-power and low-complexity communication environments. There should be an energy efficient user scheduling strategy to use a particular RIS or an IU to execute hassle-free data communication.

1.2.4 RIS group selection

For using the entire RIS, pilot signals are to be sent from each element of the RIS to measure the channel state information. This may result in a significant feedback overhead and jeopardize the anticipated performance improvements. Because of this, utilizing the full RIS

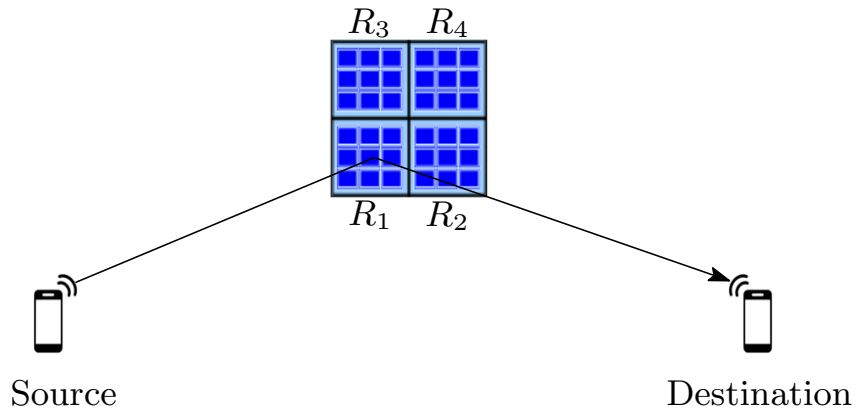

Figure 1.3: Group selection strategy.

might not be energy-efficient and could squander resources needlessly. To address this issue, there are several works [19] that suggest grouping strategies where the nearby RIS elements are grouped together into smaller non-overlapping surfaces with identical phase shifts in order to avoid the massive channel estimation overhead in RIS-based systems. Therefore, in a particular instance, more than one group may be available to facilitate the successful information transfer. In this context, the aspect of choosing an appropriate group at the RIS is important because there is always a chance that the best group, which serves our objective, is preoccupied or committed to serving another requesting pair. This may lead to select the k-th best group for a successful communication. Besides, an RIS is a 'nearly' passive device, meaning it requires a small but nonzero amount of energy for its phase-shifting operations. To support this energy requirement, a self-sustainable RIS configuration is developed, in which the RIS can harvest the required energy from the incoming signals [38]. Therefore, the k-th best group selection strategies must also consider the energy harvesting parameters for a self-sustainable RIS-assisted D2D communication scenario.

1.3 Literature review and research gap

In this thesis, we first present a RIS placement strategy taking care of single as well as double reflections. Next, considering the multi-hop cooperative framework, we select appropriate RISs and IUs for successful data communication. Then, we develop a user scheduling strategy when multiple requests arrive to a particular RIS or IU. Finally, we investigate the k-th best group selection scheme when the best group is occupied by other user pair. In the

following subsections, we emphasize the literature review related the works presented in the thesis and identify the research gaps.

1.3.1 RIS deployment taking care of both single and double reflections

Nowadays, RIS-assisted D2D communication forms a new research direction [39, 40, 41], and the majority of recent research focuses on RIS usage by assuming that RISs are already setup and accessible. The aspect of RIS-assisted D2D communications [42, 43] form an interesting direction of research. The work in [42] investigates the role of RISs for enhancing the energy efficiency of a D2D communication network. The authors in [43] focus on the uplink communication of a RIS assisted D2D enabled cellular networks. The objective of obtaining high-speed data rates is efficiently fulfilled by the use of high-frequency signals, such as the mmWaves [44], for short-distance communication. However, mmWaves suffer from its own set of shortcomings like significantly high penetration and propagation losses. Thus, RIS-assisted D2D network is the solution for such scenarios, where the direct LoS is not of sufficient quality to support mmWave-based communication [45]. As a result, RISs are strategically placed at locations where they have clear LoS links with both the users intending to communicate with each other. In this context, a novel RIS deployment strategy in the presence of phase errors is developed in [41] by keeping in mind the fair and acceptable restriction of the total number of RIS elements. In order to improve the coverage by optimizing the RIS orientation and horizontal distance, the authors in [37], develop an optimization problem for RIS placement. In a recent study in [46], a large number of RISs are strategically placed on the wall of the randomly located obstacles, like buildings, so that the coverage area can be improved significantly. A graph-based RIS deployment strategy to serve a maximum number of device pairs is discussed in [35]. The authors in [36], convert the RIS placement problem to a set cover problem and provided a greedy algorithm to enhance the system coverage area.

Most of the works on RIS deployment discussed above assumed single reflection only [35, 36, 37, 46]. Note that a few device pairs may not be able to communicate with each other via a single reflection, depending on the shape and position of the obstacles. In practice, the secondary reflections are not insignificant, especially in metropolitan settings where the RISs are not widely dispersed. Therefore, in a few cases, double reflections can be impactful when a single reflection is insufficient for RIS-assisted communication. However, the role of triple and higher-order reflections is usually ignored due to significant effective

path loss [17, 47]. Accordingly, the work in [48, 47] demonstrates that by proper tuning of the RISs, the multi-RIS secondary reflection can be leveraged to significantly enhance the range of communication. Additionally, by allowing double reflections, we can serve more obstructed device pairs without deploying more RIS. The work in [49], proposed a joint passive beamforming design for two consecutive RIS-assisted communications. However, all the above works assumed that the RISs were already deployed rather than developing any deployment strategy for double reflection [48, 47, 49]. In this thesis, we developed a RIS deployment strategy for an urban setup considering single as well as double reflections and shown that sometimes double reflections may be more beneficial than single reflection.

1.3.2 Routing in mmWave D2D communication scenario

Note that D2D communication has a small effective coverage range, and it is a short-range communication service. In particular, if two D2D users are located far apart or if the channel conditions between them are significantly fading, the D2D communication between them will be disrupted [50]. Therefore, the multi-hop D2D connection is an efficient way to further enhance the coverage area of two device pairs where the IUs can be used as a relay node [51]. Therefore, D2D relay communication mode can improve network stability, increase network deployment flexibility, and clearly lower communication strain and request latency [52]. The authors in [52], proposed a relay selection algorithm with low computational complexity to obtain an appropriate relay node for D2D links by controlling the power. Based on the anticipated data rate, a probabilistic approach for relay selection is investigated in [53]. Note that we cannot totally depend on the IUs. This is because, if the communication between two users depends only on the IUs, reliability in terms of delay-constrained information transfer cannot be ensured due to the idle IU unavailability. In that case, the time for the entire communication process will be entirely dependent on the traffic characteristics of these IUs. That is, we cannot provide the aspect of guaranteed, reliable communication.

On the other hand, as discussed earlier, both primary and secondary reflections can be used to greatly increase the communication range by appropriately adjusting the RISs [47, 48]. In [48], the authors investigated a double RIS-assisted wireless communication system in which two RISs facilitate communication via double-reflection links from a BS to several users. The work in [14], proposes a practical hybrid beamforming architecture for multi-hop RIS-empowered wireless communication networks. The author in [54],

considered RISs as intermediate relay nodes that facilitate multi-flow multipath routing. However, RIS may not be available at all for serving a particular device pair.

A possible solution to this problem is to adopt a cooperative multihop approach, where, apart from the RISs, the other IUs present in the surroundings, depending on whether they are busy or idle, can be used as relays, to facilitate the communication. IUs may decode and forward or amplify and forward [17] the incoming signal. While AF relays have low processing cost, DF relays have high reliability as they forward only the decoded information portion to the next hop and not the entire received information-plus-noise mixture [18]. Thus, the option of having the idle IUs to act as DF relays seems beneficial. Thus, to address applications with delay limitations such as URLLC [55], IUs must also be used along with RISs. In this thesis, we developed a multihop routing scheme for cooperative D2D communication using both IUs and single and double RIS as intermediate relay nodes. To the best of our knowledge, this is the first study to provide a multihop routing method that combines IUs with double RIS-assisted communication.

1.3.3 User scheduling at RIS and IU

Multiple device pairs may require the same RIS for their multihop routing. In that case, a proper scheduling of the users must be done in order to effectively use the concerned RIS. In this context, there exist some works that investigate various aspects of routing in RIS-aided multihop networks. A feasible hybrid beamforming architecture for multi-hop RIS-powered wireless communication networks is proposed in [14]. A graph convolutional network-based method with user interference relationship as the main input is used in [56] to tackle the link scheduling problem. Similarly, [57] solves the link scheduling problem using location data and a deep learning-based graph embedding technique. Taking energy-efficiency (EE) into account as one of the key difficulties, the author in [58] simultaneously optimizes the beamforming vector, transmit power, and phase shifts for RIS-assisted multihop networks. However, the aspect of user scheduling in RIS taking care of energy efficiency is not yet investigated.

Moreover, as far as the structure of a RIS is concerned, certain aspects are critical to be considered and analyzed in this multihop framework. Firstly, the arrays of the reconfigurable elements are very narrowly spaced, which implies that the channels between the consecutive reflecting elements and the source/destination are spatially correlated [59, 60]. Hence, to avoid the huge channel estimation overhead in RIS-based systems, the works in [22, 19]

propose grouping strategies where the nearby RIS elements are grouped together into smaller non-overlapping surfaces with identical phase shifts. Secondly, most existing works assume a continuous nature of the phase shifts that are offered by a RIS whereas in practical systems, they are actually discrete in nature [61]. Hence, these limited phase shifts do have a significant impact on the system performance. These aspects of a RIS cannot be overlooked if we are interested in investigating the practically feasible cooperative multihop framework. Furthermore, the least remaining distance (LRD)-based approach [62] is a standard procedure in the literature to establish a multihop connection between two users, whether the sole objective is to reduce the effective distance between the two in each hop [63]. But, this LRD approach appears good if and only if we do not take the channel conditions and the availability of the IUs into consideration. Therefore, in this thesis, we develop a priority-aware multi-user scheduling in a multi-hop scenario to support a hassle-free communication taking care of the channel correlations.

1.3.4 Generalized group selection

The traditional RIS reflects the incident signal in the desired direction by controlling the phase of each element. Thus training overhead is in direct proportion to the size of the RIS [19], which could lead to a large feedback overhead and compromise the expected performance gains. Hence utilizing the full RIS may not be energy efficient and could lead to needless resource waste. Therefore, the studies in [22, 19] offer grouping solutions where the surrounding RIS elements are grouped together into smaller non-overlapping surfaces with identical phase shifts in order to reduce the enormous channel estimation overhead in RIS-based systems. The work in [23] proposes grouping-based RIS, but without considering the impact of spatial correlation. Note that, as the inter-element spacing in an RIS decreases, the aspect of spatial correlation becomes more and more crucial. By incorporating this aspect, we can investigate a grouping-based RIS-aided multihop communication scenario. Note that the aspect of choosing an appropriate group at the RIS is important because there is always a chance that the best group, which serves our objective, is preoccupied or committed to serving another requesting user pair. However, this aspect of looking at group selection strategies in the RIS, by taking into account the aspect of spatial correlation, has not been adequately explored for the D2D communication scenario.

Besides, an RIS is a ‘nearly’ passive device, meaning it requires a small but nonzero amount of energy for its phase-shifting operations. In this direction, the work in [38]

proposes a self-sustainable RIS configuration, where the RIS can harvest the required energy from the incoming signals. Depending on the energy harvesting (EH) process, the authors propose two separate architectures: power splitting (PS) and time switching (TS). In the PS configuration, the signal power is divided into two streams: one is used for EH at the RIS, and the other is used to reflect the signal in the desired direction. On the contrary, in the TS configuration, the incident signal is solely used for EH during specific time intervals and at other times, it reflects the incoming signal. The authors in [64] propose optimized transmission strategies for self-sustainable RIS-aided simultaneous wireless information and power transfer. As a result, this particular class of RISs is ideal for operation with minimal or zero external energy supply. Hence, it is ideal for scenarios where autonomous operation is beneficial, resulting in an efficient and sustainable wireless communication network. However, different RIS groups may have different levels of harvested energy, as they harvest their energy from the incoming signals. Thus, the best group for a particular device pair depends on the level of energy harvested by different elements of the RIS. Note that the same group may found to be the best for different device pairs. In that case, we must rely on the k-th best group. However, these aspects have not been adequately addressed yet for group selection. Accordingly, in this thesis, we develop various generalized k-th best group selection strategies by considering the self-sustainable RIS-aided scenarios.

1.4 Scope of the thesis

In order to meet the necessary demand of various 5G and beyond services, it is imperative to overcome the significant operational challenges associated with effectively utilizing RIS in real-world 5G wireless systems. Some of the main difficulties have been noted in this thesis, and algorithms to address them have been developed.

In Chapter 2, we first develop a set cover-based RIS deployment strategy that helps to get an indirect LoS link between a transmitter and receiver pair in order to establish communication when there is no direct LoS link between them by considering both single and double reflection. After deploying the RISs, if a device pair wants to communicate with each other, multiple RIS may be available to assist their communication. However, due to the obstacles' shape and density, a few device pairs may not get indirect LoS via a single reflection. In such cases, double reflection can help them to get an indirect LoS. This, in turn, increases the number of served blind pairs. Moreover, double reflection has also been demonstrated to lower the number of RIS needed. Additionally, we have mathematically

proved that under certain conditions, double reflections are more energy-efficient than single reflections, which is quite counter-intuitive. Next, we have demonstrated that three reflections may provide only a slightly higher throughput, but the corresponding power consumption is reasonably high. As a result, triple or higher reflections may not be as good as a double reflection in terms of energy efficiency. This further justifies the widespread assumptions of ignoring the triple and higher-order reflections in the literature. Furthermore, it is shown that the approximation ratio of our set cover-based RIS deployment algorithm is $O(\log |B|)$, where $|B|$ represents the total number of blind pairs. This ratio is the best possible, as no polynomial-time algorithm for set cover can give a better approximation ratio than $O(\log n)$ unless P = NP. Then, each RIS is divided into a number of non-overlapping subgroups to reduce the channel estimation overhead. Subsequently, we propose an energy-efficient algorithm to find the appropriate subgroups of an RIS to achieve higher sum throughput. Finally, through the numerical results we show that our approach outperforms a random and a recent deployment strategy.

Chapter 3 is based on the already deployed RISs and the users in the surroundings. It describes the procedure by which information transfer takes place from a particular user to its desired counterpart. Moreover, we assume that the RISs are strategically placed in the environment and that idle IUs agree to act as a DF relay node. Our priority is to make more use of the idle IUs over the RISs due to the following reasons. Firstly, the RISs reflect the entire incoming signal including the noise in the desired direction, whereas a DF relay separates the noise from the information to transmit only the latter to the next user. Secondly, being a passive device, too many RISs installation in the surroundings leads to unnecessary wastage of resources. Lastly, opting for RIS over an idle IU as a hop implies frequent restart of the former, which creates problems for other users that are being served by this particular RIS at that time. However, the importance of the RISs cannot be ruled out completely. Being solely dependent on the IUs for information transfer may also hamper the reliability of the entire process, as it will fully rely on the IU availability and traffic characteristics. Moreover, the IUs are considered capable of energy harvesting and as a result, they do not waste their own energy in the process of volunteering to act as a relay for other users. Considering these insights, in this chapter, we propose a double-RIS assisted multihop routing scheme (DRAMS) for a D2D communication network. Moreover, useful information related to the proposed routing scheme is also obtained, where we characterize the maximum acceptable delay under different scenarios. Finally, the numerical results

demonstrate the benefit of DRAMS in terms of reduced RIS usage, enhanced data rate, and energy efficiency, respectively, with respect to the existing benchmark scheme.

In Chapter 4, we consider the aspect of multihop routing in a grouping-based RIS-assisted wireless network with spatially correlated channels. Effective grouping implies that a single RIS can cater to multiple pairs of devices simultaneously. Between a given pair of devices, our aim is to find a sequence of appropriate RIS group and IUs acting as relays when a direct LoS does not exist between them. Moreover, it may so happen that multiple relay requests arrive at a particular RIS or IU. In that case, IU must choose which request to fulfill and which RIS group to use. In this context, based on the respective delay constraint and the channel condition, we propose a metric that takes this decision. Here, instead of choosing the LRD as the criteria for selecting the next hop, we choose that particular IU as next hop, which provides the best data rate depending on the channel condition. In this context, we have used adaptive modulation for calculating the data rate obtained among the IUs. It is important to note that our priority is to make more use of the IUs over the RISs as explained earlier for delay-sensitive scenarios. Accordingly, we propose an intelligent scheduling strategy to handle multiple requests arriving at an IU by taking into account their delay constraints, respective channel conditions, and also the activity status (idle/busy) of the concerned IU. Finally, the numerical results demonstrate the benefits of the proposed framework, which results in enhanced data rate, reduced energy consumption, and enhanced energy efficiency, respectively, with respect to the existing benchmark schemes.

In Chapter 5, we consider a grouping-based self-sustainable RIS-aided single-hop communication setup with a finite number of groups. By taking into account both the power splitting (PS) and time splitting (TS) configurations of the RIS, we propose appropriate bounds on the choice of system parameters. The analysis takes into account a simplified linear EH model and also a practical non-linear EH model. Accordingly, a single group at the RIS is selected for information transmission from the source to the destination. Next, by considering the aspect of spatial correlation at the RIS, various group selection strategies are proposed. Specifically, the proposed strategies depend on the end-to-end signal-to-noise ratio (SNR) and the energy harvested at the groups. By employing tools from high-order statistics, we propose generalized group selection strategies and also characterize the outage (both information and energy) probability for each of these schemes. In particular, a complete analytical framework for the performance of the k-th best group selection at the RIS is presented. Finally, by using tools from the extreme value theory (EVT), we investigate the asymptotic performance of the system, where the number of groups is significantly

large. Extensive Monte Carlo simulations validate the proposed analytical framework. We observe that the strategic group selection strategy outperforms its random selection-based counterpart. Moreover, we compare our method with an existing framework that groups the RISs without considering spatial correlation, and demonstrate how spatial correlation at the RIS affects the outage performance of the proposed strategies in terms of inter-patch spacing. Furthermore, the impact of the value of k in the proposed generalized k-th best group selection strategy can also be seen. Finally, the results also depict the effect of having a large number of groups available for grouping on the system outage performance.

Finally, Chapter 6 concludes our work, and here, we mention a few future research directions of the investigated works.

1.5 Thesis organisation

In Chapter 2, a novel RIS placement strategy has been discussed by considering both single and double reflections. Next, in Chapter 3, based on the already deployed RISs, novel double-RIS assisted adaptive modulation-based multihop routing scheme for D2D wireless networks, which takes into account the aspect of multi-RIS secondary reflection. Furthermore, to handle multiple requests, a novel priority-aware channel-dependent scheduling strategy has been investigated for RIS-assisted multihop D2D communication, which also takes into account the aspect of element grouping at the RIS. A order statistics-based generalized group selection strategies for a self-sustainable RIS-assisted D2D communication set-up in a Rician fading scenario, which takes into account the aspect of correlated channels, has been discussed in Chapter 5. Lastly, the thesis is concluded and future research directions are discussed in Chapter 6.

Chapter 2

Double Reflections Aided RIS Deployment and Energy-efficient Group Selection Strategy [1]

2.1 Introduction

RIS-assisted mmWave D2D communication is a promising technique in 5G and beyond wireless network systems. Since mmWave suffers from high propagation and penetration loss, a LoS link is required in the aforementioned communication system. However, Static obstacles like trees and buildings can easily obstruct the direct LoS connectivity between a device pair. In this context, RIS placement plays a crucial role in improving the system performance. More specifically, RIS deployment strategy for both single and double reflection is a very challenging issue in D2D communication. Therefore, in this chapter, we suggest a set cover-based RIS deployment approach for D2D communication with single and double RIS assistance. We have specifically shown that allowing reflections through two consecutive RISs can significantly reduce the environment's RIS density, avoiding resource waste and allowing more obstructed device pairs to be served. We also offer an energy-efficient group selection criterion for information transfer following the RIS deployment. Furthermore, we demonstrate that, contrary to popular belief, there are instances in which double reflections are preferable to single reflections. Simulation results justified our claim. The symbols used in this chapter and their respective meanings are given in Table 2.

[1] This chapter is based on the following publication:
L. Sau and S. C. Ghosh, "RIS deployment and group selection strategy in double-RIS assisted mmWave D2D communication", **IEEE Transactions on Green Communication and Networking**, Vol. 10, pp. 723-736, 2026.

2.2 Chapter Organization

This chapter is organized as follows. We have discussed the system model and preliminaries in Section 2.3. Mathematically, the problem formulation is discussed in Section 2.4. The strategic deployment of RISs, the group selection strategy, and their analysis are discussed in Section 2.5. Thereafter in Section 2.6, we have discussed the simulation results and compared this with the existing placement strategies. Finally, in Section 2.7, we give concluding remarks and the future direction of the research.

2.3 System Model and Preliminaries

2.3.1 Network Topology

Consider a wireless communication system that operates in a rectangular area that is partitioned into small squares or grids of unit size, which is shown in Fig. 2.1. The area of the rectangle consists of M_r rows and M_c columns. We assume that each unit square grid is identical with respect to their center and we also assume that the center of the leftmost corner square is the origin. It is noted that the device that will operate in this setting will have highly directed antennas. The position of a user is approximated to the center of the grid within which it lies. We assume that a device can communicate with another directly if there is a LoS link between them and they are within a threshold distance r. This is because, as the signal gain diminishes with increasing distance, it will become insufficient for communication beyond a certain range.

Now, we are presenting a few definitions below, which will be used throughout our discussion.

Definition 1 (Direct LoS link)**.** *If there is no blockage between two users u and v and they are within a distance r then the link between them is called a direct LoS link [46].*

Definition 2 (Blind pair)**.** *A device pair (u, v) lies within a distance r is said to be a blind pair if there is no direct LoS link between them.*

Definition 3 (single reflection)**.** *A device pair (u, v) is said to be coverable via single reflection if there is no direct LoS link between u and v but they are connected via an intermediate RIS, i.e., there is a direct LoS link between u to an RIS and that RIS to v.*

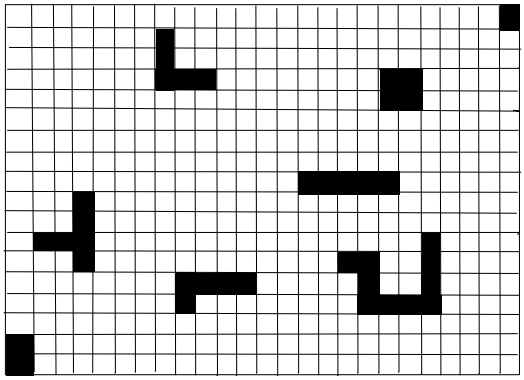

Figure 2.1: Grid and obstacle model.

Definition 4 (Double reflections)**.** *The device pair (u, v) lie within a distance r is said to be coverable via double reflections if u and v can communicate with each other in two-hop using two consecutive RISs R_i and R_j, i.e., there is a direct LoS link between u to R_i, R_i to R_j, and R_j to v, respectively.*

Definition 5 (Coverable blind pairs)**.** *If a device pair (u, v) is coverable via single reflection or double reflections, or both of them, then it is considered as a coverable blind pair, else it is called a totally blind pair.*

2.3.2 Characteristics of the Users and Environmental Obstacles

We consider all the devices in this communication scenario to be pseudo-stationary [53], i.e., during communication time, a device does not move outside the grid. We also assume that a device follows any mobility model within a grid at any time instance. However, we presume that a device's location in a unit grid is roughly determined by the grid's center. It is noted that if we consider a device is within a grid that means it lies at the center of the grid.

Here, we position the obstacle inside the grids following the acquisition of the satellite images. We assume that the satellite images give the proper position of the obstacles. In Fig. 2.1, we consider that the black cells represent the location of the obstacles. We assume that, if a grid/cell is blocked, it means the whole cell is blocked and there will not be any partially blocked cells. Multiples of these blocked zones combine to build a polygon that closely resembles the shape and size of the obstruction. Within a block cell, a device can not lie, i.e., a device can lie only within the free cells. It is noted that an RIS can not be placed within a block cell, it will be strategically placed on poles in the free zones. For simplicity

and mathematical tractability, we discretize the service area into unit-size grids as in [36] and thus approximate the real-life 3D environment to a 2D plane.

2.3.3 RIS Grouping

Obstacles prevent a device pair from directly communicating with one another. Therefore, to provide an indirect LoS between them, we use single and double reflections via one and two consecutive RISs. Let us assume that an RIS R_i consists of N_r rows and N_c columns, which are effectively controlled to adjust both the amplitude and phase of the incident waveform. However, only the phase is tuned or optimized, and the amplitude factor is fixed to unity for the purposes of simplicity and mathematical tractability [22]. We use a grouping approach in order to minimize the channel estimation overhead [65]. Furthermore, for a RIS that consists of a large number of reflecting elements, the phase shift computation is very high, and a minimum energy is required for each phase shift. Therefore, we divide R_i into K_g number of non-overlapping subgroups R_i^t to minimize the energy consumption where $1 \leq t \leq K_g$, and each R_i^t consists of $N_g \times N_g$ number of patches, i.e, $K_g \times N_g \times N_g = N_r \times N_c$. It is noted that the number of partitions and the ensuing sub-surfaces are decided upon beforehand [22], and each subgroup is capable of providing a desired throughput. In this scenario, R_i^t can be in one of two states: ON or OFF. An incident signal's phase can be altered to a desired direction when an element is in the ON state; when it is in the OFF state, it cannot reflect [22]. Here, we use one particular subgroup instead of using total RIS, and we also assume that a subgroup can serve a single request at a particular instant [66]. Our objective is to select the energy-efficient subgroups for information transfer.

2.3.4 Computation of Throughput and Energy-efficiency

In this communication scenario, let there be n_d number of devices that lie within the free zones. We assume that any two devices u and v want to communicate with each other and they lie within the free zones z_1 and z_2, respectively. Now, depending on the position of the obstacles, u and v can communicate in three different ways as follows: (i) directly, u and v can communicate directly if there is no obstacle in between them, i.e., there is a LoS link between them. (ii) via single reflection, and (iii) via double reflections. We suppose that the wireless link experiences both small-scale block fading and large-scale path loss effects. The direct channel from u to v exhibits small-scale fading and their corresponding path loss factor is $\rho_L^{\frac{1}{2}} d_{uv}^{-\frac{\alpha}{2}}$, where ρ_L is the path loss at one meter distance, α is the path loss exponent and d_{uv} denote the distance between u and v.

We also assume that each group R_i^t of an RIS R_i consists of $N_g \times N_g$ number of elements. Let $\mathbf{h}_{uR_i^t} \in \mathbb{C}^{N_g \times 1}$, $\mathbf{h}_{R_i^t R_j^s} \in \mathbb{C}^{N_g \times N_g}$ and $\mathbf{h}_{R_i^t/R_j^s v} \in \mathbb{C}^{1 \times N_g}$ be the channel matrix from u to R_i^t, R_i^t to R_j^s and, R_i^t/R_j^s to v, respectively. Note that, unlike the conventional RIS-based approach, the grouping-based approach does not involve a diagonal phase shift matrix of non-zero $N_g \times N_g$ elements [22]. A common phase shift is applied on the incoming signals, and the product of each point-to-point link determines the total path loss for each of these channel matrices [47]. As a result, the effective channel gain for single reflection and double reflection is given by $\mathbf{h}_{R_i^t v}\mathbf{h}_{uR_i^t} \times e^{j\phi_{i,t}}$ and $\mathbf{h}_{R_j^s}\mathbf{h}_{R_i^t R_j^s}\mathbf{h}_{uR_i^t} \times e^{j(\phi_{i,t}+\phi_{j,s})}$, where $e^{j\phi_{i,t}}$ and $e^{j\phi_{j,s}}$ are the common phase shift of R_i^t and R_j^s, respectively.

Now, we define a metric, data rate that will be used to quantify the performance of our proposed strategy. Here, we assume orthogonal frequency-division multiplexing (OFDM) [31] is used in our communication scenario. Let P_{tx} be the transmitted power, then the signal-to-noise-ratio (SNR) at the receiver for single RIS-assisted communication is

$$\gamma_{\text{sr}} = \frac{P_{\text{tx}}\rho_{\text{L}}^2 d_{R_i^t v}^{-\alpha} d_{uR_i^t}^{-\alpha}}{\sigma_0^2}\left|\mathbf{h}_{R_i^t v} \times \mathbf{h}_{uR_i^t} \times e^{j\phi_{i,t}}\right|^2, \tag{2.1}$$

and SNR for double RISs reflected communication is

$$\gamma_{\text{dr}} = \frac{P_{\text{tx}}\rho_{\text{L}}^3 d_{R_j^s v}^{-\alpha} d_{uR_i^t}^{-\alpha} d_{R_i^t R_j^s}^{-\alpha}}{\sigma_0^2}\left|\mathbf{h}_{R_j^s} \times \mathbf{h}_{R_i^t R_j^s} \times \mathbf{h}_{uR_i^t} \times e^{j(\phi_{i,t}+\phi_{j,s})}\right|^2, \tag{2.2}$$

where σ_0^2 is the variance of the circularly symmetric zero mean additive white Gaussian noise. Note that, we adjust the common phase shift of (2.1) and (2.2) to attain the optimal SNR. Therefore, from Shannon's capacity formula, we can get the throughput $T(\gamma) = \log(1+\gamma_{\text{sr/dr}})$. Hence, by calculating the throughput, we can compare the performances.

Now, we define the energy-efficiency metric (E_{eff}), which will be used to measure how well our suggested approach performs in terms of energy utilization. Let $T(\gamma)$ be the throughput obtained at the receiver end. Additionally, it requires a total $\text{E}_{\text{c}}^{\text{i}}$ amount of energy for information transfer via a single RIS R_i, where

$$\text{E}_{\text{c}}^{\text{i}} = \beta_k \times \alpha_k \times \frac{1}{T_i(\gamma)} \times \Big(P_{\text{tx}} + P_{\text{ph}}(R_i)\Big). \tag{2.3}$$

For two consecutive RIS (R_i and R_j) assisted communication the total energy consumption is denoted by $\text{E}_{\text{c}}^{\text{i,j}}$ where

$$\mathrm{E}_{\mathrm{c}}^{\mathrm{i,j}} = \frac{\beta_k \alpha_k}{T_{i,j}(\gamma)} \Big(P_{\mathrm{tx}} + P_{\mathrm{ph}}(R_i) + P_{\mathrm{ph}}(R_j) \Big), \tag{2.4}$$

β_k is the number of packets each with α_k bits, P_{tx} is the transmitted power, and $P_{\mathrm{ph}}(R_i)$ is phase shift power for RIS R_i.

Therefore, the energy-efficiency for single reflection and double reflections are defined by $\mathrm{E}_{\mathrm{eff}}^{\mathrm{i}} = \frac{T_i(\gamma)}{\mathrm{E}_{\mathrm{c}}^{\mathrm{i}}}$ and $\mathrm{E}_{\mathrm{eff}}^{\mathrm{i,j}} = \frac{T_{i,j}(\gamma)}{\mathrm{E}_{\mathrm{c}}^{\mathrm{i,j}}}$, respectively. Moreover, we use this metric to select an appropriate subgroup for the information transfer of each blind pair.

2.4 Problem Formulation

Our objective is to place the minimum number of RISs in strategic locations and for each information transfer, we aim to find an energy-efficient subgroup for abstracted device pair. Therefore, we formulate the problem and break it down into two separate parts: i) RIS deployment and ii) Group selection. Now we are describing these two parts in detail below:

2.4.1 RIS Deployment

In the first part, we want to formulate an optimization problem to cover a maximum number of blind pairs using the least number of RISs. It is noted that we do not consider those device pairs that have direct LoS and are totally blind. Here, let $\mathcal{B}$ be the set of all coverable blind pairs, i.e., no element of $\mathcal{B}$ remains uncovered after deploying the RISs. Moreover, to formulate the optimization problem, we define a few notations below.

Let i and j be two locations and a_{ij} be an indicating variable that describes the status of having LoS between them, where $1 \leq i, j \leq n^2$. That is,

$$a_{ij} = \begin{cases} 1, & \text{dist } (i,j) \leq r \ \& \ \exists \ \text{ LoS between i and j} \\ 0, & \text{else} \end{cases} \tag{2.5}$$

Additionally, let S_i be the set of all blind pairs covered by an RIS at the i-th cell. That is,

$$S_i = \Big\{ (p,q) : \quad a_{pi} + a_{iq} = 2 \Big\} \quad \forall \ i. \tag{2.6}$$

Note that a blind pair of $\mathcal{B}$ may be visible via a single or double reflections. Therefore, we also consider D_{ij} as a set of all blind pairs that are coverable via double reflections using two

RISs located at i-th and j-th cells, but not coverable by either i-th or j-th RIS via a single reflection. Hence, D_{ij} can be represented as

$$D_{ij} = \Big\{(p,q): \quad (p,j) \in S_i \ \ \& \quad (i,q) \in S_j, \quad (p,q) \notin S_i, \\ (p,q) \notin S_j \Big\} \quad i < j.$$

However, we define Z_{ij} as a set of all blind pairs that are coverable via single as well as double reflections using RIS placed at i-th and j-th locations. That is,

$$Z_{ij} = S_i \cup S_j \cup D_{ij}, \quad i < j. \tag{2.7}$$

We now introduce the following binary variable:

$$x_i = \begin{cases} 1, & \text{i-th cell is selected for RIS deployment,} \\ 0, & \text{else.} \end{cases}$$

Hence, we formulate the optimization problem as follows:

$$\text{Minimize} \quad \sum_{i=1}^{n^2} x_i \tag{2.8}$$

$$\text{such that} \quad \bigcup_{i,j:i\le j} Z_{ij} x_i x_j = \mathcal{B} \ \ \forall \ \ i < j. \tag{8.a}$$

This integer program can be linearized by using an intermediate binary variable y_{ij} as follows:

$$\text{Minimize} \quad \sum_{i=1}^{n^2} x_i \tag{2.9}$$

$$\text{such that} \quad \bigcup_{i,j:i\le j} Z_{ij} y_{ij} = \mathcal{B}, \tag{9.a}$$

$$y_{ij} \le x_j \quad \forall \ \ i < j, \tag{9.b}$$

$$y_{ij} \le x_i \quad \forall \ \ i < j, \tag{9.c}$$

$$y_{ij} \ge x_i + x_j - 1 \quad \forall \ \ i < j. \tag{9.d}$$

Note that the above integer linear program (ILP) is nothing but a classical set cover problem which is a well-known NP-hard problem. Therefore, in Section 2.5.1, we present a greedy solution for the RIS deployment problem.

2.4.2 Group selection

In the second part, for group selection, we assume that RISs have already been deployed. Moreover, we also know which blind pair will be covered by which RISs. Note that, a blind pair may be covered by single as well as double reflections. Hence, for a blind pair, more than one subgroup may be available to complete the information transfer. However, we allow a single subgroup for information transfer because of the scenario of energy constraints. Therefore, our primary objective is to identify a specific energy-efficient subgroup for each blind pair. Let us assume that there are n_b number of blind pairs, and R number of RISs are deployed in the surroundings, and each of them is subdivided into l number of subgroups. Let $\mathrm{G_i^s}$ be the set of all subgroups that can provide an indirect LoS link to the i-th blind pair via single reflection. Hence, we can represent $\mathrm{G_i^s}$ as

$$\mathrm{G_i^s} = \Big\{ R_j^k : i\text{-th pair is visible via } k\text{-th subgroup of RIS } R_j \Big\}.$$

Similarly, let $\mathrm{G_i^d}$ be the set of all subgroups that can provide an indirect LoS link to the i-th blind pair via double reflections. That is,

$$\mathrm{G_i^d} = \Big\{ R_{l,m}^{p,q} \quad : i\text{-th pair is visible via } p\text{-th subgroup of RIS } R_l \ \&\ q\text{-th subgroup of RIS } R_m \Big\}.$$

Hence, if a blind pair is visible by single reflection, our problem is to find a more energy-efficient subgroup $R_{j^*}^{k^*}$ from $\mathrm{G_i^s}$ such that

$$\mathrm{E_{eff}^{k^*}}(j^*) = \mathrm{argmax}\Big(\mathrm{E_{eff}^{k}}(j)\Big).$$

If a blind pair is visible via double reflections, we select $R_{l^*,m^*}^{p^*,q^*}$ as energy-efficient subgroups from $\mathrm{G_i^d}$ such that

$$\mathrm{E_{eff}^{p^*,q^*}}(l^*, m^*) = \mathrm{argmax}\Big(\mathrm{E_{eff}^{p,q}}(l, m)\Big).$$

Note that if a blind pair is visible via single as well as double reflections, we will select the more energy-efficient case for them. In Section. 2.5.2, we have discussed the group selection strategy in detail.

Algorithm 1: Visibility Algorithm

Input: $L, z_i \in Z, (u, v)$
Output: Visible or not

Join uz_i and z_iv
if $uz_i \| z_iv$ intersect at least one line segment of L **then**
    not visible via z_i
else
    Visible via z_i

2.5 Proposed Strategy

Here we discuss the RIS deployment and group selection strategy by considering both single and double reflections. Accordingly, we divide this section into two parts: i) RIS deployment strategy and ii) Group selection criteria. In the first part, we propose a greedy deployment strategy, and in the second part, we investigate an energy-efficient group selection criteria.

2.5.1 Proposed RIS Deployment Strategy

In our proposed RIS deployment strategy, we first identify which blind pairs are present in the surroundings. After identifying the blind pairs, we will find the candidate locations for RIS deployment, and finally select the candidate locations for final deployment. All these steps are now discussed in detail below.

2.5.1.1 Blind Pairs Identification

Let there be n_o obstacles and n_d device pairs in a region, whose locations are known. We assume that the sides of an obstacle are formed by line segments and L is the set of all line segments of n_o obstacles. Additionally, we assume that a device pair (u, v) can communicate with each other if they reside within r distance. Let Z be the set of all free cells. Algorithm 1 finds whether a device pair (u, v) is visible via a free cell $z_i \in Z$ or not. Here, we aim to find all the blind pairs in a region. To achieve this, we first find the set of all device pairs that may be obstructed by a particular obstacle. Finally, continuing this process for all obstacles, we get the set of all blind pairs, which is described below.

Let O_i be the i-th obstacle, L_i be the set of all line segments that constitute O_i, and

$$C_i = \Big\{(x_t, y_t) : \quad t = 1, \cdots n_i\Big\} \tag{2.10}$$

Algorithm 2: Blind Pairs Identification Algorithm

Input: L_i, D
Output: B

Initialize: $B = \phi$;
for $i \in \{1, \cdots, n_o\}$ **do**
  $B_i = \phi$, $D_i = \phi$;
  for (u^t, v^t) *in* D **do**
    if $x_i^{\min} - r \leq u_x^t, v_x^t \leq x_i^{\max} + r$ *and* $y_i^{\min} - r \leq u_y^t, v_y^t \leq y_i^{\max} + r$ **then**
      $D_i = D_i \cup \{(u^t, v^t)\}$
  for (u^t, v^t) *in* D_i **do**
    for $l \in L_i$ **do**
      if l intersect $u^t v^t$ **then**
        $B_i = B_i \cup \{(u^t, v^t)\}$
        Break;
  $B = B \cup B_i$
Return B

be the set of all n_i vertices of O_i. Therefore, let

$$\begin{aligned} x_i^{\max} &= \max\{x_t : \quad t = 1, \cdots n_i\}, \\ x_i^{\min} &= \min\{x_t : \quad t = 1, \cdots n_i\} \text{ and} \\ y_i^{\max} &= \max\{y_t : \quad t = 1, \cdots n_i\}, \\ y_i^{\min} &= \min\{y_t : \quad t = 1, \cdots n_i\} \end{aligned}$$

be the maximum and minimum x-coordinate and y-coordinate of the vertices of O_i, respectively. Let

$$\begin{aligned} D &= \left\{(u^t, v^t) \ : \quad t = 1, \cdots, n_d\right\} \\ &= \left\{((u_x^t, u_y^t), (v_x^t, v_y^t)) : \quad t = 1, \cdots, n_d\right\} \end{aligned}$$

be the set of x and y coordinates of all the device pairs. Let D_i be the set of device pairs that could potentially be obstructed by O_i. That is,

$$D_i = \left\{(u^t, v^t) \in D \ : \ x_i^{\min} - r \leq u_x^t, v_x^t \leq x_i^{\max} + r,\right.$$

$$y_i^{\min} - r \leq u_y^t, v_y^t \leq y_i^{\max} + r \Big\}. \tag{2.11}$$

Let $\mathcal{B}_i$ be a set of all blind pairs that could potentially be obstructed by O_i. That is,

$$\mathcal{B}_i = \{(u^t, v^t) \in D_i \quad : \quad u^t v^t \text{ intersect at least one line segment of } L_i\}. \tag{2.12}$$

Continuing this process, for each obstacle, we can compute the set B of all blind pairs as follows:

$$\mathcal{B} = \mathcal{B}_1 \cup \mathcal{B}_2 \cup \cdots \cup \mathcal{B}_{n_o} = \bigcup_{i=1}^{n_o} \mathcal{B}_i. \tag{2.13}$$

The complete process of blind pair identification is shown in Algorithm 2. Note that our main motivation is to serve a maximum number of blind pairs using indirect LoS via single or double reflections. In this context, we use a novel technique to find out the candidate zones for RIS deployment below.

2.5.1.2 Finding Candidate Locations for RIS Deployment

Our goal is to find the candidate locations for RIS deployment such that we can serve a maximum number of blind pairs with fewer RISs. Since the grid consists of N_r rows and N_c columns, there are $N_r \times N_r$ zones in the grid. Out of $N_r N_c$ zones, few are covered by obstacles, and the remaining are obstacle-free zones. Let there be p free zones where $p < N_r N_c$ and Z be the set of all free zones. That is,

$$Z = \Big\{ z_i : i = 1, 2, \cdots, p \Big\}, \tag{2.14}$$

where z_i denotes the i-th free zone.

Let A_i be the set of all blind pairs that are *visible* via z_i, i.e., for blind pair $(u, v) \in A_i$ there is a direct LoS between u to z_i and z_i to v. Additionally, we denote the cardinality of A_i as $card(A_i)$. Let A be an array of p elements whose i-th element represents the cardinality of A_i, i.e., $card(A_i)$. Let $\max(A)$ be the maximum element of A, and t be the corresponding index of $\max(A)$ in the array A. Therefore, z_t is the corresponding zone from where the maximum number of blind pairs can be served. Hence, we select z_t as the first candidate location for RIS deployment and A_t be the set of all blind pairs that are *visible* via z_t. Here we rename the set A_t as A_1^m and z_t as z_c^1. Therefore, after finding the initial RIS location, let B_{rem}^1 represent the set of all the remaining blind pairs, i.e.,

$$B_{rem}^1 = B \setminus A_1^m = \left(A_1^m\right)^c, \tag{2.15}$$

where X^c denotes the complement of the set X.

After fixing the first candidate location z_c^1, the remaining blind pairs may be visible via i) single reflection or ii) double reflections. In particular, the remaining blind pairs in B_{rem}^1 may be visible via single reflection using any free cell other than z_c^1, or via double reflections using z_c^1 plus one of the remaining free cells. Therefore, we select that free cell as a second candidate location for RIS deployment from where the maximum number of elements of B_{rem}^1 will be served using single or double reflections. Let us denote z_c^2 as the second candidate zone for RIS deployment, and B_{rem}^2 as the set of remaining blind pairs. In a similar way, we can find out the other candidate locations. Therefore, after finding the k-th candidate location, the remaining set of blind pairs is given by

$$B_{rem}^k = \left(A_1^m \cup A_2^m \cdots \cup A_{k-1}^m \cup A_k^m\right)^c = B_{rem}^{k-1} \setminus A_k^m \tag{2.16}$$

where A_k^m is the set of all blind pairs that are served by the k-th candidate location, and B_{rem}^{k-1} is the set of all remaining blind pairs before finding the k-th candidate location and the process will stop if $B_{rem}^k = B_{rem}^{k-1}$ or $B_{rem}^k = \phi$. Finally, we receive the set Z_c of all candidate zones from where we can cover the greatest number of blind pairs. The RISs will actually be placed at the center of each free zone $z_i \in Z_c$. The proposed strategy is described in Fig. 2.2.

Complexity and approximation ratio of the proposed algorithm

Let there be p free cells and $|\mathcal{B}|$ many blind pairs. According to our proposed strategy, for selecting the first RIS location, we consider each free cell and compute the number of blind pairs that can be served by it using single reflection only. This requires $p|\mathcal{B}|$ complexity. Next, for finding the k-th RIS location ($k \geq 2$), we consider each of the remaining $(p-k+1)$ free cells and compute how many blind pairs can be covered by it using single as well as double reflections. This requires $(p-k+1)|\mathcal{B}| + (k-1)(p-k+1)|\mathcal{B}| + \binom{k-1}{2}|\mathcal{B}|$ complexity. Hence, the worst-case complexity of the proposed algorithm is $O(p^2|\mathcal{B}|)$. This greedy algorithm is indeed the classic set cover greedy algorithm, which has a well-known approximate ratio of $O(\log n)$ [67]. The approximation ratio of our suggested RIS deployment algorithm is therefore $O(\log|\mathcal{B}|)$, where $|B|$ represents the total number of blind pairs. In fact, it is also well-known that no polynomial-time algorithm for set cover can give a better approximation ratio than $O(\log n)$ unless P = NP [67].

From the above discussion and observation, we get the following remarks.

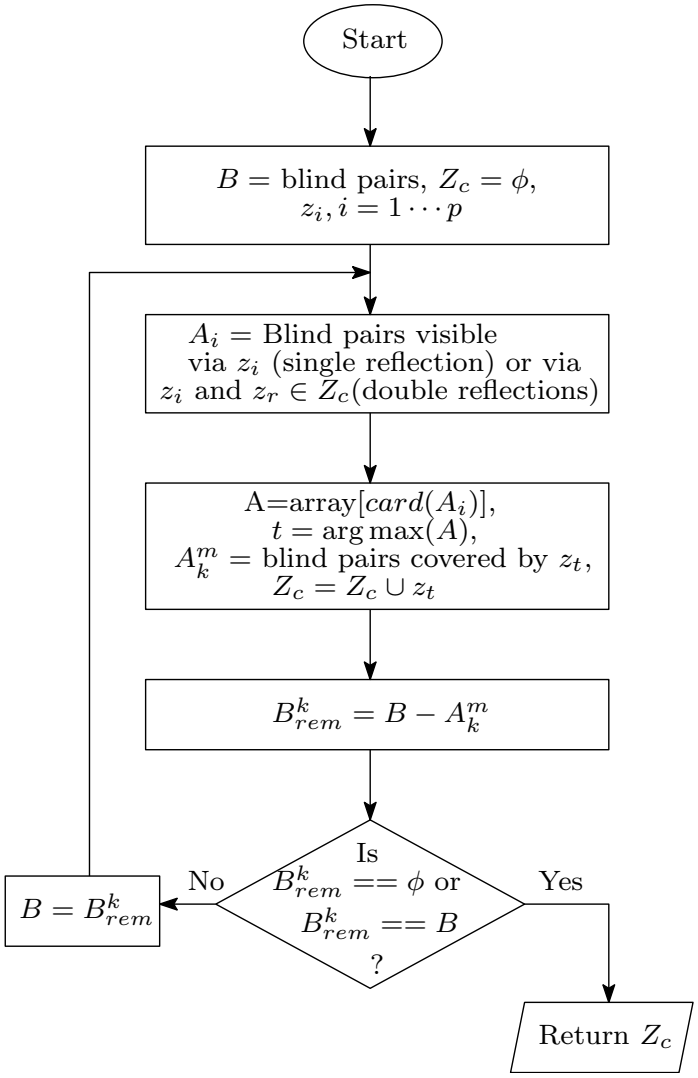

Figure 2.2: Proposed strategy for finding candidate locations.

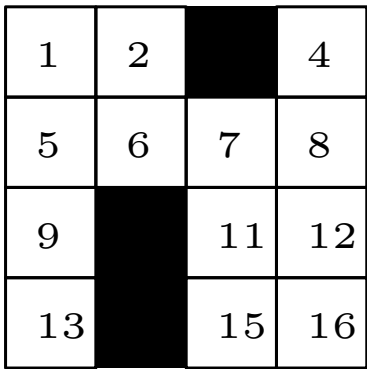

Figure 2.3: Example of a communication environment

Remark 1. *If $B^k_{rem} \neq \phi$ and $B^k_{rem} = B^{k-1}_{rem}$ holds then $B_{un} = B^k_{rem}$ is the total number of uncovered blind pairs. That is, $B_{un} = \left(A^m_1 \cup A^m_2 \cdots \cup A^m_{k-1} \cup A^m_k\right)^c$.*

Remark 2. *If only k number of RISs are allowed to deploy, then the total number of blind pairs that can be served is given by $\left(B^1_{rem} \cap B^2_{rem} \cap \cdots \cap B^k_{rem}\right)^c = \mathcal{B} \setminus B^k_{rem}$.*

Remark 3. *In a particular scenario, if no blind pair is visible via double reflections, then our proposed strategy will be converted into the RIS deployment strategy for single reflection.*

Below, we have illustrated the proposed RIS deployment strategy using an example.

2.5.1.3 Illustrative Example of the Proposed Deployment Strategy

A specific scenario of our proposed strategy is demonstrated in Fig. 2.3. Here we consider a grid that consists of four rows and four columns. As this grid consists of sixteen cells, we label these cells from 1 to 16. Moreover, we assume that the obstacles are located in the black cells, which correspond to the cell numbers $3, 10$, and 14. We also consider that a device can lie only within a free cell. Here, $\{1,2,4,5,6,7,8,9,11,12,13,15,16\}$ is the set of all free cells. Here, we assume that each pair of cells is within r distance apart from each other. Therefore, in this communication environment,

$$\begin{aligned} B = \{&(1,4),(1,8),(1,11),(1,15),(1,16),(2,4),(2,7),(2,8),\\ &(2,13),(2,12),(2,15),(4,5),(4,6),(4,7),(4,9),(4,13),\\ &(5,12),(5,11),(5,15),(5,16),(6,9),(6,11),(6,13),\\ &(6,15),(6,16),(7,9),(7,13),(8,9),(8,13),(9,11),(9,12), \end{aligned}$$

$$(9,15),(9,16),(11,13),(12,13),(13,15),(13,16)\}$$

is the complete set of all the blind pairs. Specifically, there is no direct LoS link between any device pair of B. As obstacles block the direct LoS of the blind pairs, RISs can be strategically deployed to provide an indirect LoS link. It can be observed that each of the blind pairs in $\{(4,9),(4,13),(9,15),(11,13),(12,13),(13,15),(13,16)\}$ can not be covered via single reflection, even if we deploy RISs in all the free cells. However, in our proposed strategy, we can serve more blind pairs using double reflections along with the single reflection. It can be observed that the maximum number of blind pairs can be served by placing an RIS at cell 12. Thus, our strategy will choose cell 12 as the first RIS location. Also, note that cells 1 and 12 together can serve all the remaining blind pairs using single and double reflections. That is, according to our proposed strategy, $\{1,12\}$ will be the set of locations for RIS deployment.

In the following Subsection 2.5.2, we will address which subgroup of an RIS will be selected for information transformation.

2.5.2 Group Selection Criteria

In Section 2.5.1 above, we have strategically found R, the set of all deployed RISs, and the set of all coverable blind pairs $\mathcal{B}_\rfloor = B \setminus B_{un}$. A blind pair $(u,v) \in \mathcal{B}_\rfloor$ can be covered in three different ways: i) via only single reflection, ii) via only double reflections, and iii) via both single and double reflections. Since energy consumption is a very important parameter in wireless communication scenarios, we discuss in the following the process to find the energy-efficient group considering the above-mentioned three cases.

2.5.2.1 Energy-efficient Subgroup Selection for single reflection

In this case, u sends all the packets to v using one subgroup of an RIS as an intermediate reflector. Let $S_{u,v}$ be the set of RISs each of which can provide indirect LoS between u and v via single reflection. That is, $S_{u,v} = \{R_i : \ R_i \text{ is visible from both u and } v\}$. Since each RIS is partitioned into k non-overlapping subgroups, different subgroups may provide different data rates. In this context, from Subsection 2.3.4, the required energy $\mathrm{E_c(i)}$ for information transfer from u to v using i-th subgroup of s-th RIS is given by

$$\mathrm{E_c^s}(i) = \beta_k \times \alpha_k \times \frac{1}{T_s^i(\gamma)} \times \Big(P_{\mathrm{tx}} + P_{\mathrm{ph}}(R_s^i)\Big), \tag{2.17}$$

where $P_{\text{phase}}(R_s^i)$ is the phase shift power of i-th subgroup of R_s.

Therefore, the energy-efficiency $\mathrm{E}_{\text{eff}}^{\text{s}}(i)$ for a particular (u, v) pair using i-th subgroup is

$$\mathrm{E}_{\text{eff}}^{\text{s}}(i) = \frac{T_s^i(\gamma)}{\mathrm{E}_{\text{c}}^{\text{s}}(i)}. \tag{2.18}$$

Now, we form an optimization problem to select an energy-efficient subgroup as below:

$$\begin{aligned} \max \quad & \mathrm{E}_{\text{eff}}^{\text{s}}(i) && (2.19)\\ \text{s.t.} \quad & T_s^i(\gamma) \geq T_{th},\ i = 1, \cdots k \ \text{ and } \ s \in S_{u,v}, && (19.a)\\ & \mathrm{E}_{\text{c}}^{\text{s}}(i) > 0 \quad i = 1, \cdots k \ \text{ and } \ s \in S_{u,v}, && (19.b) \end{aligned}$$

where T_{th} is a predefined threshold.

2.5.2.2 Energy-efficient Subgroup Selection for Double Reflections

In this communication environment, u transfers the packets to v using two consecutive RISs R_i and R_j, respectively. We also assume that $D_{u,v}$ be the set of RISs each of which can provide indirect LoS between u and v. That is, $D_{u,v} = \{(R_i, R_j) : \ (R_i \text{ is visible from } u \text{ and } R_j) \ \& \ (R_j \text{ is visible from } v)\}$. Since each RIS is partitioned into k non-overlapping subgroups, one subgroup from R_i and another from R_j will be selected for complete information transfer from u to v. Therefore, from (2.4), the required energy for complete information transfer using l-th and m-th subgroup of R_i and R_j respectively, is given by

$$\mathrm{E}_{\text{c}}^{\text{i,j}}(l, m) = \frac{\beta_k \alpha_k}{T_{i,j}^{l,m}(\gamma)} \Big(P_{\text{tx}} + P_{\text{ph}}(R_i^l) + P_{\text{ph}}(R_j^m) \Big), \tag{2.20}$$

where, $P_{\text{ph}}(R_j^m)$ and $P_{\text{ph}}(R_i^l)$ are the phase shift power for m-th and l-th subgroup of R_j and R_i, respectively. Moreover, we can compute the energy-efficiency as

$$\mathrm{E}_{\text{eff}}^{\text{i,j}}(l, m) = \frac{T_{i,j}^{l,m}(\gamma)}{\mathrm{E}_{\text{c}}^{\text{i,j}}(l, m)}. \tag{2.21}$$

Now, we formulate an optimization problem to select the energy-efficient subgroups as follows:

$$\begin{aligned} \max \quad & \mathrm{E}_{\text{eff}}^{\text{i,j}}(l, m) && (2.22)\\ \text{s.t.} \quad & T_{i,j}^{l,m}(\gamma) \geq T_{th},\ l, m = 1, \cdots k \ \& \ i, j \in D_{u,v} && (22.a) \end{aligned}$$

Algorithm 3: Group Selection Algorithm

Input: $R, (u, v)$

Output: $R_{s^*}^{i^*}, R_{i^*,j^*}^{l^*,m^*}$

```
% Single Reflection
for s ∈ R do
    if (u, v) visible via R_s then
        for i ∈ R_s do
            compute E_eff^s(i)
        E_eff^{s*}(i*) = argmax ( E_eff^s(i) )
    else
        E_eff^{s*}(i*) = 0
% Double Reflection
for i ∈ R do
    for j ∈ R do
        if (u, v) visible via R_i and R_j then
            for l ∈ R_i do
                for m ∈ R_j do
                    if (u, v) visible via R_i^l and R_j^m then
                        Compute E_eff^{i,j}(l, m)
            E_eff^{i*,j*}(l*, m*) = argmax ( E_eff^{i,j}(l, m) )
        else
            E_eff^{i*,j*}(l*, m*) = 0
% Both Single and Double Reflection
if E_eff^{s*}(i*) ≥ E_eff^{i*,j*}(l*, m*) then
    Return R_{s*}^{i*}
else
    Return R_{i*,j*}^{l*,m*}
```

$$\mathrm{E}_{\mathrm{c}}^{\mathrm{i,j}}(l,m) > 0 \quad l,m = 1,\cdots k \;\&\; i,j \in D_{u,v}. \tag{22.b}$$

2.5.2.3 Energy-efficient Subgroup Selection for both Single and Double Reflections

In this communication environment, a device pair (u, v) is covered by both single and double reflections. That is, $S_{u,v} \neq \phi$ and $D_{u,v} \neq \phi$. Therefore, from 2.5.2.1, we get a

subgroup that provides the maximum energy-efficiency for single reflection. Similarly, using case 2.5.2.2 above, we get a pair of subgroups that provide the maximum energy-efficiency for double reflections. Finally, we select the best among them for information transfer between u and v. Note that once the RISs are deployed, the time required for establishing the connection for a particular requesting pair (u, v) is $O(|Z_c|)$, where $|Z_c|$ denotes the total number of RISs deployed.

In the following propositions, we will prove two interesting facts for a device pair covered via both single and double reflections.

Proposition 2.5.1. *Let a device pair (u, v) be visible through R_i^l using single reflection, and through R_i^l and R_j^m together via double reflections. In that case, single reflection are always more energy-efficient than double reflections.*

Proof. Let (u, v) be a blind pair that is visible via R_i^l using single reflection. Let $d_{R_i^l u}$ and $d_{R_i^l v}$ be the distances between u and R_i^l, and R_i^l and v, respectively. It is also given that (u, v) is visible via R_i^l and R_j^m together using double reflections, where R_i^l is a common subgroup that is used in both single and double reflections. Let $d_{R_i^l R_j^m}$ and $d_{R_j^m v}$ be the distances between R_i^l and R_j^m, and R_j^m and v, respectively. Additionally, we assume that $d_{R_i^l R_j^m} > 1$, $d_{R_j^m v} > 1$ and the channel conditions for single and double-reflected communication are the same. Therefore, using triangular inequality, we can claim that

$$d_{R_i^l u} < d_{R_i^l R_j^m} + d_{R_j^m v}. \tag{2.23}$$

Moreover, from (2.2), we have

$$\begin{aligned}
&P_{\text{tx}} |\mathbf{h}_{R_j^m} \times \mathbf{h}_{R_i^l R_j^m} \times \mathbf{h}_{u R_i^l} \times e^{j(\phi_{i,l} + \phi_{j,m})}|^2 \times \rho_{\text{L}}^3 d_{R_j^m v}^{-\alpha} d_{u R_i^l}^{-\alpha} d_{R_i^l R_j^m}^{-\alpha} \\
&\leq P_{\text{tx}} |\mathbf{h}_{R_j^m} \times \mathbf{h}_{R_i^l R_j^m} \times \mathbf{h}_{u R_i^l} \times e^{j(\phi_{i,l} + \phi_{j,m})}|^2 \\
&\qquad \times \rho_{\text{L}}^2 d_{R_j^m v}^{-\alpha} d_{u R_i^l}^{-\alpha} d_{R_i^l R_j^m}^{-\alpha} \quad (\because\ 0 < \rho < 1) \\
&\leq P_{\text{tx}} |\mathbf{h}_{R_j^m} \times \mathbf{h}_{R_i^l R_j^m} \times \mathbf{h}_{u R_i^l} \times e^{j(\phi_{i,l} + \phi_{j,m})}|^2 \\
&\quad \times \rho_{\text{L}}^2 d_{u R_i^l}^{-\alpha} d_{R_i^l v}^{-\alpha} \text{ (from (2.23) and } d_{R_i^l R_j^m} > 1, d_{R_j^m v} > 1)
\end{aligned} \tag{2.24}$$

Therefore, from (2.24), (2.2) and (2.1), we can claim that

$$\frac{P |\mathbf{h}_{R_j^m} \times \mathbf{h}_{R_i^l R_j^m} \times \mathbf{h}_{u R_i^l} \times e^{j(\phi_{i,l} + \phi_{j,m})}|^2 \times \rho_{\text{L}}^3 d_{R_j^m v}^{-\alpha} d_{u R_i^l}^{-\alpha} d_{R_i^l R_j^m}^{-\alpha}}{\sigma^2}$$

$$\leq \frac{P|\mathbf{h}_{R_j^m} \times \mathbf{h}_{R_i^l R_j^m} \times \mathbf{h}_{uR_i^l} \times e^{j(\phi_{i,l}+\phi_{j,m})}|^2 \times \rho_{\mathrm{L}}^2 d_{uR_i^l}^{-\alpha} d_{R_i^l v}^{-\alpha}}{\sigma^2}$$
$$\implies \gamma_{dr} \leq \gamma_{sr} \implies T_{i,j}^{l,m}(\gamma) \leq T_i^l(\gamma)$$
$$\implies T_i^l(\gamma) - T_{i,j}^{l,m}(\gamma) \geq 0. \tag{2.25}$$

Now, from (2.18) and (2.21), we have

$$\begin{aligned}
\mathrm{E}_{\mathrm{eff}}^{\mathrm{i}}(l) - \mathrm{E}_{\mathrm{eff}}^{\mathrm{i,j}}(l,m) &= \frac{T_i^l(\gamma)}{\frac{\beta_k \phi_k}{T_i^l(\gamma)} \times \left(P_{\mathrm{tx}} + P_{\mathrm{ph}}(R_i^l)\right)} \\
&\quad - \frac{T_{i,j}^{l,m}(\gamma)}{\frac{\beta_k \phi_k}{T_{i,j}^{l,m}(\gamma)} \times \left(P + P_{\mathrm{ph}}(R_i^l) + P_{\mathrm{ph}}(R_j^m)\right)} \\
&= \frac{1}{\beta_k \phi_k} \times \left\{ \frac{\left(P_{\mathrm{tx}} + P_{\mathrm{ph}}(R_i^l) + P_{\mathrm{ph}}(R_j^m)\right)\left(T_i^l(\gamma)\right)^2}{\left(P_{\mathrm{tx}} + P_{\mathrm{ph}}(R_i^l) + P_{\mathrm{ph}}(R_j^m)\right)\left(P_{\mathrm{tx}} + P_{\mathrm{ph}}(R_i^l)\right)} \right. \\
&\quad \left. - \frac{\left(P_{\mathrm{tx}} + P_{\mathrm{ph}}(R_i^l)\right)\left(T_{i,j}^{l,m}(\gamma)\right)^2}{\left(P_{\mathrm{tx}} + P_{\mathrm{ph}}(R_i^l) + P_{\mathrm{ph}}(R_j^m)\right)\left(P_{\mathrm{tx}} + P_{\mathrm{ph}}(R_i^l)\right)} \right\} \\
&= \frac{1}{\beta_k \phi_k} \times \left\{ \frac{\left(P_{\mathrm{tx}} + P_{\mathrm{ph}}(R_i^l)\right)\left(\left(T_i^l(\gamma)\right)^2 - \left(T_{i,j}^{l,m}(\gamma)\right)^2\right)}{\left(P_{\mathrm{tx}} + P_{\mathrm{ph}}(R_i^l) + P_{\mathrm{ph}}(R_j^m)\right)\left(P_{\mathrm{tx}} + P_{\mathrm{ph}}(R_i^l)\right)} \right. \\
&\quad \left. + \frac{P_{\mathrm{ph}}(R_j^m)\left(T_i^l(\gamma)\right)^2}{\left(P_{\mathrm{tx}} + P_{\mathrm{ph}}(R_i^l) + P_{\mathrm{ph}}(R_j^m)\right)\left(P_{\mathrm{tx}} + P_{\mathrm{ph}}(R_i^l)\right)} \right\} \\
&\geq 0 \quad \left(\because \quad \left(T_i^l(\gamma)\right)^2 - \left(T_{i,j}^{l,m}(\gamma)\right)^2 \geq 0 \ \text{(from (2.25))} \right. \\
&\qquad \left. \text{and} \quad P_{\mathrm{ph}}(R_j^m)\left(T_i^l(\gamma)\right)^2 \geq 0 \right) \qquad (2.26) \\
&\implies \mathrm{E}_{\mathrm{eff}}^{\mathrm{i}}(l) - \mathrm{E}_{\mathrm{eff}}^{\mathrm{i,j}}(l,m) \geq 0. \qquad (2.27)
\end{aligned}$$

Therefore, we can conclude from (2.23) that the transmitted signals from u require a longer route for double reflections than for single reflection in order to reach v. As a result, due to having a longer path and substantial path loss, the achievable data rate at v for

double reflections are lower than the single reflection when utilizing a common subgroup. Hence, from (2.27), we can conclude that if a device pair is coverable by single and double reflections using a common subgroup, single reflection are more beneficial than double reflections which is quite intuitive. □

From (2.17) and (2.20), we observe that energy consumption is a function of data rate, transmit power, and phase shift power. Again, the data rate is a function of distance. Moreover, if a device pair (u, v) is visible via R_s^t using single reflection, and R_i^l and R_j^m for double reflections where R_s^t, R_i^l and R_j^m are three distinct subgroups, the result may be quite different, which is counter-intuitive. More specifically, in the following proposition, we prove that double reflections may be more energy-efficient than single reflection depending on the power consumption and the distance traveled by the signal.

Proposition 2.5.2. *Let a device pair (u, v) be visible through R_s^t using single reflection, and through R_i^l and R_j^m together via double reflections, where R_s^t, R_i^l and R_j^m are three distinct subgroups. If the following conditions hold:*

$$\text{i)}\ \ P_{\text{tx}} + P_{\text{ph}}(R_s^t) \leq P_{\text{tx}} + P_{\text{ph}}(R_i^l) + P_{\text{ph}}(R_j^m)\ \ \textit{and}$$
$$\text{ii)}\ \ \rho_{\text{L}} d_{R_s^t v} d_{u R_s^t} \geq d_{R_j^m v} d_{u R_i^l} d_{R_i^l R_j^m}$$

then double reflections are more energy-efficient than single reflection.

Proof. Here we want to prove that double reflections may be more beneficial than single reflection in some specific scenarios. In this context, $\text{E}_{\text{eff}}^{\text{s}}(t)$ for single reflection must be less than $\text{E}_{\text{eff}}^{\text{i,j}}(l, m)$ for double reflections. Therefore, from (2.18) and (2.21), we have

$$\begin{aligned} \text{E}_{\text{eff}}^{\text{i,j}}(l, m) \geq \text{E}_{\text{eff}}^{\text{s}}(t) &\iff \frac{T_{i,j}^{l,m}(\gamma)}{\text{E}_{\text{c}}^{\text{i,j}}(l, m)} \geq \frac{T_s^i(\gamma)}{\text{E}_{\text{c}}^{\text{s}}(\text{i})} \\ &\iff \frac{T_{i,j}^{l,m}(\gamma)}{T_s^i(\gamma)} \geq \frac{\text{E}_{\text{c}}^{\text{i,j}}(\text{l}, \text{m})}{\text{E}_{\text{c}}^{\text{s}}(\text{i})}. \end{aligned} \tag{2.28}$$

Now, by using $\text{E}_{\text{c}}^{\text{i,j}}(l, m)$ and $\text{E}_{\text{c}}^{\text{s}}(i)$ from (2.17) and (2.20), respectively, we obtain

$$\left(\frac{T_{i,j}^{l,m}(\gamma)}{T_s^i(\gamma)} \right)^2 \geq \frac{P_{\text{tx}} + P_{\text{ph}}(R_i^l) + P_{\text{ph}}(R_j^m)}{P_{\text{tx}} + P_{\text{ph}}(R_s^t)}. \tag{2.29}$$

From the stated condition (i), the required phase shift power for double reflections is always greater than the required phase shift power for single reflection. That is,

$$\left(P_{\text{tx}} + P_{\text{ph}}(R_s^t)\right) \leq \left(P_{\text{tx}} + P_{\text{ph}}(R_i^l) + P_{\text{ph}}(R_j^m)\right) \tag{2.30}$$

$$\iff \frac{P_{\text{tx}} + P_{\text{ph}}(R_i^l) + P_{\text{ph}}(R_j^m)}{P_{\text{tx}} + P_{\text{ph}}(R_{\text{s}}^t)} \geq 1. \tag{2.31}$$

Therefore, from (2.29) and (2.31), we can claim that

$$\begin{aligned}
&\left(\frac{T_{i,j}^{l,m}(\gamma)}{T_s^i(\gamma)}\right)^2 \geq 1 \\
&\iff T_{i,j}^{l,m}(\gamma) - T_s^t(\gamma) \geq 0 \left(\because T_{i,j}^{l,m}(\gamma) > 0 \text{ and } T_s^i(\gamma) > 0\right) \\
&\iff \frac{\begin{aligned} &P_{\text{tx}} |\mathbf{h}_{R_j^m} \times \mathbf{h}_{R_i^l R_j^m} \times \mathbf{h}_{uR_i^l} \times e^{j(\phi_{i,l}+\phi_{j,m})}|^2 \\ &\qquad \times \rho_{\text{L}}^3 d_{R_j^m v}^{-\alpha} d_{uR_i^l}^{-\alpha} d_{R_i^l R_j^m}^{-\alpha} \end{aligned}}{\sigma_0^2} \\
&\qquad - \frac{P_{\text{tx}} |\mathbf{h}_{R_s^t v} \times \mathbf{h}_{uR_i^t} \times e^{j\phi_{s,t}}|^2 d_{R_s^t v}^{-\alpha} d_{uR_s^t}^{-\alpha} \rho_{\text{L}}^2}{\sigma_0^2} \geq 0.
\end{aligned} \tag{2.32}$$

Now, from the stated conditions (ii), we can show that

$$\begin{aligned}
&\rho_{\text{L}} d_{R_s^t v} d_{uR_s^t} \geq d_{R_j^m v} d_{uR_i^l} d_{R_i^l R_j^m} \\
&\iff \rho_L^3 d_{R_j^m v}^{-\alpha} d_{uR_i^l}^{-\alpha} d_{R_i^l R_j^m}^{-\alpha} \geq \rho_L^2 d_{R_s^t v}^{-\alpha} d_{uR_s^t}^{-\alpha}.
\end{aligned} \tag{2.33}$$

Therefore, from (2.32) and (2.33), we can claim that

$$|\mathbf{h}_{R_j^m} \times \mathbf{h}_{R_i^l R_j^m} \times \mathbf{h}_{uR_i^l} \times e^{j(\phi_{i,l}+\phi_{j,m})}|^2 \geq |\mathbf{h}_{R_s^t v} \times \mathbf{h}_{uR_s^t} \times e^{j\phi_{s,t}}|^2. \tag{2.34}$$

That is, the power gain at the receiver end is greater in double reflections than in single reflection. Moreover, from (2.34), we can conclude that if a device pair is visible via single and double reflection and it satisfies the stated conditions, then double reflection is more beneficial than single reflection. □

In the following subsection, we illustrate with an example, the situation where double reflections are more energy-efficient than single reflection.

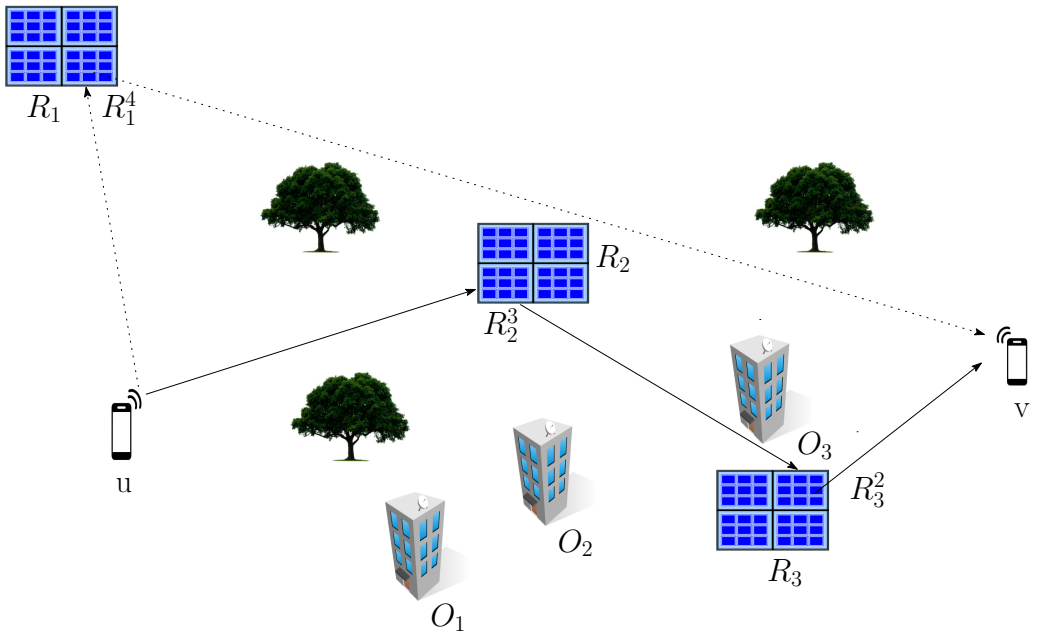

Figure 2.4: Double reflections may be more beneficial than single reflection.

2.5.2.4 Illustrative Example where Double Reflection is more Beneficial than Single Reflection

In Fig. 2.4, u wants to communicate with v and two possible paths are available in between them, one is via R_1^4 using single reflection, and another one via R_2^3 and R_3^2 together using double reflections. Since R_1^4 is located far away from u and v, the achieved data rate at v is not very high. Moreover, due to the close proximity of u to R_2^3, R_2^3 to R_3^2, and R_3^2 to v the achievable data rate at v is more than the achievable data rate via the path using R_1^4, which follows from Proposition 2.5.2. Therefore, in this case, the second path is more energy-efficient. As a result, u selects the path via R_2^3 and R_3^2 for complete information transfer using double reflections.

2.6 Simulation Results

Thereafter in this section, we conduct comprehensive simulations to verify the effectiveness of our suggested approach and compare it with the closest available methods [37], [40] and [48]. Here we consider a two-dimensional square area of 400×400 m^2 [36]. Furthermore, we assume that two devices can communicate only if they lie within a specific coverage radius. Moreover, we anticipate that D2D communication will occur at a frequency of 60 GHz with a 500 MHz bandwidth [68]. The transmit power P is 30 dBm and $P_{\text{phase}} = 5$

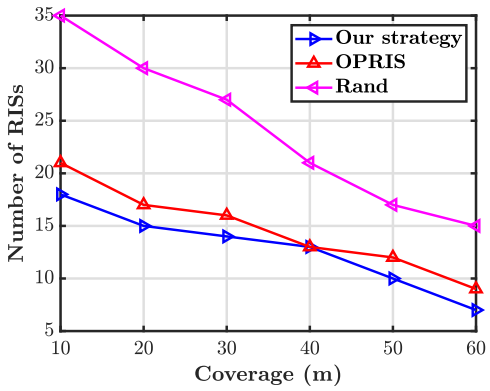

Figure 2.5: Impact of coverage area on number of RISs.

dBm [69]. Here, we consider a Rician fading scenario [70], incorporating a Rician factor $K = 10$ dB. The default parameters taken into account are: path loss at one-meter distance $\rho_L = 10^{-3.53}$ [71], the path loss exponent is $\alpha = 2$ and the packet length is 1000 bits. Below we briefly describe the existing methods [37], [40] and [48] with which we have compared our proposed approach.

- OPRIS [37]: This work investigates the optimal placement of RISs for a single reflected scenario. In other words, it does not allow double reflections.
- Rand [40]: In this work, the RISs are placed arbitrarily in the geographically separated locations. Here too, the authors investigate the aspect of single reflection.
- DAR [48]: This work proposes an approach to connect a particular device pair by considering the aspect of double reflections. However, it does not include the feature of RIS grouping in the communication scenarios.

Fig. 2.5 shows how many RISs are needed to cover the largest possible region as a function of coverage radius. Here, we consider three different scenarios with three different RIS placement strategies. Consequently, we look at the number of RISs used in these scenarios to get the maximum coverage. Note that, with increasing coverage radius, the number of RISs used exhibits a non-increasing trend, which is quite intuitive. We observe that our strategy outperforms both `OPRIS` and `Rand`. This is because, there are many device pairs which are visible via double reflections, but for a single reflection, we need to install a new RIS. As a result, our strategy brings down the requirement of RISs in comparison to `OPRIS` and `Rand`, as they did not allow double reflections.

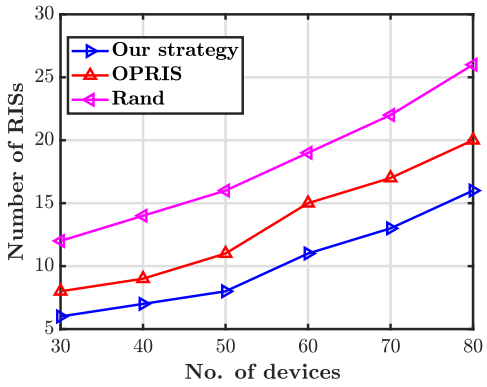

Figure 2.6: Impact of number of devices on number of RISs.

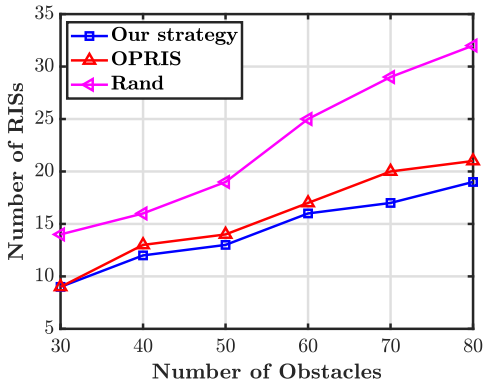

Figure 2.7: Impact of number of obstacles on number of RISs.

Fig. 2.6 and Fig. 2.7 show how many RISs are needed to cover the largest possible region as a function of device density and number of obstacles, respectively. Accordingly, we look at the number of RISs used in three different scenarios to get the maximum coverage. We find that, for a given situation, the number of RISs increases with the growing density of devices (obstacles), which is quite intuitive. Here too, we observed that our strategy outperforms `OPRIS` and `Rand` for the same reason as stated earlier.

Fig. 2.8 demonstrates the impact of obstacle density on the sum throughput, where the sum throughput is calculated by using (2.1) and (2.2). Here, we observe that, for a particular scenario, the sum throughput shows a decreasing trend with an increasing number of obstacles. Moreover, our proposed strategy outperforms `OPRIS` and `Rand` in terms of sum throughput. This is because in our proposed strategy, we can serve more blind pairs due to considering the double reflections.

From Fig. 2.9, we observe that, in relation to the growing obstacles, the number of

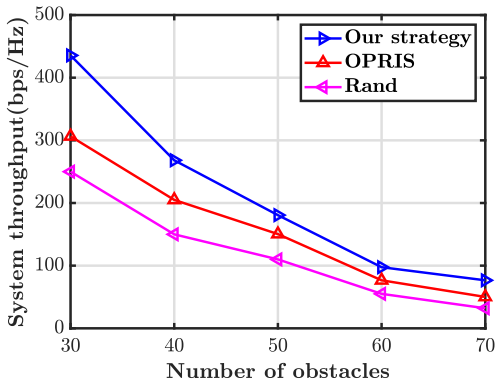

Figure 2.8: Impact of the number of obstacles on sum throughput.

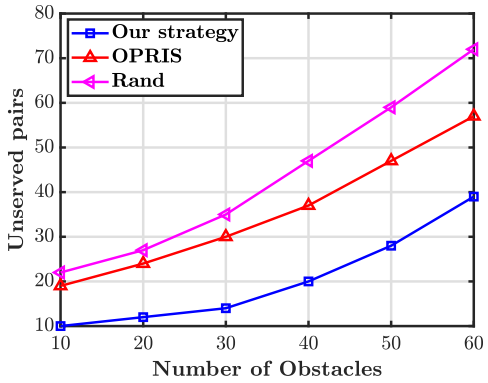

Figure 2.9: Impact of the number of obstacles on Unserved pairs.

unserved device pairs exhibits an increasing trend. As the number of obstacles increases, the number of blind pairs also increases. As a result, the likelihood of having more blind pairs that are not served rises. Note that using double reflections, sometimes we can serve some blind pairs that are not possible to serve by single reflection even after deploying more RISs. As a result, our proposed strategy outperforms the performance of `OPRIS` and `Rand` in terms of number of unserved blind pairs.

The significance of RIS grouping on the achievable throughput and energy-efficiency, as a function of the number of elements in a RIS, is shown in Fig. 2.10. In particular, we examine the effects of distinguishing between a grouping-based scenario (GBS) and a non-grouping-based scenario (nGBS). In nGBS, the entire RIS is used for information transfer, whereas in GBS, the RIS is divided into four equal-sized groups, and only one of them is used for information transfer. Here, we observe that in both cases, achievable throughput follows an increasing trend with the growing number of elements. This is

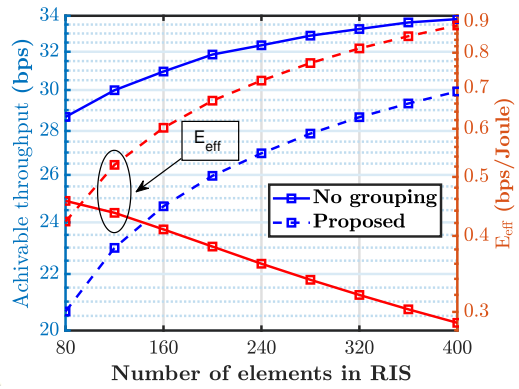

Figure 2.10: Impact of the number of elements in a group on energy consumption.

because a growing number of patches support better throughput. As a result, nGBS provides higher data throughput as compared to GBS. This makes sense because, in contrast to GBS, nGBS makes use of the entire RIS, whereas GBS only uses a portion of the RIS's total number of patches. We also observe from (2.10) that, in relation to the rising number of elements in a RIS, the E_{eff} for nGBS is in a decreasing trend whereas it is in an increasing trend for GBS. This is because the required phase shift power in nGBS is proportional to the number of patches of an RIS, whereas a common phase shift power is used for GBS. As a result, usage of the GBS leads to better E_{eff} performance.

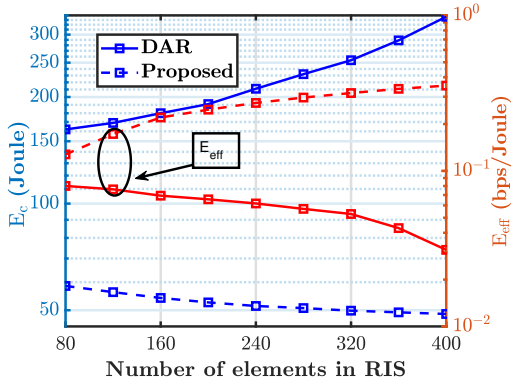

Figure 2.11: Impact of the number of elements in a group on energy-efficiency.

In Fig. 2.11, a comparison of energy consumption (E_c) and energy-efficiency (E_{eff}) between the proposed strategy and the existing benchmark `DAR`, are shown. Here, as mentioned in 2.10, we partitioned a RIS into four equal parts and chose one of them to facilitate communication. Additionally, we consider a scenario, where both strategies use double reflections. In 2.11, we observed that in relation to the growing number of patches of

an RIS, $E_c(E_{eff})$ exhibits an increasing (decreasing) trend in DAR, and $E_c(E_{eff})$ exhibits a decreasing (increasing) trend in our proposed strategy. This improvement is because of the fact that the required phase shift power in DAR is proportional to the number of patches of an RIS as it uses the entire RIS, whereas a particular group is being used, and a common phase shift power is used in our proposed strategy.

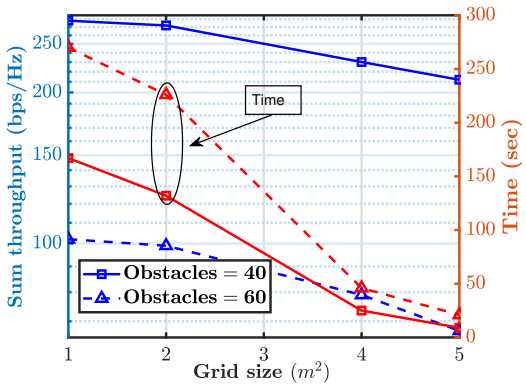

Figure 2.12: Performance trade-off investigation: different obstacles.

Fig. 2.12 shows the impact of grid size on both sum throughput and computation time for different numbers of obstacles. Here, grid size a signifies that the service area is discretized as $a \times a$ squares. Here, we observe that as the grid size increases, both the sum throughput and the computation time exhibit a decreasing trend. As stated in the system model, we assumed that an obstacle occupies the entire grid, even if it just occupies a portion of it. Consequently, the total number of LoS links decreases significantly, leading to a downward trend in the sum throughput. On the other hand, as the size of the grid increases, the overall computation time decreases, as computation time is a function of the number of grids. Additionally, the performance of 40 obstacles is superior to that of 60 obstacles, which is also quite intuitive.

Fig. 2.13 illustrates the importance of double and triple reflections on the achievable throughput and energy efficiency E_{eff} as a function of the number of obstacles. The sum throughput exhibits a decreasing trend with the number of obstacles for both double and triple reflections, which is quite intuitive. It can be observed that the sum throughput for triple reflection is only marginally higher than double reflections. Moreover, this difference is more towards the higher number of obstacles, i.e., for the extremely obstructed environments. On the other hand, the energy-efficiency is not as good as that of double reflections. It can be observed that the improvement in sum throughput is significant when

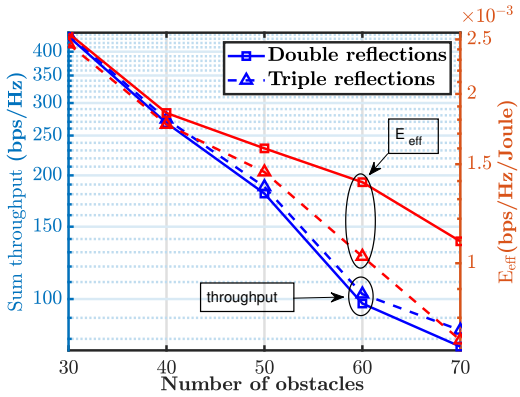

Figure 2.13: Performance trade-off investigation: double and triple reflections.

we take into account the second reflections. However, due to the inclusion of the third reflections, the improvement in sum throughput is found to be only marginal. Moreover, this marginal improvement in sum throughput is obtained at the cost of significantly more energy consumption. This, in turn, reduces the energy efficiency for triple reflections. This further justifies the widespread assumption of ignoring the triple and higher order reflections in the literature.

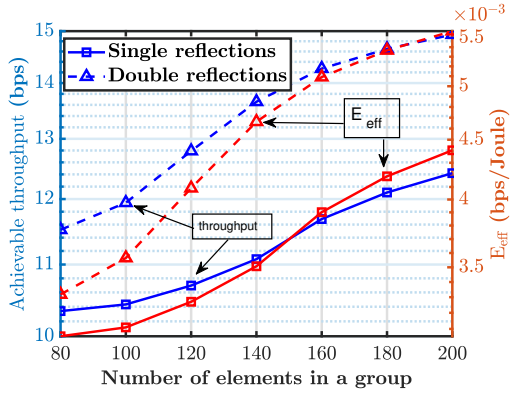

Figure 2.14: Performance trade-off investigation of Proposition 1.

Comparisons of the achievable throughput and energy-efficiency for single and double reflections using our proposed approach are presented in Fig. 2.14. According to Proposition 2.5.1, double reflection is more energy-efficient than single reflection under certain conditions. In support of this, we consider a fixed $S - D$ pair that is coverable by both single and double reflections, and it satisfies the conditions of Proposition 2.5.1. Here, we observe that, in relation to the growing number of elements of a group, the achievable throughput and energy-efficiency for both single and double reflections exhibit an increasing trend and

saturate after a certain number of elements of a group. Here, our proposed strategy for double reflection outperforms the performance of single reflection in terms of achievable throughput and energy-efficiency, which is quite counter-intuitive. The reason for this is the longer distance between S and RIS, as well as RIS and D, for single reflection. Whereas, for double reflection, the $S - D$ pair is served by multiple short hops using two consecutive RISs.

2.7 Conclusion

In this chapter, we proposed a novel RIS deployment strategy in the double RIS-assisted D2D wireless communication scenario, which takes into account the elements grouping of an RIS. The proposed strategy prevents resource wastage by deploying the RIS strategically taking care of both single and double reflections and partitioning the RIS into non-overlapping sub-groups. Subsequently, we proposed an energy-efficient group selection strategy for a device pair to complete their communication. It is interesting to note that under some conditions, double reflections are more energy-efficient than single reflection. The simulation results show that a significant reduction in the number of RISs is achievable by allowing double reflections. In addition, double reflections provide more energy efficient communication, and also bring down the number of unserved blind pairs in comparison to some existing benchmarks.

Chapter 3

Double-RIS Assisted Multihop Routing Scheme for D2D Communication[1]

3.1 Introduction

RIS is a promising solution for enhancing the performance of mmWave D2D multi-hop wireless communication networks. In the previous chapter, we discussed a novel RIS deployment strategy. In this chapter, we present a double-RIS-assisted multihop routing scheme for a D2D communication network, considering that the RISs are already strategically placed in the environment. In particular, the plan relies on the nearby users and RISs that are already operational. This work focuses on utilizing the current intermediate users (IUs), which can serve as relays, in addition to the RISs. Thus, it is possible to cut down on the density of RIS deployment in the environment, preventing resource waste. However, relying exclusively on the IUs would require total reliance on their availability for relaying, which would make it impossible to guarantee the reliability of delay-constrained information transfer. Additionally, the IUs are thought to be able to harvest energy, so they don't waste their own energy volunteering to serve as relays for other users. Finally, helpful insights regarding the scheme design are also provided, where we characterize the maximum acceptable delay at each hop under various setups. Numerical results show the advantage of the suggested scheme over some existing approaches.

[1]This chapter is based on the following publication:
L. Sau, P. Mukherjee, and S. C. Ghosh, "DRAMS: Double-RIS assisted multihop routing scheme for device-to-device communication", **Computer Communications (Elsevier)**, Vol. 220, pp.52-63, Apr. 2024.

3.2 Chapter Organization

The rest of this chapter is organized as follows: Section 3.3 describes the system model and the problem formulation, Section 3.4 presents the proposed strategy, and Section 3.5 analyses the delay associated with information transfer. Numerical results are presented in Section 3.6 and finally, Section 3.7 concludes the work.

3.3 System Model

3.3.1 Network topology

A wireless network topology is considered, which consists of a source S, N_R RISs $R_1, R_2, \ldots, R_{N_R}$, N_I IUs $U_1, U_2, \cdots, U_{N_I}$, and destination D[2], respectively. Each transmitter, i.e., the source S or an IU U_j $j = 1, \cdots, N_I$ transmits with the same fixed power P_{tx} and the RIS R_i $i = 1, \cdots, N_R$ has N_i reflecting elements, respectively. Table 2 shows the list of variables used, along with the descriptions. In general, each RIS is effectively controlled to adjust both the amplitude and phase of the incident waveform. However, for the sake of simplicity and mathematical tractability, the amplitude factor is set to unity and it is only the phase that is tuned or optimized [72, 73]. Moreover, we assume that no direct LoS exists between S and D and that S relies on the IUs and/or RISs to communicate to D. Each IU U_j communicates with its own associated receiver and acts as a DF relay for other users, when idle. Lastly, each IU is equipped with a buffer of sufficient capacity and all the D2D pairs follow time-slotted synchronous communication [74], with slot duration T_s. An example of this topology is presented in Fig. 3.1, for $N_R = 3$ and $N_I = 4$, respectively, where S can communicate with D via IUs and/or RISs.

3.3.2 User Traffic Characterization

It is noted that in a typical wireless communication scenario, data generally arrives in bursts to the users. As a result, the IUs $U_1, U_2, \cdots, U_{N_I}$ in this work are characterized by exponentially distributed OFF and ON period lengths, with means λ_k and μ_k, respectively. Without any loss of generality, T_s is assumed to be small in comparison with μ_k and λ_k [75], which prevents $U_k \; \forall \; k = 1, \cdots, N_I$ changing its status multiple times within a single T_s.

[2]Network topology with multiple $S - D$ pairs can be also considered, which is left for future work.

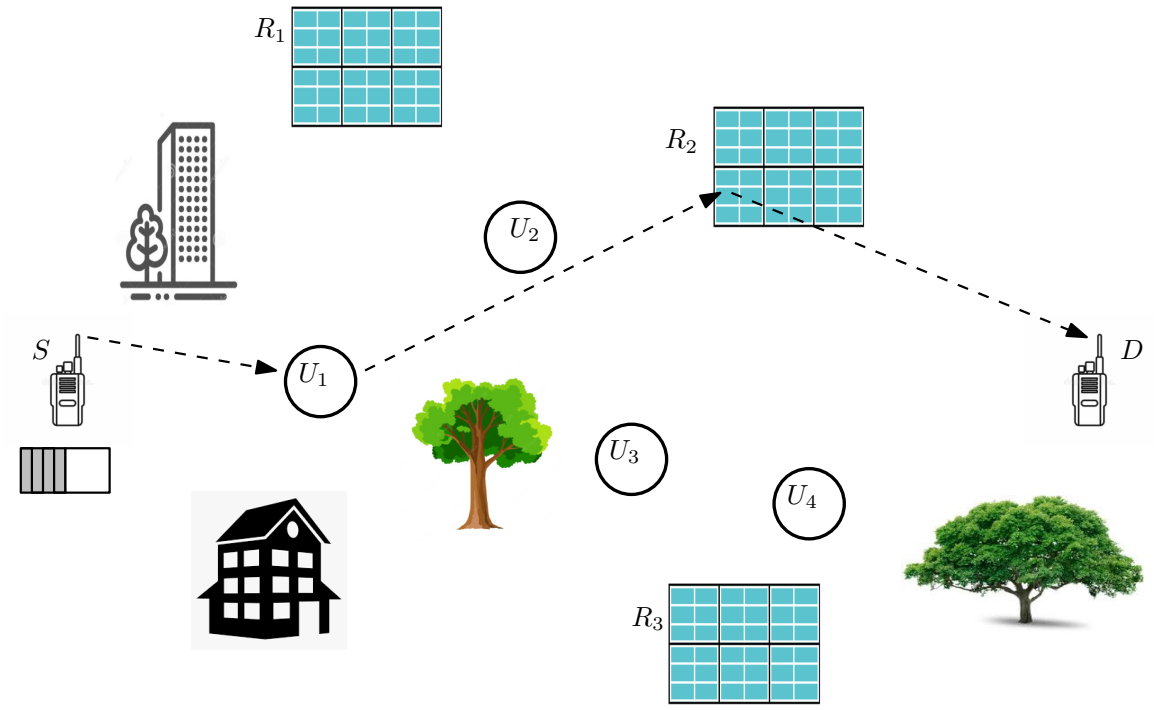

Figure 3.1: The proposed RIS-based multihop network architecture.

Thus, the state 0 and 1 represents the IU being idle and busy, respectively and the probability $p_{ij}\ \forall\ i,j \in \{0,1\}$ denotes the transition probability of the IU currently being in state i and it changes to state j in the next time slot. Accordingly, the IU activities are characterized by a discrete-time Markov chain (DTMC) with the state transition probabilities [75, 76]:

$$\mathrm{p}_{10} = \int_0^{T_s} \frac{1}{\mu_k} e^{-a/\mu_k} da = 1 - e^{-T_s/\mu_k},\ \mathrm{p}_{11} = 1 - \mathrm{p}_{10}, \tag{3.1}$$

$$\mathrm{p}_{01} = \int_0^{T_s} \frac{1}{\lambda_k} e^{-b/\lambda_k} db = 1 - e^{-T_s/\lambda_k},\ \text{and}\ \mathrm{p}_{00} = 1 - \mathrm{p}_{01}.$$

Accordingly the state transition matrix $\mathcal{P}$ is:

$$\mathcal{P} = \begin{bmatrix} \mathrm{p}_{00} & \mathrm{p}_{01} \\ \mathrm{p}_{10} & \mathrm{p}_{11} \end{bmatrix} = \begin{bmatrix} e^{-T_s/\lambda_k} & 1 - e^{-T_s/\lambda_k} \\ 1 - e^{-T_s/\mu_k} & e^{-T_s/\mu_k} \end{bmatrix}. \tag{3.2}$$

3.3.3 Channel Model

Depending on the availability of the IUs, it is possible to connect S to D with or without taking the help of any RIS. When RIS is being used, the signal from an arbitrary U_i can

reach U_{i+1} via any of the following paths: (i) primary reflection, i.e., the signal from U_i reaches U_{i+1} by using only one RIS and (ii) secondary reflection, i.e., there exist two consecutive RISs via which the signal from U_i reaches U_{i+1}. In this work, due to large effective path loss, we neglect the aspect of triple or higher order reflections [47]. However, the secondary reflection are not negligible in practice, especially in urban environments, where the RISs are not deployed too far from each other. This problem can be modeled as a graph, where the devices represent the vertices. These vertices have an edge in between if and only if the corresponding nodes can communicate, i.e., they reside within some threshold distance. We assume that the wireless links suffer from both large-scale path loss effects and small-scale block fading, and the modulus of the channel follows the Rician distribution. The channels $S \rightarrow U_j$, $U_j \rightarrow D$, and $U_j \rightarrow U_k \; \forall \; j,k = 1,\cdots,N_I$ exhibit small-scale fading and their corresponding path-loss factors are $\rho_{\mathrm{L}}^{1/2} d_{SU_j}^{-\alpha/2}$, $\rho_{\mathrm{L}}^{1/2} d_{U_jD}^{-\alpha/2}$, and $\rho_{\mathrm{L}}^{1/2} d_{U_jU_k}^{-\alpha/2}$, respectively, where ρ_{L} is the pathloss at one meter distance, α is the path-loss exponent and d_{mn} denotes the distance between m and n.

Let $\boldsymbol{h}_{S/UR_i} \in \mathbb{C}^{M\times 1}$, $\boldsymbol{h}_{R_iR_j} \in \mathbb{C}^{M\times M}$, and $\boldsymbol{h}_{R_jD/U} \in \mathbb{C}^{1\times M}$ denote the channel matrix from S or IU to i-th RIS, i-th to j-th RIS $(i \neq j)$, and j-th RIS to an IU or D, respectively. In addition, the phase-shift matrix of the i-th RIS is denoted by $\boldsymbol{\Phi}_i = \mathrm{diag}(\phi_1,\cdots,\phi_M) \in \mathbb{C}^{M\times M}$, i.e., a diagonal matrix accounting for the response of the RIS elements, where $\phi_n = \exp(j\theta_n)$, $n = 1,\cdots,M$ and $\theta_n \in [0, 2\pi]$ is the phase shift applied by the RIS elements [77]. Lastly, the total path-loss for each of these channel matrix is the product of the path-loss of each point-to-point link [47]. Accordingly, the effective channel gain in case of single and double reflection is $\boldsymbol{h}_{R_iD/U}\boldsymbol{\Phi}_i\boldsymbol{h}_{S/UR_i}$ and $\boldsymbol{h}_{R_jD/U}\boldsymbol{\Phi}_j\boldsymbol{h}_{R_iR_j}\boldsymbol{\Phi}_i\boldsymbol{h}_{S/UR_i}$, respectively.

3.3.4 Energy Harvesting Model

As stated earlier, it is for an idle IU $U_j \; \forall \; j = 1,\cdots,N_I$ to decide whether to act as a relay or not. Moreover, there must be some 'reward' for the same or else, there is no point for the user to waste its own energy in transferring data packets from S to D. In this context, we assume that each U_j is equipped with an EH unit, which can extract DC power from the received electromagnetic waves [78]. If an idle U_j agrees to act as a relay, we incentivize it in the form of a reward, i.e., it is able to harvest energy from the incoming signal and use the same to transfer the received information. For a transmission power P_{tx}, the power harvested at IU is [79]

$$P_{\text{harv}} = \frac{M_h(1 - e^{-aP_{\text{tx}}\rho_{\text{L}}d^{-\alpha}|h|^2})}{1 + e^{-a(P_{\text{tx}}\rho_{\text{L}}d^{-\alpha}|h|^2 - b)}}, \tag{3.3}$$

where M_h is the maximum harvested power corresponding to the saturated EH circuit, h is the complex channel gain, d is the associated distance, and finally, a and b are the respective circuit parameters.

3.3.5 Delay-constrained Transmission

Shannon capacity is the largest data rate at which the information can be transmitted with an arbitrarily small error probability, provided that the number of channel uses is infinitely large [80]. However, for applications such as delay-constrained scenarios, the number of channel uses cannot be very large. As a result, the error probability will not be arbitrarily small and it needs reconsideration. In such scenarios, the maximum instantaneous achievable data rate $T(\gamma)$ is approximated as [81]

$$T(\gamma) = \log_2(1+\gamma) - \frac{Q^{-1}(\varepsilon)}{\ln 2}\sqrt{\frac{\gamma^2 + 2\gamma}{M_b(1+\gamma)^2}}, \tag{3.4}$$

where γ is SNR, $\varepsilon \in [0, 1]$ is the error probability, M_b is the number of channel uses, and $Q(x) = \frac{1}{\sqrt{2\pi}}\int_x^\infty e^{-\frac{t^2}{2}}dt$ is the Gaussian Q function. For delay unconstrained scenarios, i.e., when $M_b \to \infty$, we have $T(\gamma) \to \log_2(1+\gamma)$. When a RIS is selected to pass the signal due to unavailability of idle IUs, we consider this achievable data rate R while searching for an IU in the next hop.

3.4 DRAMS: The Proposed Strategy

This section discusses the proposed multihop framework DRAMS in detail, where the novelty lies in the joint IU traffic characteristics and double-RIS assisted dynamic framework. As we are considering a delay-constrained scenario, the data from S must reach D within time T_d in this set-up. Here we assume that a device cannot communicate with another beyond a distance r and S has α packets of information to send D with φ bits in each. Pictorially, we connect the location of S and D by a virtual straight line and consider it to be the x-axis. Accordingly, we consider another virtual line as the y-axis at S, which is

perpendicular to the x-axis. We intend to connect S to D via some IUs/RISs. Firstly, we scan the right half circle[3] of radius r at S to identify the idle IUs. Secondly, after the idle IU identification, we decide on the appropriate modulation scheme and its corresponding energy requirement. Thirdly, in case of multiple idle IU availability, we chose the appropriate IU based on the LRD from D and the acceptable delay constraint. Two IUs are said to be directly connected if there exists a LoS in between them and they reside within a distance r of each other. Else, we identify suitable RISs for this purpose. Finally, we also provide an illustrative example of the proposed DRAMS.

3.4.1 Identification of the Idle IUs

We identify the idle IUs by beacon transmission within a radius r, in the direction of D [82], which can act as potential DF relays. We define $\Omega = \{U_1, \cdots, U_\epsilon\}$ as the set of all U_js that are present in the right half circle of radius r centred at S, where $\epsilon < N_I$ and $U_k = 1/0$, depending on whether the k^{th} IU is busy/idle. As we intend to reduce the LRD in each hop, we consider only the right half circle for identifying the potential relays. Accordingly, we define the set of idle/busy IUs as

$$\Omega_I = \{u_I^1, u_I^2, \cdots, u_I^{\epsilon_I}\} \text{ and } \Omega_B = \{u_B^1, u_B^2, \cdots, u_B^{\epsilon_B}\}, \tag{3.5}$$

where $\epsilon_I + \epsilon_B = \epsilon$ denotes the total number of IUs in the concerned region. On the basis of the traffic characteristics of a particular idle (busy) IU, we estimate the time for which it continues to remain idle (busy) given that it is currently idle (busy).

Definition 6. *Duration of Idleness (DoI) ν_I: It is the time duration during which a particular IU is estimated to be idle, given that it is currently idle.*

From the transition probability matrix (3.2), we know that the p_{00} corresponding to the idle IU U_k is $p_{00} = e^{-T_s/\lambda_k}$. As we are considering exponentially distributed idle and busy periods, due to the memoryless property [83], we obtain ν_I^k, i.e., ν_I for the IU U_k, as follows. For an acceptable error threshold δ, we desire to have

[3]It is to be noted that in our proposed framework, we search for appropriate IU/RIS in the right half circle. The reason for this is attributed to the fact that we have assumed to have D in the right-hand side of S. However, if D happens to be on the left-hand side, the framework still works and it is just that we then search for appropriate IU/RIS in the left-hand circle at each hop. By generalizing this, it can be said that we search for IU/RIS in the direction of D from S.

$$\mathrm{p}_{00}^{\nu_I^k} \geq 1-\delta \implies \nu_I^k \leq \frac{\lambda_k}{T_s} \ln\left(\frac{1}{1-\delta}\right). \tag{3.6}$$

Since we are interested in considering the maximum time for which an IU is expected to be idle for a given δ, we consider $\nu_I^k = \frac{\lambda_k}{T_s} \ln\left(\frac{1}{1-\delta}\right)$. Hence, corresponding to Ω_I, we have φ_I, where $\varphi_I = \{\nu_I^1, \nu_I^2, \cdots, \nu_I^{\epsilon_I}\}$. Similarly, we define a metric 'Duration of Busyness' (DoB).

Definition 7. *DoB ν_B: It is the time duration during which a particular IU is estimated to be busy, given that it is currently busy.*

By considering $\mathrm{p}_{11} = e^{-T_s/\mu_k}$ from (3.2) and adopting a similar procedure as DoI, the DoB ν_B^k, i.e., ν_B for U_k, is obtained as

$$\nu_B^k = \frac{\mu_k}{T_s} \ln\left(\frac{1}{1-\delta}\right). \tag{3.7}$$

Hence, corresponding to Ω_B, we obtain $\varphi_B = \{\nu_B^1, \nu_B^2, \cdots, \nu_B^{\epsilon_B}\}$.

3.4.2 Choosing Appropriate Modulation at the IUs

The objective of this work is not only to transfer data from S to D, but also with minimum energy consumption. In the process of doing so, we introduce the aspect of rate adaptation at the IUs. Moreover, the idle IUs employ rate adaptation if and only if there is a direct connection between the users and there is no RIS used to connect them[4]. The IUs adopt a modulation scheme m_q from the set $\mathbb{M} = \{m_1, m_2, \cdots, m_{|\mathbb{M}|}\}$, which corresponds to a data rate $D_q = \log_2(m_q)\ \forall\ q = 1, \cdots, |\mathbb{M}|$. The choice of m_q depends on the wireless channel between the two consecutive IUs, where the complex channel gain h, bit error rate (BER) P_b, constellation size m_q, and the received power $P\rho_{\mathrm{L}} d^{-\alpha}|h|^2$ are related as [84]:

$$P_b = c_1 \exp\left(\frac{-c_2 P \rho_{\mathrm{L}} d^{-\alpha}|h|^2}{\sigma^2(m_q^{c_3} - c_4)}\right). \tag{3.8}$$

Here σ^2 is the noise power, and $c_1, \cdots, c_4$ are modulation-specific constants, respectively. The above equation explains the relation between the chosen modulation scheme and

[4]The aspect of RIS-enabled rate adaptation is not considered here, as this is beyond the scope of the current work. However, the proposed framework can also be extended to such scenarios with suitable adjustments like optimal RIS beam alignment [47].

the application-specific acceptable BER. By considering a transmission power P and a modulation scheme m_q, the time required for complete transfer of α_k information packets of the IU U_k with φ_k bits in each is $\tau_{\text{req}}(k,q) = \left\lceil \frac{\alpha_k \varphi_k}{D_q} \right\rceil$ slots, where $\left\lceil \cdot \right\rceil$ denotes the ceiling function. Accordingly, if P_{proc} is the processing power, the corresponding energy required for complete information transfer is characterized as

$$E_{\text{req}}(k,q) = (P_{\text{tx}} + P_{\text{proc}})\tau_{\text{req}}(k,q)T_s, \tag{3.9}$$

which is not a fixed quantity, but a function of the chosen constellation size.

3.4.3 Selection of the Appropriate IUs

Till now, we have identified the pool of busy and idle IUs within the radius r towards D. Now, among the idle ones, we identify the ones that can be leveraged upon to act as DF relays in forwarding the information from S to D. Towards this direction, we define the set $\mathcal{Y}_{k,q}$ as

$$\mathcal{Y}_{k,q} = \left\{ \tau_{\text{req}}(k,q) : U_k \in \Omega_I,\ m_q \in \mathbb{M},\ \tau_{\text{req}}(k,q) \leq \nu_I^k \right\}. \tag{3.10}$$

Specifically, $\mathcal{Y}_{k,q}$ is the set of those IU $U_k \in \Omega_I$ and their associated modulation scheme $m_q \in \mathbb{M}$ such that they satisfy what we define as the *availability constraint* $\tau_{\text{req}}(k,q) \leq \nu_I^k$, i.e., the required time for complete information transfer from U_k is less than its estimated idle time ν_I^k. Accordingly, S chooses the appropriate IU U_{k^*} along with its modulation scheme m_{q^*} as

$$(k^*, q^*) = \underset{k,q}{\operatorname{argmin}}\, \mathcal{Y}_{k,q}. \tag{3.11}$$

Note that the computational complexity of this entire process is $|\Omega_I| \times |\mathbb{M}|$. However, at times we have $\mathcal{Y}_{k,q}$ to be a null set as $\tau_{\text{req}}(k,q) > \nu_I^k(U_k)\ \forall\ U_k \in \Omega_I$, i.e., DoI corresponding to all the elements of Ω_I is less than the time required by U_k for continuous complete information transfer by using a constellation of size m_q. As it is necessary to complete the entire information transfer in a single phase, S decides to avoid transmission and waits for an interval of η_w slots with the hope that some $U_k \in \Omega_B$ may become idle in the near future. In the following subsection, we derive the analytical expression for the quantity η_w.

3.4.3.1 Calculation of η_w

In such scenarios, S identifies the pool of busy IUs in the right half circle of radius r, i.e., Ω_B from (3.5). Accordingly, it estimates the time interval of $\eta_{I,n}$ slots after which $U_n \in \Omega_B$ will become idle, i.e., we have $U_n \in \Omega_I$ after $\eta_{I,n}$ slots. This can be effectively modeled as a geometric distribution [83], where we map the event of U_n being idle and busy as success and failure, respectively. Therefore, given that $U_n \in \Omega_B$, we are interested in finding out the number of trial required till the first success, which in this case, is $\eta_{I,n}$. From the transition probability matrix $\mathcal{P}$ in (3.2), we obtain the probability of success in the $\eta_{I,n}$-th slot as $\mathrm{p}_{11}^{\eta_{I,n}-1}\mathrm{p}_{10}$, which needs to be greater than an acceptable threshold probability p_{th}, i.e.,

$$\begin{aligned} &\mathrm{p}_{11}^{\eta_{I,n}-1}\mathrm{p}_{10} \geq p_{\text{th}} \\ &\implies \left(e^{-T_s/\mu_k}\right)^{\eta_{I,n}-1}\left(1-e^{-T_s/\mu_k}\right) \geq p_{\text{th}}, \end{aligned} \tag{3.12}$$

which after some trivial algebraic manipulations yield

$$\eta_{I,n} \leq \frac{\mu_k}{T_s} \ln\left(\left(\frac{1-e^{-T_s/\mu_k}}{p_{\text{th}}}\right)^{+}\right) + 1, \tag{3.13}$$

where we define $x^{+} = \max(x,1)$. Since we are interested in maximizing the chance of an IU availability, for a given p_{th}, we consider $\eta_{I,n} = \frac{\mu_k}{T_s} \ln\left(\left(\frac{1-e^{-T_s/\mu_k}}{p_{\text{th}}}\right)^{+}\right) + 1$. Furthermore, as this is a delay-constrained scenario, we cannot afford to wait for a significant amount of time. Hence, S chooses not to transmit for η_w slots, where

$$\eta_w = \min_{U_n \in \Omega_B} \eta_{I,n}. \tag{3.14}$$

Since S waits for η_w slots, we have the reduced delay bound $T_d^{'}$, where $T_d^{'} = T_d - \eta_w T_s$. Hence, we can say that the acceptable delay bound becomes tighter with every transmission deferral. In this context, a detailed delay analysis is provided later in Section 3.5. Now after a time interval of η_w slots, S again scans the right half circle of radius r to classify the idle IUs and accordingly, it solves (3.11) again to obtain U_{k^*} along with the appropriate modulation m_{q^*}. If even now, the solution is a null set, S proceeds with a RIS as the next hop.

Remark 4. *We adopt a cooperative framework in this work, i.e., a particular IU agrees to act as a DF relay whenever it is idle. A scenario, where an idle IU may not agree to act as a*

relay for a particular $S-D$ pair, in spite of being idle, is not considered here but left for future work.

3.4.3.2 Harvested Energy

As stated earlier, we incentivize the selected IU in terms of harvested energy, i.e., U_{k^*} harvests energy from the signal it received from S. From (3.3), when a particular constellation m_q is selected, we obtain the harvested energy at U_{k^*} as

$$E_{\text{harv}}(k^*, q^*) = \frac{M_h(1 - e^{-aP\rho_L d_{SU}^{-\alpha}|h_{SU}|^2})}{1 + e^{-a(P\rho_L d_{SU}^{-\alpha}|h_{SU}|^2 - b)}} \tau_{\text{req}}(k^*, q^*), \tag{3.15}$$

where $h_{SU} \sim \mathcal{CN}(0,1)$ is the channel gain and $d_{SU}^{-\alpha}$ is the corresponding path-loss factor. Moreover, we observe from (3.15) that the harvested energy is a function of the chosen constellation m_q. Furthermore, (3.11) chooses the IU with the best channel condition and as E_{harv} is a monotonic function of $|h_{SU}|^2$, this results in better EH performance at U_{k^*}.

This entire procedure of identifying idle IUs within radius r to act as relays is described later pictorially in Fig. 3.2. However, if only IUs are to made act as relays, then the information transfer from S to D will solely rely on the IU traffic characteristics and activities. To overcome this problem, we take help of the already strategically placed RISs in the surroundings [36, 35], which always guarantees communication in the absence of appropriate IUs. This also implies that the location of the RISs are known to all the IUs in the surroundings.

3.4.4 Identification of RIS in case of Idle IU Unavailability

In case of directly connected idle IU unavailability, S searches for a RIS within the right half circle of radius r, which reduces the LRD for the next hop. The location of the idle IU in the proximity of the RIS is known to S by the reverse path forwarding procedure [82] via the RIS, when an IU receives the beacon signal transmitted by S. In a multi-user scenario, by assuming that there are L device pairs being supported by that particular RIS and there exists an idle IU in the right half circle of radius r that satisfies the constraints as stated in (3.10), the signal-to-interference-plus-noise-ratio (SINR) corresponding to this particular device pair is

$$\gamma_{\text{sr}} = \frac{P_{\text{tx}} |\boldsymbol{h}_{R_i D/U} \boldsymbol{\Phi}_i \boldsymbol{h}_{S/UR_i}|^2 d_{R_i D/U}^{-\alpha} d_{S/UR_i}^{-\alpha} \rho_{\text{L}}^2}{\sum\limits_{\substack{l=1 \\ l \neq i}}^{L} P_{\text{tx}} \rho_{\text{L}}^2 |\boldsymbol{h}_{R_l D/U} \boldsymbol{\Phi}_l \boldsymbol{h}_{S/UR_l}|^2 d_{R_l D/U}^{-\alpha} d_{S/UR_l}^{-\alpha} + \sigma_0^2}, \tag{3.16}$$

where σ_0^2 is the variance of the circularly symmetric zero mean AWGN, the effective channel gain between S and the idle IU is $\boldsymbol{h}_{R_i D/U} \boldsymbol{\Phi}_i \boldsymbol{h}_{S/UR_i}$ and, $\rho_{\text{L}}^2 d_{R_i D/U}^{-\alpha} d_{S/UR_i}^{-\alpha}$ is the effective path-loss factor as defined in Section 3.3.3. Accordingly, the phase shift matrix of this particular RIS is optimized, such that the sum throughput of all the users being served by the RIS is maximized. Moreover, note that we are considering a delay-constrained scenario here, i.e., the data rate that we aim to maximize is obtained by replacing $\gamma = \gamma_{\text{sr}}$ in (3.4) as

$$T(\gamma_{\text{sr}}) = \log_2(1 + \gamma_{\text{sr}}) - \frac{Q^{-1}(\varepsilon)}{\ln 2} \sqrt{\frac{\gamma_{\text{sr}}^2 + 2\gamma_{\text{sr}}}{M_b (1 + \gamma_{\text{sr}})^2}}, \tag{3.17}$$

where M_b denoting the total number of channel uses, is a finite quantity and ε is the acceptable probability of error.

For the scenario of a single-user system, (3.16) reduces to

$$\gamma_{\text{sr}} = \frac{P_{\text{tx}} |\boldsymbol{h}_{R_i D/U} \boldsymbol{\Phi}_i \boldsymbol{h}_{S/UR_i}|^2 \rho_{\text{L}}^2 d_{R_i D/U}^{-\alpha} d_{S/UR_i}^{-\alpha}}{\sigma_0^2}, \tag{3.18}$$

where we have $\boldsymbol{h}_{R_i D/U} = \left[\zeta_1 e^{-j\theta_{\zeta,1}}, \cdots, \zeta_N e^{-j\theta_{\zeta,N}}\right]$, $\boldsymbol{h}_{S/UR_i} = \left[\omega_1 e^{-j\theta_{\omega,1}}, \cdots, \omega_N e^{-j\theta_{\omega,N}}\right]$, and $\boldsymbol{\Phi}_i = \text{diag}(\phi_1, \cdots, \phi_N)$ with $\phi_n = \exp(j\theta_n)$, $n = 1, \cdots, N$. Here, the optimal choice of $\boldsymbol{\Phi}_i$ which maximizes γ_{sr} is

$$\phi_n = \theta_{\zeta,n} + \theta_{\omega,n} \ \forall \ n = 1, \cdots, N \tag{3.19}$$

and accordingly, we obtain

$$\gamma_{\text{sr}}^{\text{opt}} = \frac{P_{\text{tx}} \left(\sum\limits_{i=1}^{N} \zeta_i \omega_i \right)^2 \rho_{\text{L}}^2 d_{R_i D/U}^{-\alpha} d_{S/UR_i}^{-\alpha}}{\sigma_0^2}. \tag{3.20}$$

Furthermore, the received power at the IU can be expressed as $P_{\text{tx}} |\boldsymbol{h}_{R_i D/U} \boldsymbol{\Phi}_i \boldsymbol{h}_{S/UR_i}|^2 \rho_{\text{L}}^2 d_{R_i D/U}^{-\alpha} d_{S/UR_i}^{-\alpha}$ and accordingly, the harvested power, in this case, is obtained from (3.3), i.e.,

$$P_{\text{harv}} = \frac{M_h \left(1 - e^{-aP_{\text{tx}}|\boldsymbol{h}_{R_iD/U}\boldsymbol{\Phi}_i\boldsymbol{h}_{S/UR_i}|^2\rho_{\text{L}}^2 d_{R_iD/U}^{-\alpha} d_{S/UR_i}^{-\alpha}}\right)}{1 + e^{-a\left(P_{\text{tx}}|\boldsymbol{h}_{R_iD/U}\boldsymbol{\Phi}_i\boldsymbol{h}_{S/UR_i}|^2\rho_{\text{L}}^2 d_{R_iD/U}^{-\alpha} d_{S/UR_i}^{-\alpha} - b\right)}}, \tag{3.21}$$

which can be further analytically characterized if the probability distribution function of $\boldsymbol{h}_{R_iD/U}$ and $\boldsymbol{h}_{S/UR_i}$ are known [85]. Finally, based on (3.20), the maximum harvested power at the IU for a single user system is

$$P_{\text{harv}}^{\text{opt}} = \frac{M_h \left(1 - e^{-aP_{\text{tx}}\left(\sum_{i=1}^{N}\zeta_i\omega_i\right)^2\rho_{\text{L}}^2 d_{R_iD/U}^{-\alpha} d_{S/UR_i}^{-\alpha}}\right)}{1 + e^{-a\left(P_{\text{tx}}\left(\sum_{i=1}^{N}\zeta_i\omega_i\right)^2\rho_{\text{L}}^2 d_{R_iD/U}^{-\alpha} d_{S/UR_i}^{-\alpha} - b\right)}}. \tag{3.22}$$

Remark 5. *The optimal phase shift matrix for a single-user system is obtained in* (3.19). *However, finding the same for the scenario involving an arbitrary number of users is not as straightforward as above and the said problem has been formulated as an optimization problem in [43, 47, 73].*

Note that it may happen as to there is no idle IU in the right half circle of radius r centred at the RIS, which satisfies the desired criteria as mentioned in (3.10). However, we are sure to find another RIS, as we assume that the RISs are already strategically placed in the surroundings [36]. Hence, the RIS directs the signal towards this newly found RIS in its range. Finally, if there is no idle IU in the coverage area, i.e., a right half circle of radius r, from this RIS, the communication stops. However, if an idle IU exists, the received power at this idle IU is

$$\begin{aligned} P_{\text{dr}} = {} & P_{\text{tx}}|\boldsymbol{h}_{R_jD/U}\boldsymbol{\Phi}_j\boldsymbol{h}_{R_iR_j}\boldsymbol{\Phi}_i\boldsymbol{h}_{S/UR_i}|^2 \\ & \times \rho_{\text{L}}^3 d_{R_jD/U}^{-\alpha} d_{S/UR_i}^{-\alpha} d_{R_iR_j}^{-\alpha} \end{aligned} \tag{3.23}$$

and by assuming that there are L D2D pairs being served by this RIS at this point of time, the resulting doubly reflected SINR in this case is evaluated as

$$\gamma_{\text{dr}} = \frac{\begin{aligned} & P_{\text{tx}}|\boldsymbol{h}_{R_jD/U}\boldsymbol{\Phi}_j\boldsymbol{h}_{R_iR_j}\boldsymbol{\Phi}_i\boldsymbol{h}_{S/UR_i}|^2 \\ & \times \rho_{\text{L}}^3 d_{R_jD/U}^{-\alpha} d_{S/UR_i}^{-\alpha} d_{R_iR_j}^{-\alpha} \end{aligned}}{\begin{aligned} \sum_{\substack{l=1 \\ l\neq i}}^{L} & P_{\text{tx}}|\boldsymbol{h}_{R_jD/U}\boldsymbol{\Phi}_j\boldsymbol{h}_{R_lR_j}\boldsymbol{\Phi}_l\boldsymbol{h}_{S/UR_l}|^2 \\ & \times \rho_{\text{L}}^3 d_{R_jD/U}^{-\alpha} d_{S/UR_l}^{-\alpha} d_{R_lR_j}^{-\alpha} \end{aligned} + \sigma_0^2}. \tag{3.24}$$

Our aim is to maximize $R(\gamma_{\mathrm{dr}})$, which is obtained by replacing $\gamma = \gamma_{\mathrm{dr}}$ in (3.4). As stated earlier in Remark 5, we optimize the phase shift matrix by using any of the existing available techniques. Lastly, the harvested power, in this context of a doubly RIS reflected signal, is obtained from (3.3) as

$$P_{\mathrm{harv}} = \frac{M_h(1 - e^{-aP_{\mathrm{dr}}})}{1 + e^{-a(P_{\mathrm{dr}} - b)}}, \tag{3.25}$$

where P_{dr} is the received power as defined in (3.23). Once the information reaches an idle IU in one of the hops, then the same process, as described above, is used to identify the next idle IU or the nearby RIS, until the information reaches D.

The complete process of information transfer, as described above, from S to D within a time limit of T_d is the proposed framework DRAMS and this has been pictorially presented by a concise and compact flowchart in Fig. 3.2.

The overall procedure is demonstrated by an illustrative example in Fig. 3.3, where there is no direct LoS link between S and D and the corresponding delay constraint for the complete data transfer is T_d. To select the intermediate hops (IU/RIS), we consider a semi-circle of radius r at S in the LRD direction from S to D. We observe from the figure that there are no available IUs within the half-circle C_1, which is centered at S and satisfies the conditions as stated in (3.10). Hence, S estimates the waiting time interval of η_w slots and the delay constraint T_d is accordingly updated as $T_d^{'} = T_d - \eta_w T_s$. After waiting for η_w slots, S again scans the semi-circle of radius r but still it cannot find an appropriate IU that can act as a relay. Accordingly, S does not wait any further but observes that RIS R_1, R_9 and R_{10} can act as potential reflectors for the first hop. As the reflected signal, via R_1, traverses the maximum distance in the LRD direction, R_1 is selected among the three. Since r is the coverage distance for each RIS and idle U_2, U_3 lies inside this region, (3.11) is solved over these two IUs to select U_3 as the next hop.

By adopting a similar technique, we consider a right half circle of radius r at U_3 to observe that there are no idle IUs in this region and R_3 is the only RIS that reduces the LRD from U_3 to D. Moreover, R_4 is selected to act as the next hop of this framework due to two reasons: firstly, there are no idle IUs available in the concerned region and secondly, as stated earlier, double reflections are non-negligible in practice. As U_5 covers the LRD towards D and three consecutive RIS selection results in significant signal degradation [47], U_5 is chosen to act as the next relay node. In a similar logic, U_7 and U_9 are selected to act as the corresponding hops of the proposed framework. Therefore, the signal from S reaches D within a time limit of T_d by using the path $S, R_1, U_3, R_3, R_4, U_5, U_7, U_9, D$.

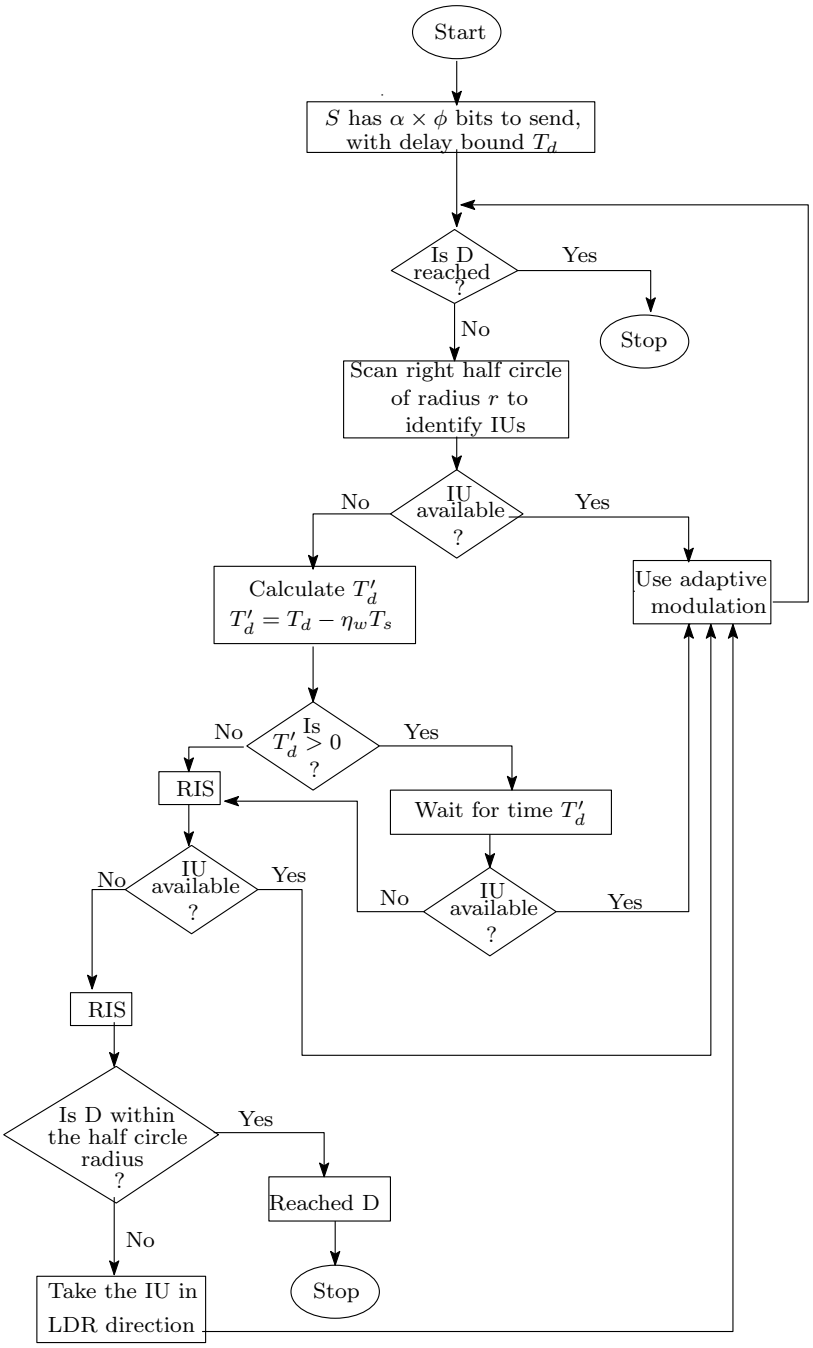

Figure 3.2: Flowchart of the proposed strategy.

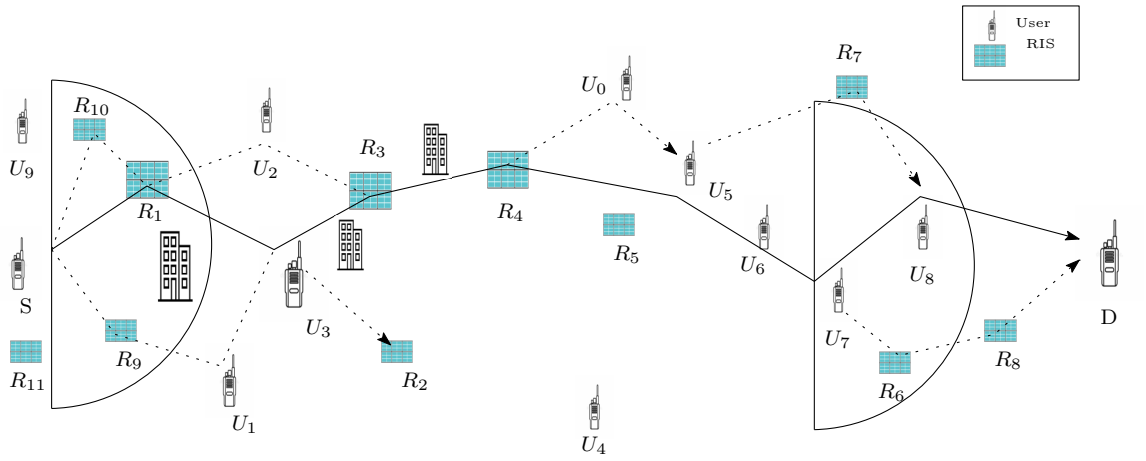

Figure 3.3: Illustrative Example

3.5 Delay Analysis

As stated earlier in Section III-C, here we investigate DRAMS in terms of the delay for information transfer from S to D. Based on the choice of IUs and RISs as hops of this framework, we can have the following scenarios: (i) only IUs (both busy and idle) and (ii) both IUs and RISs are being used. Now we look at all the scenarios in detail.

3.5.1 Only IUs

Here we observe that the information packets from S reach D through a finite number of busy/idle IUs and no RIS is being used in this scenario. On arrival of information, S immediately locates an idle IU U_1 within the right half circle of radius r, which is also in the LRD direction and can act as a DF relay. However, if S cannot locate an idle IU in the desired region that satisfies the constraints from (3.10), before proceeding with a RIS, S waits for a finite amount of time to identify the next node in the proposed framework. We assume that there must be an IU that meets the constraints in (3.10) within this waiting time. In this context, we estimate the maximum acceptable waiting time T_{d_i} at IU U_i, such that the overall delay constraint of time T_d is not violated.

Let l be the Euclidean distance from S to D and any IU can transmit to a maximum distance r. Hence, the minimum number of hops required to send a data packet from S to D is $\Psi = \left\lceil \frac{l}{r} \right\rceil$. Therefore, the maximum acceptable delay and actual delay at S is $T_{d_0} = \frac{T_d}{\Psi}$ and t_0, respectively. In case the actual waiting time t_i at U_i is less than T_{d_i}, we propose that

the leftover waiting time $T_{d_i} - t_i$ is carried forward to U_{i+1}, i.e., the maximum acceptable delay $T_{d_{i+1}}$ at U_{i+1} is now updated as $T_{d_{i+1}} + (T_{d_i} - t_i)$.

Remark 6. *In this work, we consider a scenario, where IUs cannot communicate beyond a distance r, i.e., the IUs do not have a global knowledge of the system topology. Therefore, U_i passes on $T_{d_i} - t_i$ to U_{i+1}, as it is unaware of exactly how many hops will be required in DRAMS for the complete information transfer from S to D.*

Accordingly, we characterize T_{d_i} as

$$T_{d_i} = \frac{T_d - \sum_{k=0}^{i-2} \beta_k t_k - T_{d_{i-1}}}{\Psi - \Psi_i} + (T_{d_{i-1}} - \beta_{i-1} t_{i-1}) \quad i \geq 2,$$

where $\Psi_i = \left\lfloor \frac{||S - U_i||}{r} \right\rfloor$, $\lfloor \cdot \rfloor$ is the floor function, $T_{d_0} = \frac{T_d}{\Psi}$, $T_{d_1} = \frac{T_d - T_{d_0}}{\Psi - \Psi_1} + (T_{d_0} - \beta_0 t_0)$, and

$$\beta_i = \begin{cases} 0, & \text{Idle } U_i, \\ 1, & \text{Busy } U_i. \end{cases} \tag{3.26}$$

Moreover, based on the value of β corresponding to a particular U_i, we can have the following extreme cases:

1. $\beta_z = 0 \; \forall \; z < i$, i.e., no waiting at $U_1, \cdots, U_{i-1}$ and
2. $\beta_z = 1 \; \forall \; z < i$, i.e., waiting at $U_1, \cdots, U_{i-1}$.

Both these cases are investigated below.

Case I: $\beta_z = 0 \; \forall \; z < i$.

Here we investigate the scenario when the information from S has not faced any waiting at $U_1, \cdots, U_{i-2}, U_{i-1}$ till U_i. Accordingly, the maximum acceptable delay at U_i is given by the following theorem.

Theorem 3.5.1. *Without any delay in information transfer from S through the IUs $U_1, \cdots, U_{i-2}, U_{i-1}$, the maximum acceptable delay at U_i is given by*

Table 3.1: Summary of results.

Cases	IU	RIS	Maximum acceptable delay at U_i
1	✓	×	$T_{d_i} = \begin{cases} \frac{T_d}{\Psi}, & i = 0, \\ \frac{T_d - T_{d_0}}{\Psi - \Psi_1} + (T_{d_0} - \beta_0 t_0), & i = 1, \\ \frac{T_d - \sum_{k=0}^{i-2} \beta_k t_k - T_{d_{i-1}}}{\Psi - \Psi_i} + (T_{d_{i-1}} - \beta_{i-1} t_{i-1}) & i \geq 2. \end{cases}$
2	✓	✓	$T_{d_i} = \begin{cases} \frac{T_d}{\Psi}, & i = 0, \\ \frac{T_d - T_{d_0}}{\Psi - \Psi_1} + (T_{d_0} - (c_0 t'_0 + (1 - c_0) t''_0)), & i = 1, \\ \frac{T_d - \sum_{k=0}^{i-2} c_k t'_k - \sum_{k=0}^{i-2} (1 - c_k) t''_k - T_{d_{i-1}}}{\Psi - \Psi_i} + (T_{d_{i-1}} - (c_{i-1} t'_{i-1} + (1 - c_{i-1}) t''_{i-1})) & i \geq 2. \end{cases}$

$$T_{d_i} = T_d \left(\sum_{p=1}^{i} \left(\frac{1}{\Psi - \Psi_p} \right) \prod_{q=p+1}^{i} \left(1 - \frac{1}{\Psi - \Psi_q} \right) + \frac{1}{\Psi} \prod_{n=1}^{i} \left(1 - \frac{1}{\Psi - \Psi_n} \right) \right). \tag{3.27}$$

Proof. By replacing $\beta_z = 0 \; \forall \; z < i$ in (3.26), we obtain

$$T_{d_i} = \frac{T_d - T_{d_{i-1}}}{\Psi - \Psi_i} + T_{d_{i-1}} \quad i \geq 1, \tag{3.28}$$

where $T_{d_0} = \frac{T_d}{\Psi}$. After trivial manipulations, T_{d_1} can be alternatively written as

$$T_{d_1} = \frac{T_d - T_{d_0}}{\Psi - \Psi_1} + T_{d_0} = T_d \left(\frac{1}{\Psi - \Psi_1} + \frac{1}{\Psi} \left(1 - \frac{1}{\Psi - \Psi_1} \right) \right). \tag{3.29}$$

Similarly, we obtain T_{d_2} as a function of T_{d_1}, which in turn, can be further simplified in terms of T_{d_0} as

$$\begin{aligned} T_{d_2} &= \frac{T_d}{\Psi - \Psi_2} + \left(1 - \frac{1}{\Psi - \Psi_2} \right) T_{d_1} \\ &\overset{(a)}{=} \frac{T_d}{\Psi - \Psi_2} + \left(1 - \frac{1}{\Psi - \Psi_2} \right) \\ &\qquad \times \left(\frac{T_d}{\Psi - \Psi_1} + \left(1 - \frac{1}{\Psi - \Psi_1} \right) T_{d_0} \right) \\ &= T_d \left(\frac{1}{\Psi - \Psi_2} + \frac{1}{\Psi - \Psi_1} \left(1 - \frac{1}{\Psi - \Psi_2} \right) \right. \end{aligned}$$

$$+\frac{1}{\Psi}\left(1-\frac{1}{\Psi-\Psi_1}\right)\left(1-\frac{1}{\Psi-\Psi_2}\right)\Bigg), \tag{3.30}$$

where (a) follows from (3.29). By proceeding in the same way for $i \geq 1$, we get

$$T_{d_i} = T_d\left(\sum_{p=1}^{i}\left(\frac{1}{\Psi-\Psi_p}\right)\prod_{q=p+1}^{i}\left(1-\frac{1}{\Psi-\Psi_q}\right) + \frac{1}{\Psi}\prod_{n=1}^{i}\left(1-\frac{1}{\Psi-\Psi_n}\right)\right). \tag{3.31}$$

Moreover, it can also be observed that by putting $i = 2$ in (3.31) results in (3.30). □

We observe from Theorem 3.5.1 that the maximum acceptable delay T_{d_i} at IU U_i is expressed in terms of the overall delay constraint T_d. Furthermore, it can also be observed that T_{d_i} increases monotonically with i, i.e., $T_{d_i} \leq T_{d_{i+1}}\ \forall\ i$.

Case II: $\beta_z = 1\ \forall\ z < i$.

This implies that the information from S has suffered delay at all the IUs till U_i, i.e., in this case, we obtain the maximum acceptable delay at U_i from (3.26) as

$$T_{d_i} = \frac{T_d - \sum_{k=0}^{i-2} t_k - T_{d_{i-1}}}{\Psi-\Psi_i} + (T_{d_{i-1}} - t_{i-1}) \quad i \geq 2, \tag{3.32}$$

where $T_{d_0} = \dfrac{T_d}{\Psi}$ and $T_{d_1} = \dfrac{T_d - T_{d_0}}{\Psi-\Psi_1} + (T_{d_0} - t_0)$.
By simplifying T_{d_1} in (3.32), we obtain

$$\begin{aligned} T_{d_1} &\overset{(a)}{=} T_d\left(\frac{1}{\Psi-\Psi_1}\left(1-\frac{1}{\Psi}\right)+\frac{1}{\Psi}\right) \\ &\quad - \mu_1 \ln\left(\left(\frac{1-e^{-T_s/\mu_1}}{p_{\text{th}}}\right)^{+}\right) - T_s \\ &\overset{(b)}{=} T_d\left(\frac{1}{\Psi-\Psi_1}\left(1-\frac{1}{\Psi}\right)+\frac{1}{\Psi}\right) - \mu_1 \ln\left(\left(\frac{T_s}{\mu_1 p_{\text{th}}}\right)\right) - T_s, \end{aligned} \tag{3.33}$$

where (a) follows from $T_{d_0} = \dfrac{T_d}{\Psi}$ and (3.13). Furthermore, (b) follows from the Taylor expansion of e^{-T_s/μ_1} and neglecting its higher order terms as we know from Section 3.3.2

that $T_s/\mu_1 < 1$ and finally, by considering an appropriate p_{th} such that $\frac{T_s}{\mu_1 p_{\text{th}}} > 1$ holds.

Remark 7. *Note that for* $x \geq 1$, $x \ln\left(\frac{1}{x}\right)$ *is a monotonically decreasing function with its maxima at* $x = 1$, *when* $x \ln\left(\frac{1}{x}\right) = 0$. *Hence, we can observe from* (3.33), *that* T_{d_1} *increases with* μ_1 *when other parameters are constant. It is interesting to observe, that the same intuition is also provided by the term* p_{10} *in the transition probability matrix stated in* (3.2).

Instead of making a claim specifically with respect to U_1 as in Remark 7, we can make a generalization as follows. From (3.32), we obtain

$$\begin{aligned} T_{d_i} &= \frac{T_d - T_{d_{i-1}}}{\Psi - \Psi_i} + T_{d_{i-1}} - \frac{\sum_{k=0}^{i-2} t_k}{\Psi - \Psi_i} - t_{i-1} \qquad i \geq 2 \\ &= \frac{T_d - T_{d_{i-1}}}{\Psi - \Psi_i} + T_{d_{i-1}} - \left(\frac{i-1}{\Psi - \Psi_i} + 1\right) T_s \\ &\quad \underbrace{- \left(\frac{1}{\Psi - \Psi_i} \sum_{k=1}^{i-1} \mu_k \ln\left(\frac{T_s}{\mu_k p_{\text{th}}}\right) + \mu_i \ln\left(\frac{T_s}{\mu_i p_{\text{th}}}\right)\right)}_{\text{function of } \mu_1, \cdots, \mu_i}, \end{aligned} \tag{3.34}$$

which is based on (3.13).

Remark 8. *We observe from* (3.34) *that* T_{d_i} *is a joint function of* $\mu_1, \cdots, \mu_i$. *This implies that the average acceptable time delay at an arbitrary intermediate user is dependent on the traffic characteristics of all the previous intermediate users.*

Since we have investigated the two extreme scenarios, i.e., no delay at $U_1, \cdots, U_{i-1}$ and waiting at all of $U_1, \cdots, U_{i-1}$, the actual T_{d_i} corresponding to U_i will be in between the two. The reason behind this observation is attributed to the practical scenario of $\beta = 0$ for some of the IUs and $\beta = 1$ otherwise.

3.5.2 RIS and IUs

This is the most general scenario, which involves IUs, both idle and busy, and RISs in the process of information transfer from S to D. In this setup, if S has information packets to transfer, first it will search for idle IUs within the right half circle of radius r in the LRD direction. If one of the IUs is available that meets all the criteria as stated in (3.10) within

the acceptable waiting time, this particular IU will serve as the DF relay node but otherwise, S goes for a RIS. This process of IU or RIS selection is repeated at each hop until D is reached. In this context, we come across namely two types of delays at an arbitrary IU U_i as follows.

1. Delay t_i': waiting time at U_i, when it transfers the data packets to the following IU and
2. Delay t_i'': time after which U_i chooses an RIS to do the transfer due to reasons such as the unavailability of an appropriate IU.

It is to be noted that both t_i' and t_i'' occur at U_i for information transfer to U_{i+1}. Towards this direction, U_i after suffering a delay t_i'', immediately chooses a RIS and if there are no suitable IU in the LRD direction of the RIS, it immediately directs the signal to its adjacent RIS. This is based on the fact that double-RIS-aided information transfer is a non-negligible phenomenon [47] and the corresponding channel model is described in Section 3.3.3. Moreover, we assume that the RISs are strategically placed [36] and as a result, there is always another RIS in the right half circle of radius r. Furthermore, in the context of maximum acceptable delay calculation at an IU, here also we propose $T_{d_i} - t_i$ of being carried forward to only U_{i+1}.

With the motivation and the framework for this variant already stated in the previous section, we proceed along similar lines to obtain the maximum acceptable delay T_{d_i} corresponding to U_i.

$$T_{d_i} = \frac{T_d - \sum_{k=0}^{i-2} c_k t_k' - \sum_{k=0}^{i-2} (1-c_k) t_k'' - T_{d_{i-1}}}{\Psi - \Psi_i} + \left(T_{d_{i-1}} - (c_{i-1} t_{i-1}' + (1-c_{i-1}) t_{i-1}'')\right) \qquad i \geq 2, \tag{3.35}$$

and $T_{d_1} = \dfrac{T_d - T_{d_0}}{\Psi - \Psi_1} + (T_{d_0} - (c_0 t_0' + (1-c_0) t_0''))$, where

$$c_i = \begin{cases} 1, & \text{for D2D delay,} \\ 0, & \text{else} \end{cases} \tag{3.36}$$

Note that for a particular U_i, both t_i' and t_i'' cannot exist at the same time.

Hence in this section, we have analyzed the transmission delay for all the possible cases of the proposed framework. Finally, Table 3.1 presents a summary of the main analytical results derived in this section.

Table 3.2: Transmission Modes for $P_b = 10^{-6}$.

SNR interval (dB)	Modulation	Rate (bits/sym.)
$(-\infty, 9.8554)$	No transmission	0
$[9.8554, 12.8657)$	BPSK	1
$[12.8657, 14.6266)$	QPSK	2
$[14.6266, 15.8760)$	8-QAM	3
$[15.8760, 16.8451)$	16-QAM	4
$[16.8451, 17.6369)$	32-QAM	5
$[17.6369, 18.3063)$	64-QAM	6
$[18.3063, 18.8863)$	128-QAM	7
$[18.8863, +\infty)$	256-QAM	8

3.6 Numerical Results

In this section, we carry out extensive simulations to validate the performance of DRAMS and also compare with the nearest existing approach. Here we consider data transmission in a Rician fading scenario, where we assume Rician factor $K = 10$ dB. The default parameters considered are: slot duration $T_s = 100$ μs [75], IU transmission power $P_{\text{tx}} = 30$ dBm, IU processing power $P_t = 10$ dBm, path loss at one-meter distance $\rho_{\text{L}} = 10^{-3.53}$ [86], pathloss exponent $\alpha = 4.2$ between two consecutive IUs and $\alpha = 2$ elsewhere, the number of elements in each RIS $M = 250$, and acceptable delay bound $T_d = 50$ ms [87]. The parameters related to energy harvesting at the IUs are $N_I = 24$ mW, $a = 150$, and $b = 0.014$ [88]. Based on (3.8), we consider M-ary quadrature amplitude modulation (M-QAM) transmission between consecutive IUs and a BER of $P_b = 10^{-6}$ results in $\frac{P_{\text{tx}}\rho_{\text{L}} d^{-\alpha}|h|^2}{\sigma^2} = 9.6724(m_q - 1)$, where m_q is constellation size as defined in Section 3.4.2. Accordingly, we obtain the transmission modes (TM) as stated in Table 3.2 and these TM are used in this section. Moreover, in this work, when an RIS is chosen due to the unavailability of IUs, we consider parameters $M_b = 1000$ and $\varepsilon = 10^{-4}$ [89]. Next we demonstrate the performance of DRAMS and also validate the proposed analytical framework against Monte Carlo simulation. Finally, we compare DRAMS with the existing approaches.

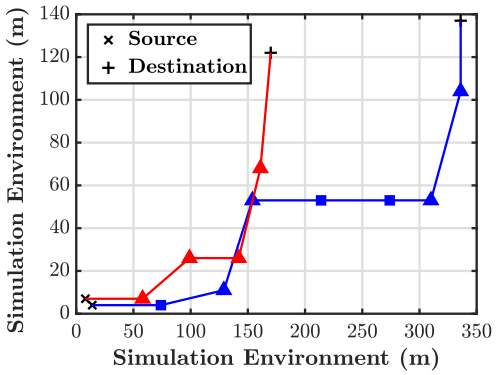

Figure 3.4: DRAMS trajectories for two different scenarios; Δ corresponds to IU and □ corresponds to RIS.

3.6.1 Performance of DRAMS

An illustration of the DRAMS-based multihop trajectory is presented in Fig. 3.4. In this scenario, we consider a two-dimensional squared area of 400×400 m^2, where the IUs and the RISs are randomly and strategically placed, respectively, as shown in Fig. 3.4. Moreover, we assume an IU coverage of 60 m, where 'coverage' refers to the maximum distance at which a particular IU can communicate. We consider two separate instances, when a randomly selected $S - D$ pair wants to communicate. In the process of doing so, DRAMS establishes a multi-hop connection, which effectively brings out the advantages of the proposed scheme as follows.

1. IUs are preferred over RISs in establishing the $S - D$ connection, i.e., the figure demonstrates that if IUs are available to act as relays without violating the delay constraint, RISs are completely overlooked by DRAMS.

2. On the other hand, the RISs are considered as an option only in the case of IU unavailability. Furthermore, to take advantage of the RISs significantly, DRAMS also leverages on the secondary reflections from the RISs, which can also be observed by the choice of two consecutive □s in the figure.

In this way, by prioritizing the choice of IUs over RISs, DRAMS avoids the aspect of unnecessary resource wastage. However, it is to be noted that this benefit does not come at a cost of violating the delay constraint and the corresponding analysis is already explained in Section 3.5.

Fig. 3.5 illustrates the number of RISs used to connect S to D as a function of the IU coverage. We consider a particular $S - D$ pair and three different scenarios with IU

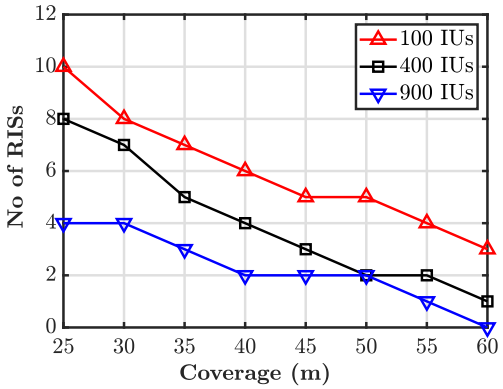

Figure 3.5: Effect of IU coverage.

density 100, 400, and 900, respectively. Accordingly, we look at the number of RISs used to establish a multi-hop connection from S to D. For a particular IU density, we observe that the number of RISs used to connect $S - D$ follows a non-increasing trend with respect to increasing IU coverage. This is justified by the fact that a smaller coverage implies more number of hops to connect $S - D$. Moreover, we know that higher carrier frequency results in higher data rate but lower coverage. Hence, the figure demonstrates that for identical IU density, higher carrier frequency (lower coverage) results in higher number of RISs being used and vice-versa. Finally, we also note that irrespective of the IU density, the number of RISs used asymptotically reaches zero with increasing IU coverage.

Fig. 3.6 depicts the number of RISs used to connect S to D as a function of the IU density. In this figure, we establish a connection between a $S - D$ pair for three different IU coverage of 30, 45, and 60 m, respectively. It is observed here that a lesser number of RISs are being used as the IU density increases and here also, irrespective of the IU coverage radius, the value asymptotically reaches zero. In other words, for an environment with a significantly large IU density, it is possible to completely avoid the usage of RISs.

From Fig. 3.5 and Fig. 3.6 we observe that depending on the carrier frequency (i.e., the IU coverage) and density of IUs in the surroundings, it is possible to establish a multihop $S - D$ connection consisting of only IUs and not RISs. This further strengthens our claim of exploiting the IU traffic characteristics to reduce the dependency on the RISs. It is to be noted that our proposed DRAMS avoids wastage of resources but not at the cost of performance degradation.

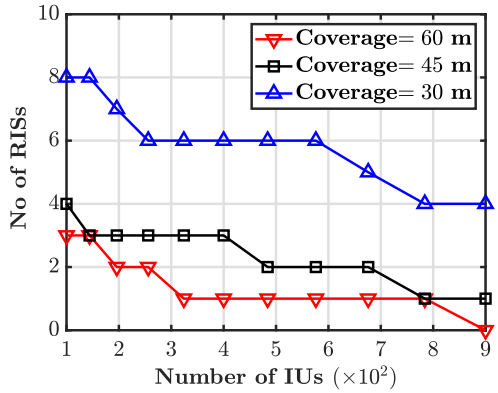

Figure 3.6: Effect of IU density.

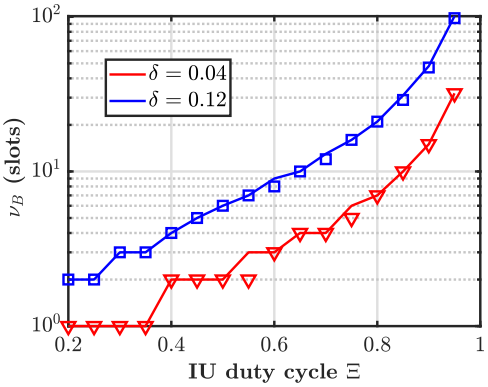

Figure 3.7: Verification of ν_B estimation; lines correspond to analysis and markers correspond to simulation results.

3.6.2 Verification of ν_B and ν_I by Monte Carlo Simulation

Here for the generation of results, we define the average IU activity duty cycle as $\Xi = \frac{\mu_k}{\mu_k + \lambda_k} \ \forall \ k$, which is the average fraction of the total time that an IU remains busy communicating with its own dedicated receiver.

Fig. 3.7 compares the analytically obtained ν_B in (3.7) with the Monte Carlo simulations, where we consider the average 'OFF' duration $\lambda_k = 4$ ms $\forall \ k$. It is observed that ν_B increases monotonically with Ξ and moreover, the rate of increase exponentially shoots up as $\Xi \to 1$. This is also intuitive, as increasing Ξ implies that the IU will remain busy most of the time and hence, the time duration for which it will remain busy given that it is currently busy will also increase. Furthermore, we also observe that for a particular Ξ, a higher value of δ implies a greater value of ν_B and vice-versa, as evident from (3.7).

We compare the analytically obtained ν_I with the corresponding Monte Carlo simulations in Fig. 3.8, where we consider the average 'ON' duration $\mu_k = 4$ ms $\forall \ k$. We observe that,

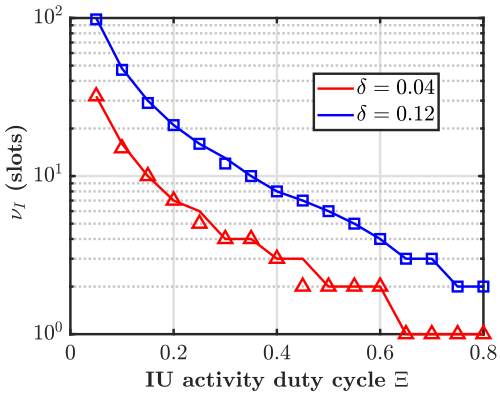

Figure 3.8: Verification of ν_I estimation; lines correspond to analysis and markers correspond to simulation results.

irrespective of δ, the value of ν_I decreases with increasing Ξ, unlike ν_B. This is intuitive too, as increasing the duty cycle implies that the IU will remain idle for a relatively lesser amount of time. Furthermore, here also, we observe that for any particular Ξ, $\delta_1 > \delta_2$ results in ν_I corresponding to δ_1 being greater than the ν_I corresponding to δ_2. Thus, based on Fig. 3.7 and Fig. 3.8, we can state that ν_B and ν_I complement each other. Furthermore, it can also be said, that DRAMS will always have a tendency to select IUs with lower Ξ as relays.

3.6.3 Performance Comparison

Here we first define the metrics, namely data throughput and energy efficiency, which will be used to quantify the performance of DRAMS.

3.6.3.1 Data throughput $\mathcal{D}_\mathcal{T}$

By assuming that DRAMS chooses $\mathcal{X}$ IUs and a certain number of RISs to connect the k-th $S-D$ pair in $\mathcal{X}+1$ hops, the data throughput is defined as

$$\mathcal{D}_\mathcal{T} = \frac{1}{\sum_{i=1}^{\mathcal{X}+1} \frac{1-a_i}{(1-P_b)\, m_{q_i}} + \frac{a_i}{T_i(\gamma_i)}}, \tag{3.37}$$

where

$$a_i = \begin{cases} 1, & \text{if } i\text{-th hop involves RIS,} \\ 0, & \text{else.} \end{cases}$$

Here P_b is the BER and m_{q_i} is the constellation size as stated in (3.8). Moreover, in case we have a RIS selected due to idle IU unavailability, R_i is the corresponding achievable data rate as defined in (3.4).

3.6.3.2 Energy efficiency $\mathcal{E}_{\text{eff}}$

Similar to data throughput, the system energy efficiency for transferring α_k packets of data with φ bits in each packet, when the k-th $S-D$ pair gets connected in $\mathcal{X}+1$ hops is defined as

$$\mathcal{E}_{\text{eff}} = \frac{\alpha_k \varphi_k}{(P_{\text{tx}} + P_t)\, T_s \sum_{i=1}^{\mathcal{X}+1} \tau_i - T_s \sum_{j=1}^{\mathcal{X}} P_{\text{harv}}(j)\tau_j}, \tag{3.38}$$

where P_{tx} and P_t is the transmission and processing power respectively, as defined in (3.9). Moreover, τ_i is the time required (in slots) for complete information transfer in the i-th hop and finally, based on the channel condition, $P_{\text{harv}}(j)$ is the harvested power at the j-th IU when the channel between the $(j-1)$-th and j-th IU is being used for information transfer. Note that in (5.4), the numerator is essentially the amount of data transferred and the denominator denotes the net energy consumption, where the first term is the energy required for data transmission and the second term implies the amount of energy harvested. Hereafter, we compare the performance of DRAMS with the existing benchmark schemes [37, 48]. Accordingly, the variants used for this purpose are the following:

1. OPRIS [37]: The work investigates the optimal placement of RISs when the $S-D$ pair is either directly connected or connected via a single RIS only. In other words, it does not involve any aspect of connecting two devices that require multihop communication. DAR [48]: This work proposes the involvement of only double-RIS aided scenarios for the purpose of connecting S to D. It does not involve the aspect of incorporating single and/or double reflection depending on the availability of IU and/or RIS.

Fig. 3.9 (a) demonstrates an overall decreasing trend of $\mathcal{D}_{\mathcal{T}}$ with IU coverage, irrespective of the deployed scheme. This is because although increasing coverage implies lesser number of hops, the pathloss factor becomes dominant. It is observed that the performance of both DRAMS and OPRIS, without AM, are comparable and equally poor as compared to DRAMS irrespective of M_b. This degraded performance is attributed to the inability to exploit the temporal variation of the wireless channel. Moreover, we note that irrespective of coverage, DRAMS with $M_b \to \infty$ always outperforms its finite M_b counterpart and the

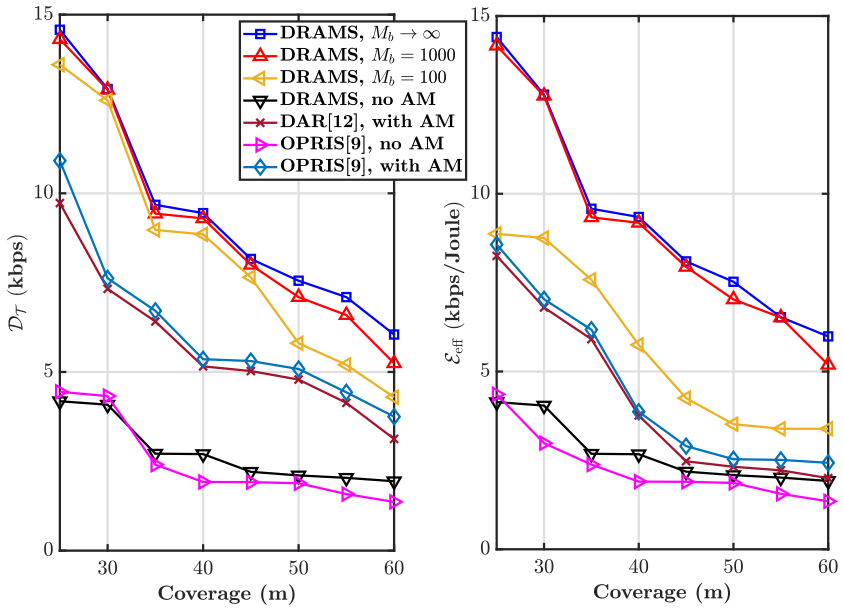

Figure 3.9: Performance comparison: (a) Data throughput (b) Energy efficiency.

performance gap increases with decreasing M_b. This is because the $M_b \to \infty$ scenario always chooses the best channel in each hop while connecting $S - D$, whereas a finite M_b scenario cannot do so always due to the application-specific delay constraints. As a result, it can be concluded that if delay is not a critical factor for the application at hand, the performance of DRAMS gets enhanced by a finite margin. It is important to note that OPRIS (DAR) always utilizes single (double) reflection in the RIS-aided networks. On the contrary, DRAMS uses either of the two, depending on the scenario, which results in reduced RIS deployment, but not at the cost of degraded data throughput. As in Fig. 3.9 (a), Fig. 3.9 (b) depicts the advantage of the proposed framework in terms of $\mathcal{E}_{\text{eff}}$, which also reduces with increasing coverage irrespective of the framework being used.

3.6.4 Impact of Mobility

Here we consider a mobile scenario, i.e., the IUs are having a particular velocity in a certain direction. Note that this will have a significant effect on the performance of the proposed scheme, as the inter-IU distance changes during the process of information transfer. In this context, Fig. 3.10 illustrates the impact of IU mobility on DRAMS, with the coverage being taken as 50 m and the mobility aspect being modeled by the standard random waypoint (RWP) model [90]. Here, we fix the maximum possible velocity V_{max} of the IUs, consider a random velocity in $[0, V_{\text{max}}]$ and observe its impact on the system data throughput. It can

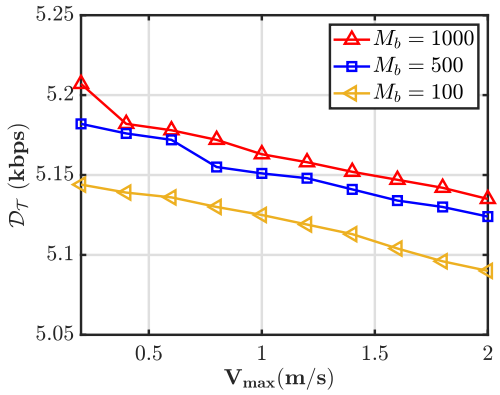

Figure 3.10: Effect of IU mobility on DRAMS.

be seen that the performance deteriorates monotonically with increasing V_{max}, which is intuitive. The reason for this is attributed to the fact that, due to mobility, a particular IU can move outside the coverage of another IU even during the communication process. This inevitably leads to outage, resulting in lesser data rate. Moreover, note that this figure with $V_{\text{max}} = 0$ is a special case corresponding to the static scenario, i.e., Fig. 3.9. Furthermore, note that for a fixed V_{max}, $\mathcal{D}_{\mathcal{T}}$ decreases with M_b, which is inline with the observation made in Fig. 3.9 as well.

3.7 Conclusion

In this chapter, we proposed a novel double-RIS assisted adaptive modulation-based multihop routing scheme for D2D wireless networks, which takes into account the aspect of multi-RIS secondary reflection. The proposed DRAMS exploits the traffic characteristics of the users present in the surroundings to bring down the dependency on the already deployed RISs, which reduces the wastage of resources. Numerical results demonstrate that double RIS assistance, at times, provide indirect LoS between the $S - D$ pair, which may not be achieved even with single RIS assistance. Moreover, we observe that, in certain cases, neighbouring IUs alone are sufficient for providing the required LoS without any RIS. Moreover, the results also showcase the significance of the proposed framework in terms of enhanced data throughput and energy efficiency. An immediate extension of this work is to investigate a non-cooperative scenario, where the users are independent to decide whether they would like to act as a relay and if they do, then for which corresponding $S - D$ pair in case of multiple requests.

Chapter 4

Priority-aware Grouping-based Multihop Routing Scheme[1]

4.1 Introduction

In the previous chapter, we proposed a routing strategy for a particular device pair. For multiple device pairs, a single RIS may be simultaneously requested by several devices to act as a relay for their seamless communications. To deal with such cases, we propose a multi-hop routing scheme based on traffic-dependent grouping of priority-aware users for a mmWave D2D communication network with spatially correlated channels that is assisted by RIS. In particular, the suggested plan takes advantage of the users' priority (based on their individual delay-constrained applications) and the spatial correlation feature in the RISs' closely spaced reflecting elements. Here, we create a multi-hop connection for information transfer from one of the users to its intended recipient based on the other users in the neighborhood, their individual traffic characteristics, and the nearby RISs that have already been deployed. The impact of considering realistic discrete phase shifts at the RIS patches rather than their ideal continuous counterpart is taken into consideration in this context. Furthermore, we assert and show that the traditional least remaining distance (LRD) based method is not always the best option due to its limitations. The benefits of the suggested approach are finally illustrated by numerical results, which show that it performs noticeably better than the current benchmark schemes on the basis of system performance metrics like data throughput, energy consumption, and energy efficiency.

[1]This chapter is based on the following publication:
L. Sau, P. Mukherjee, and S. C. Ghosh, "Priority-aware grouping-based multihop routing scheme for RIS-assisted wireless networks", **IEEE Transactions on Network Science and Engineering**, vol. 12, no. 2, pp. 1172–1185, Mar.-Apr. 2025.

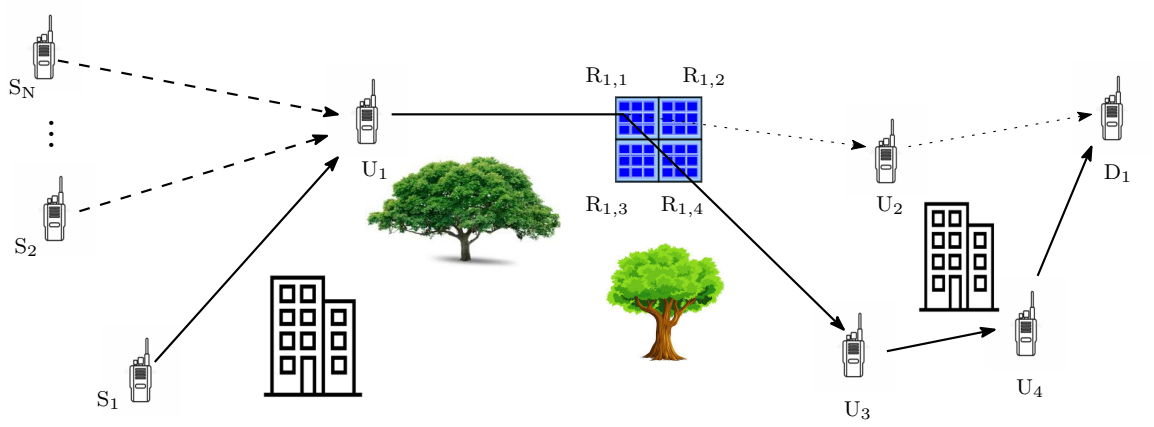

Figure 4.1: System Model

4.2 Chapter Organization

The chapter is organized as follows. Section 4.3 describes the system model, Section 4.4 presents the proposed strategy, section 4.5 describes the analysis of the proposed scheduling strategy, the numerical results are presented in Section 4.6 and finally, Section 4.7 concludes the work.

4.3 System Model

4.3.1 Network Topology

The considered topology consists of N sources $S_1, \cdots, S_N$ and their respective destinations $D_1, \cdots, D_N$, N_R RISs $R_1, \cdots, R_{N_R}$, and N_I IUs $U_1, \cdots, U_{N_I}$. In a delay-constrained scenario, all the sources transmit signals with constant power P_{tx}, where the maximum acceptable delay for $S_n - D_n$ pair is T_{d_n} $\forall\, n = 1, \cdots, N$. The sources are prioritized based on their acceptable delay limit, i.e., higher T_{d_n} implies lower priority, and vice-versa. We consider all such $S_n - D_n$ pair for which the direct LoS link does not exist. We further assume that the devices cannot communicate beyond a distance r, each IU has a sufficient capacity buffer, and all D2D pairs adhere to time-slotted synchronous communication [74] with slot duration T_s.

Each RIS has M reflecting elements, which are effectively controlled to adjust both the amplitude and phase of the incident waveform[2]. However, for the sake of simplicity

[2]Here we do not consider secondary reflections from the RISs. However, the proposed framework is

and mathematical tractability, the amplitude factor is set to unity and it is only the phase that is tuned or optimized [22]. To reduce the channel estimation overhead, we employ a grouping strategy, where nearby M_g reflecting elements are grouped together, such that all the elements belonging to the same group introduce identical phase shift [22]. Specifically, the r-th RIS R_r, consisting of M reflecting elements, is subdivided into K_g non-overlapping surfaces $R_{r,b}\ \forall\ 1 \leq b \leq K_g$ such that $M_g K_g = M$, where the number of partitions and the resulting sub-surfaces are determined a-priori [22]. Without any loss of generality, we consider that each group has an equal number of elements and a particular group can serve one service request at a time [66]. In this scenario, $R_{r,b}$ has two possible states: ON and OFF. If an element is in ON state, the phase of an incident signal can be changed to a desired direction and it cannot reflect while in OFF state. Finally, an example of the considered scenario is demonstrated in Fig. 5.3, where S_1 has the highest priority and the elements of the RIS are grouped into four non-overlapping surfaces, and the signal from S_1 reaches D_1 by using the path $S_1 - U_1 - R_{1,1} - U_3 - U_4 - D_1$.

4.3.2 Channel Model

Based on the IU availability, the $S_i - D_i$ pair communicates with or without the help of RISs. We assume that the wireless links suffer from both large-scale path-loss effects and small-scale block fading. All the channels $S_i \rightarrow U_j$, $U_j \rightarrow U_k$, and $U_k \rightarrow D_i$ $\forall\ j,k = 1,\cdots,N_I$ experience Rician fading and their corresponding path-loss factors are $\rho_{\mathrm{L}}^{1/2} d_{S,U_j}^{-\alpha/2}$, $\rho_{\mathrm{L}}^{1/2} d_{U_j,U_k}^{-\alpha/2}$, and $\rho_{\mathrm{L}}^{1/2} d_{U_k,D}^{-\alpha/2}$, respectively, where ρ_{L} is the pathloss at one meter distance, α is the path-loss exponent and $d_{m,n}$ denotes the distance between m and n. Specifically, we have the channel gain $h_{p,q}\ \forall\ \{p,q\} \in \{S_i, U_j, U_k, D_i\}$, where the distribution of $|h_{p,q}|$ is defined as[70]

$$\begin{aligned} f_{|h_{p,q}|}(\alpha, K_{p,q}) &= 2(1+K_{p,q}) e^{-K_{p,q}} \\ &\times \alpha e^{-(1+K_{p,q})\alpha^2} I_0\left(2\alpha\sqrt{K_{p,q}(1+K_{p,q})}\right),\ \alpha \geq 0. \end{aligned} \tag{4.1}$$

Here $K_{p,q}$ is the Rician factor corresponding to the channel gain $h_{p,q}$ and $I_0(\cdot)$ denotes the zero-order modified Bessel function of the first kind. Moreover, note that direct $S - D$ path does not exist, i.e., $h_{S_i,D_i} = 0\ \forall\ i$.

general and it can be readily extended to the case where the aspect of secondary reflection is incorporated [47].

Since the elements of the RIS are divided into K_g subgroups with M_g reflecting elements on each of them, the composite channel between S_i/U_j and $R_{r,b}$ is obtained as [22]

$$h_{S_i/U_j,R_{r,b}} = \sum_{n \in R_{r,b}} h_n, \tag{4.2}$$

where h_n is the channel gain between S_i/U_j and the n-th element of $R_{r,b}$ and $|h_n|$ follows identical distribution as (4.1). Similarly, the composite channel between $R_{r,b}$ and U_k/D_i is

$$g_{R_{r,b},U_k/D_i} = \sum_{m \in R_{r,b}} g_m. \tag{4.3}$$

Finally, as the reflecting elements within $R_{r,b}$ are very close to each other, it is practical to assume that the associated channels are spatially correlated. Note that in this work, we adopt the *sinc* model [59] to mathematically characterize the spatial correlation at the RISs.

4.3.3 User Traffic Characterization

In a typical wireless communication scenario, data generally arrives in bursts to the users. As a result, the IUs $U_1, \cdots, U_{N_I}$, in this work, are characterized by exponentially distributed OFF and ON period lengths, with means $\lambda_{u,k}$ and $\mu_{u,k}$, respectively. Without any loss of generality, T_s is assumed to be small in comparison with $\mu_{u,k}$ and $\lambda_{u,k}$ rest of this[75], which prevents $U_k \; \forall \; k = 1, \cdots, N_I$ changing its status multiple times within a single T_s. Thus, the IU activities are characterized by a discrete-time Markov chain (DTMC) with the state transition probabilities [75]:

$$\mathrm{P}_{\mathrm{ON}\to\mathrm{OFF}} \triangleq \mathrm{p}_{10} = \int_0^{T_s} \frac{1}{\mu_{u,k}} e^{-a/\mu_{u,k}} da = 1 - e^{-T_S/\mu_{u,k}}, \tag{4.4}$$

$$\mathrm{P}_{\mathrm{OFF}\to\mathrm{ON}} \triangleq \mathrm{p}_{01} = \int_0^{T_s} \frac{1}{\lambda_{u,k}} e^{-b/\lambda_{u,k}} db = 1 - e^{-T_S/\lambda_{u,k}}.$$

Accordingly the state transition matrix $\mathcal{P}$ is:

$$\mathcal{P} = \begin{bmatrix} \mathrm{p}_{00} & \mathrm{p}_{01} \\ \mathrm{p}_{10} & \mathrm{p}_{11} \end{bmatrix} = \begin{bmatrix} e^{-T_S/\lambda_{u,k}} & 1 - e^{-T_S/\lambda_{u,k}} \\ 1 - e^{-T_S/\mu_{u,k}} & e^{-T_S/\mu_{u,k}} \end{bmatrix}. \tag{4.5}$$

4.4 Proposed strategy

In this section, we propose a priority-aware scheduling strategy for grouping-based RIS-assisted wireless networks. Here, we consider a delay-constrained scenario, where the data from S_i must arrive at D_i within the delay bound T_{d_i}. Firstly, we characterize the achievable data rate for a grouping-based RIS-aided scenario. Secondly, based on the channel condition and the number of coding bits being used at the RIS, we comment on the suitable group selection strategy. Thirdly, depending on the channel condition as well as the delay sensitivity of the application, a novel scheduling strategy is proposed for information transfer between any two IUs. Note that, we also comment on the appropriate choice of modulation scheme and appropriate next hop selection criteria. Finally, we provide an illustrative example of the proposed framework.

4.4.1 Achievable Rate Characterization of Grouping-based RIS

Based on (4.2), the adopted *sinc* correlation model, and the theory of correlated random variables [91], we obtain

$$\begin{aligned} h_1 &= h_{I1} + j h_{Q1} \\ &\vdots \\ h_n &= \left(\mu_{1,n} h_{I1} + \sqrt{1-\mu_{1,n}^2}\, h_{In}\right) \\ &\quad + j\left(\mu_{1,n} h_{Q1} + \sqrt{1-\mu_{1,n}^2}\, h_{Qn}\right) \quad \forall \quad n \in R_{r,b}, \end{aligned} \tag{4.6}$$

where $\mu_{1,n} = \dfrac{\sin\left(\frac{2\pi}{\lambda} d_{1,n}\right)}{\frac{2\pi}{\lambda} d_{1,n}}$ is the spatial correlation and $d_{1,n}$ is the Euclidean distance between the first and n-th element of $R_{r,b}$ [59]. Moreover, h_{In}, h_{Qn} are independent Gaussian random variables denoting the in-phase and quadrature components of h_n, such that $|h_n|$ follows identical distribution as (4.1). Accordingly, from (4.2), we can derive the composite $S_i/U_j - R_{r,b}$ channel $h_{S_i/U_j,R_{r,b}}$ as

$$\begin{aligned} h_{S_i/U_j,R_{r,b}} &= \left(h_{I1} \sum_{p=1}^{M_g} \mu_{1,p} + \sum_{p=1}^{M_g} h_{Ip} \sqrt{1-\mu_{1,p}^2}\right) \\ &\quad + j\left(h_{Q1} \sum_{p=1}^{M_g} \mu_{1,p} + \sum_{p=1}^{M_g} h_{Qp} \sqrt{1-\mu_{1,p}^2}\right) \end{aligned} \tag{4.7}$$

and similarly, the composite $R_{r,b} - U_k/D_i$ channel $g_{R_{r,b},U_k/D_i}$ can also be obtained[3]. Hence, if a communication link exists between U_j and U_k via $R_{r,b}$, the resulting end-to-end achievable rate is expressed as

$$T_{j,k}^{r,b} = \left(1 - \frac{2}{T_c}\right) \log_2 \left(1 + \gamma_{j,k}^{r,b}\right), \tag{4.8}$$

where SNR $\gamma_{j,k}^{r,b}$ is defined as

$$\begin{aligned} \gamma_{j,k}^{r,b} &= \frac{P_{\text{tx}} \rho_{\text{L}}^2 \left(d_{U_j,R_r} d_{R_r,U_k}\right)^{-\alpha}}{\sigma_0^2} \left| h_{U_j,R_{r,b}} \times g_{R_{r,b},U_k} \times e^{j\phi_{r,b}} \right|^2 \\ &= \zeta \left| h_{U_j,R_{r,b}} \times g_{R_{r,b},U_k} \times e^{j\phi_{r,b}} \right|^2, \end{aligned} \tag{4.9}$$

where $\zeta = \frac{P_{\text{tx}} \rho_{\text{L}}^2 \left(d_{U_j,R_r} d_{R_r,U_k}\right)^{-\alpha}}{\sigma_0^2}$, $\phi_{r,b}$ is the associated phase shift provided at $R_{r,b}$, T_c is the channel coherence time normalized to the number of slots, and σ_0 is the power of the zero mean AWGN at U_k. Moreover, the quantity $\frac{2}{T_c}$ denotes the feedback and processing delay. Note that unlike the conventional RIS-based approach, $\gamma_{j,k}^{r,b}$ does not involve a diagonal phase shift matrix of K_g non-zero elements. On the contrary, all the elements of $R_{r,b}$ provide a common phase shift $\phi_{r,b}$ to the incoming signal. Hence, by rewriting the complex composite channels as $h_{U_j,R_{r,b}} = \left| h_{U_j,R_{r,b}} \right| e^{-j\theta_h}$ and $g_{R_{r,b},U_k} = \left| g_{R_{r,b},U_k} \right| e^{-j\theta_g}$, we obtain the optimal phase shift corresponding to $R_{r,b}$ as $\phi_{r,b}^{\text{opt}} = \theta_h + \theta_g$ such that the maximum attainable SNR is given by (4.10). Finally, as we focus on the performance of idle IUs acting as DF relays, we consider an ideal scenario where we ignore the interference from other IUs; interference mitigation can be achieved through sophisticated signal processing and equalization techniques [92].

Remark 9. *We observe from* (4.8) *and* (4.10) *that the achievable data rate* $T_{j,k}^{r,b}$ *is dependent on both the number of reflecting elements* M_g *and the spatial correlation* $\mu_{1,n}$ $\forall$ $n = 1, \cdots, M_g$. *Specifically,* $\mu_{1,n}$ *is dependent on the Euclidean distance between the first and* n*-th element of the non-overlapping surface* $R_{r,b}$ *of the RIS* R_r.

[3]Statistical characterization of both the composite channels is straightforward as it only involves the aspect of the sum of correlated random variables.

$$\gamma_{j,k}^{r,b} = \frac{P_{\text{tx}}\rho_{\text{L}}^2 \left(d_{U,R_r} d_{R_r,U_k}\right)^{-\alpha}}{\sigma_0^2} \left|h_{U_j,R_{r,b}}\right|^2 \left|g_{R_{r,b},U_k}\right|^2$$

$$\overset{(a)}{=} \frac{P_{\text{tx}}\rho_{\text{L}}^2 \left(d_{U_j,R_r} d_{R_r,U_k}\right)^{-\alpha}}{\sigma_0^2} \left(\left(h_{I1} \sum_{p=1}^{M_g} \mu_{1,p} + \sum_{p=1}^{M_g} h_{Ip} \sqrt{1-\mu_{1,p}^2} \right)^2 \right. \tag{4.10}$$

$$\left. + \left(h_{Q1} \sum_{p=1}^{M_g} \mu_{1,p} + \sum_{p=1}^{M_g} h_{Qp} \sqrt{1-\mu_{1,p}^2} \right)^2 \right)$$

$$\times \left(\left(g_{I1} \sum_{p=1}^{M_g} \mu_{1,p} + \sum_{p=1}^{M_g} g_{Ii} \sqrt{1-\mu_{1,p}^2} \right)^2 + \left(g_{Q1} \sum_{p=1}^{M_g} \mu_{1,p} + \sum_{p=1}^{M_g} g_{Qi} \sqrt{1-\mu_{1,p}^2} \right)^2 \right), \tag{4.11}$$

where (a) follows from (4.7).

4.4.2 Group Selection Criteria at an RIS

As the RIS is partitioned into K_g non-overlapping subsurfaces, the question of appropriate selection arises in the context of multiple subgroups availability. Hence, here we discuss the group selection criterion at a particular RIS. In case a communication link exists between U_j and U_k via R_r, the resulting rate, when the b-th group of R_r is opted for, is given by (4.8). By rewriting (4.9), we obtain

$$\gamma_{j,k}^{r,b} = \zeta \left| h_{U_j,R_{r,b}} \times g_{R_{r,b},U_k} \times e^{j\phi_{r,b}} \right|^2, \tag{4.12}$$

where from (4.7), we have

$$\begin{aligned} h_{U_j,R_{r,b}} = & \left(h_{I_1} \sum_{p=1}^{M_g} \mu_{1,p} + h_{I_1} \sum_{p=1}^{M_g} \sqrt{1-\mu_{1,p}^2} \right) \\ & + j \left(h_{Q_1} \sum_{p=1}^{M_g} \mu_{1,p} + h_{Q_1} \sum_{p=1}^{M_g} \sqrt{1-\mu_{1,p}^2} \right) \\ = & \left\{ \left(h_{I_1} \sum_{p=1}^{M_g} \mu_{1,p} + h_{I_1} \sum_{p=1}^{M_g} \sqrt{1-\mu_{1,p}^2} \right)^2 \right. \\ & \left. + \left(h_{Q_1} \sum_{p=1}^{M_g} \mu_{1,p} + h_{Q_1} \sum_{p=1}^{M_g} \sqrt{1-\mu_{1,p}^2} \right)^2 \right\}^{\frac{1}{2}} \end{aligned}$$

$$\times \arctan\left(\frac{h_{Q_1}\sum_{p=1}^{M_g}\mu_{1,p}+h_{Q_1}\sum_{p=1}^{M_g}\sqrt{1-\mu_{1,p}^2}}{h_{I_1}\sum_{p=1}^{M_g}\mu_{1,p}+h_{I_1}\sum_{p=1}^{M_g}\sqrt{1-\mu_{1,p}^2}}\right). \tag{4.13}$$

Similarly, we can represent $g_{R_{r,b},U_k}$ and hence, the optimal phase shift for the desired signal is

$$\phi_{r,b}^{opt}=\sum_{p\in\{h,g\}}\arctan\left(\frac{p_{Q_1}\sum_{p=1}^{M_g}\mu_{1,p}+p_{Q_1}\sum_{p=1}^{M_g}\sqrt{1-\mu_{1,p}^2}}{p_{I_1}\sum_{p=1}^{M_g}\mu_{1,p}+p_{I_1}\sum_{p=1}^{M_g}\sqrt{1-\mu_{1,p}^2}}\right) \tag{4.14}$$

Based on the considered grouping framework, $\phi_{r,b}^{opt}$ is the optimal phase shift corresponding to all the elements of $R_{r,b}$. Here, we state to differentiate our grouping framework from the one presented in [93]. This work considers a RIS-assisted aerial-terrestrial communication system, where the RIS is attached to a building, assisting the downlink communications of multiple UAV-user pairs. Here, the RIS is sub-divided into multiple groups, such that, one RIS group can serve one UAV-user pair. However, within a group, each reflecting element is allotted its own unique phase shift. On the contrary, in our proposed framework, all the elements belonging to the same group introduce identical phase shift, resulting in reduced channel estimation overhead.

Note that, in all practical cases, the phase shift $\phi_{r,b}^{c}$ is not a continuous quantity but it is chosen from the finite set of predetermined phase shifts offered by the RIS [61]. Therefore, we choose $\phi_{r,b}^{c}$ among them, which is closest to the optimal $\phi_{r,b}^{opt}$, i.e., $\theta_h+\theta_g$. It may happen, that we have $\phi_{r,b}^{c}\neq\phi_{r,b}^{opt}$ and thus, we define the corresponding error δ_p as $\delta_p=\phi_{r,b}^{opt}-\phi_{r,b}^{c}$. By assuming that each subgroup of R_b is K_b bits coded, there are 2^{K_b} phase shifts available with a constant interval of $\frac{2\pi}{2^{K_b}}$, i.e., we have

$$-\frac{2\pi}{2^{K_b+1}}\leq\delta_p<\frac{2\pi}{2^{K_b+1}}. \tag{4.15}$$

Therefore, we obtain $\phi_{r,b}^{c}=\frac{\pi r}{2^{K_b-1}}$ where $\{r : r\in\mathbb{I} \text{ and } 0\leq \mathrm{r}\leq 2^{\mathrm{K_b}-1}\}$. As a result, the suboptimal, i.e., closest to the optimal, SNR $\hat{\gamma}_{j,k}^{r,b}$ is characterized as

$$\hat{\gamma}_{j,k}^{r,b}=\zeta\left|h_{U_j,R_{r,b}}\right|^2\left|g_{R_{r,b},U_k}\right|^2\left|e^{-j\delta_p}\right|^2 \tag{4.16}$$

and accordingly, the corresponding achievable data rate is

$$\hat{T}_{j,k}^{r,b} = \left(1 - \frac{2}{T_c}\right) \log_2 \left(1 + \hat{\gamma}_{j,k}^{r,b}\right). \tag{4.17}$$

Note that we have $\hat{T}_{j,k}^{r,b} = T_{j,k}^{r,b}$ when $\delta_p = 0$. In case of multiple subgroup availability at R_r, we choose the b^*-th subgroup, where we obtain

$$b^* = \underset{b \in \mathbb{B}}{\operatorname{argmax}}\, \hat{T}_{j,k}^{r,b} \overset{(a)}{\equiv} \underset{b \in \mathbb{B}}{\operatorname{argmax}}\, \hat{\gamma}_{j,k}^{r,b}. \tag{4.18}$$

Here $\mathbb{B}$ denotes the set of available subgroups at R_r and (a) follows from the monotonic nature of $\log_2(\cdot)$. It is worth observing that the selection of a particular subgroup does not necessarily imply $\delta_p = 0$ for the same. The reason for this is attributed to the fact that, generally we have $\left|h_{U_j,R_{r,b_1}}\right| \neq \left|h_{U_j,R_{r,b_2}}\right|$ and $\left|g_{R_{r,b_1},U_k}\right| \neq \left|g_{R_{r,b_2},U_k}\right|$ for $b_1 \neq b_2$ and $b_1, b_2 \in \mathbb{B}$. Hence, the choice of the available subgroup with the minimum corresponding δ_p value does not always give the desired result.

4.4.3 Scheduling Strategy at the IU

The current state of an IU plays a crucial role if we are to comment on whether its selection as a relay is appropriate for a particular source-destination pair. Hence, we consider two separate scenarios, where a particular IU is idle or busy and accordingly decide on the scheduling strategy.

4.4.3.1 IU is presently idle

Here, we assume that none of the IUs are aware of the entire topology as they can only communicate within a circular range of radius r. As a result, by using the beacon transmission technique [82], the idle IUs U_i are first identified in that range. Thereafter, based on its traffic characteristics, we estimate the time $\kappa_{I,i}$ for which it will continue to remain idle. Accordingly, $\kappa_{I,i}$ is estimated as

$$\kappa_{I,i} = \lambda_i \ln \left(\frac{1}{1 - \delta_e}\right), \tag{4.19}$$

where δ_e is the acceptable error threshold and λ_i depends on the traffic characteristics of U_i (defined in Section 4.3.3). During this time interval, U_i acts as a relay for the other active

IUs. Suppose, at any arbitrary point of time, there are $N_A(\leq N)$ sources $S_1, \cdots, S_{N_A}$ wanting to communicate with their respective destinations $D_1, \cdots, D_{N_A}$ via the IUs. The minimum number of hops required to send packets from S_n to D_n within a delay constraint T_{d_n} is $\Psi = \left\lceil \frac{l}{r} \right\rceil$, where l is the Euclidean distance from S_n to D_n. Moreover, U_i agrees to act as a relay only for those IU pairs, whose maximum possible delay at U_i, i.e., $T_{d_{n,i}}$ $\forall\, n = 1, \cdots, N_A$ is less than $\kappa_{I,i}$ and the remaining are discarded automatically. But, an idle IU can serve a single request at a time. Therefore, if there are N_κ $(\leq N_A)$ candidates requesting for U_i, these sources are prioritized depending on their respective acceptable delay limits $T_{d_{n,i}}$ $\forall\, n = 1, \cdots, N_\kappa$.

Accordingly, let p_j $\forall\, j = 1, \cdots, N_\kappa$ be the priority of the j-th requesting pair. Also, we define a quantity q_j, which is associated with the channel condition while transmitting a signal from U_i to the next relay node of the $S_j - D_j$ pair. Accordingly, to decide among the candidate requesting pairs at U_i, we define a quantity β as a convex combination of priority and the channel condition, i.e.,

$$\beta = cp_j + (1-c)q_j \qquad \text{where} \qquad c \in [0,1]. \tag{4.20}$$

The choice of c depends on the application under consideration. Finally, the candidate with maximum β is selected and by continuing this process, the transmitted packet reaches its destination within a delay bound. To obtain more analytical insights, we consider the above-mentioned extreme scenarios, i.e., $c = 0, 1$.

4.4.3.2 When $c = 0$

This denotes a channel-aware delay unconstrained scenario, where U_i always chooses the candidate with best channel condition, irrespective of its priority status. In case the connection does not involve any RIS, adaptive modulation (discussed in Section 4.4.4) is employed and the corresponding data rate is determined. Note that, the scenario of considering $c = 0$ and not involving any RIS, essentially represents the classical problem of channel-aware scheduling in a multiple-user scenario [94].

4.4.3.3 When $c = 1$

This implies that unaware of the channel conditions, the selection decision is solely based on the priority of the requesting candidates.

In this case, suppose $S_j - D_j$ is the selected source-destination pair with T_{d_j} being the associated maximum acceptable delay. The computation of the corresponding data rate is discussed in Section 4.5.

4.4.3.4 U_i is currently busy but the time after which it becomes idle can be estimated

There may be instances where an idle IU is unavailable presently. If U_i becomes available after a certain time, it may be able to assist in signal transfer for a requesting pair. Therefore, based on the user traffic characteristic, we estimate the time $\eta_{w,i}$ after which U_i is expected to become idle, i.e., after $\eta_{w,i}$ time slot, U_i will be available. Consequently, $\eta_{w,i}$ is estimated as

$$\eta_{w,i} = \mu_i \ln \left(\left(\frac{1 - e^{1/\mu_i}}{p_{\text{th}}} \right)^+ \right) + 1. \tag{4.21}$$

where μ_i depends on user traffic characteristic of U_i, p_{th} is an acceptable threshold probability, and $x^+ = \max(x, 1)$. As this is a cooperative framework, after $\eta_{w,i}$ time slot, U_i becomes idle and it agrees to serve as a relay node. Hereafter, the quantity $\kappa_{I,i}$ from (4.19) is estimated. However, in this context, U_i agrees to act as relay only for those IU pairs, whose maximum possible delay at U_i is less than $\eta_{w,i} + \kappa_{I,i}$. We assume that there are $N_{\eta\kappa} (\leq N_A)$ requesting pairs and the approach as to how a requesting pair is served by the U_i is similar to what is described in the previous subsection.

Remark 10. *Note that, in this work, the scheduling depends on the weighted combination of the priority and channel conditions. However, if one is eager to look into some other parameters, the extension is trivial. Specifically, if there are n parameters of concern, we have*

$$\beta = \sum_{i=1}^{n} c_i x_i, \tag{4.22}$$

where $\sum_{i=1}^{n} c_i = 1$ *and* $c_i \in [0, 1] \; \forall \; i = 1, \cdots, n$.

4.4.4 Adaptive Modulation at the Intermediate Users

Based on β, a particular service request is chosen by an IU. Therefore, the IU forwards the requesting pair's data to the subsequent hop, and a strategic choice of the subsequent hop is essential in the delay constraint communication scenario. However, to select the subsequent hop, we take into account the achievable data rate at the next IU. We accomplish this by

utilizing an IU-IU connection with an adaptive modulation scheme. Note that, adaptive modulation is employed if and only if a connection is established between consecutive IUs without the involvement of any RIS. Now, we go into more detail about the adaptive modulation methods below.

The primary objective, in this case, is not simply to transfer data from S_i to D_i, but also to take care of the delay constraint. Hence, in this work, we consider channel adaptive communication [95] with fixed transmission power at the IUs. However, the IUs use rate adaptation if and only if they are in direct LoS with one another and no RIS is being used to link them. Let m_r be the modulation scheme for an IU, where $m_r \in \mathbf{M} = \{m_1, m_2, \cdots, m_{|\mathbf{M}|}\}$ and corresponding data rate is $D_r = \log_2(m_r)\ \forall\ r = 1, 2, \cdots, |\mathbf{M}|$. The choice of m_r depends on the wireless channel, where the complex channel gain h, BER P_b, constellation size m_r, and the received power $P_{\text{tx}}\rho_{\text{L}}d^{-\alpha}|h|^2$ are related as [95]:

$$P_b = c_1 \exp\left(\frac{-c_2 P_{\text{tx}}\rho_{\text{L}}d^{-\alpha}|h|^2}{\sigma_0^2(m_r^{c_3} - c_4)}\right). \tag{4.23}$$

Here σ_0^2 is the noise power, and $c_1, \cdots, c_4$ are modulation-specific constants, respectively. The above equation explains the relation between the chosen modulation scheme and the application-specific acceptable BER. The channel configuration between two IUs determines m_r. On the chosen m_r, for a complete transfer of α_k packets with ϕ_k bits each, it take $\tau(r) = \left\lceil \frac{\alpha_k \phi_k}{D_r} \right\rceil$ slots, where $\lceil \cdot \rceil$ denotes the ceiling function.

4.4.5 Next Hop Selection Criteria

It is noted that, in the considered scenario of joint RIS and IU-assisted multihop framework, the classical LRD-based approach may not always yield the optimal routing solution. The LRD-based solution necessarily focuses on the fact that in the process of information transfer of an arbitrary $S - D$ pair, we always choose that particular IU/RIS at each hop, which minimizes the minimum distance towards D from S. However, by doing so, we are overlooking aspects like the channel condition and/or the IU availability. As a result, at each hop, which can be an IU or RIS, only that candidate is chosen that has the best channel condition or sufficient idle time for which it can act as a DF relay or both, such that the respective delay constraint is not violated. In this context, an extensive delay analysis is provided in Section 4.5. Depending on the channel condition and the availability of an IU, we go for RIS or IU. In our next hop selection process, by considering the channel condition

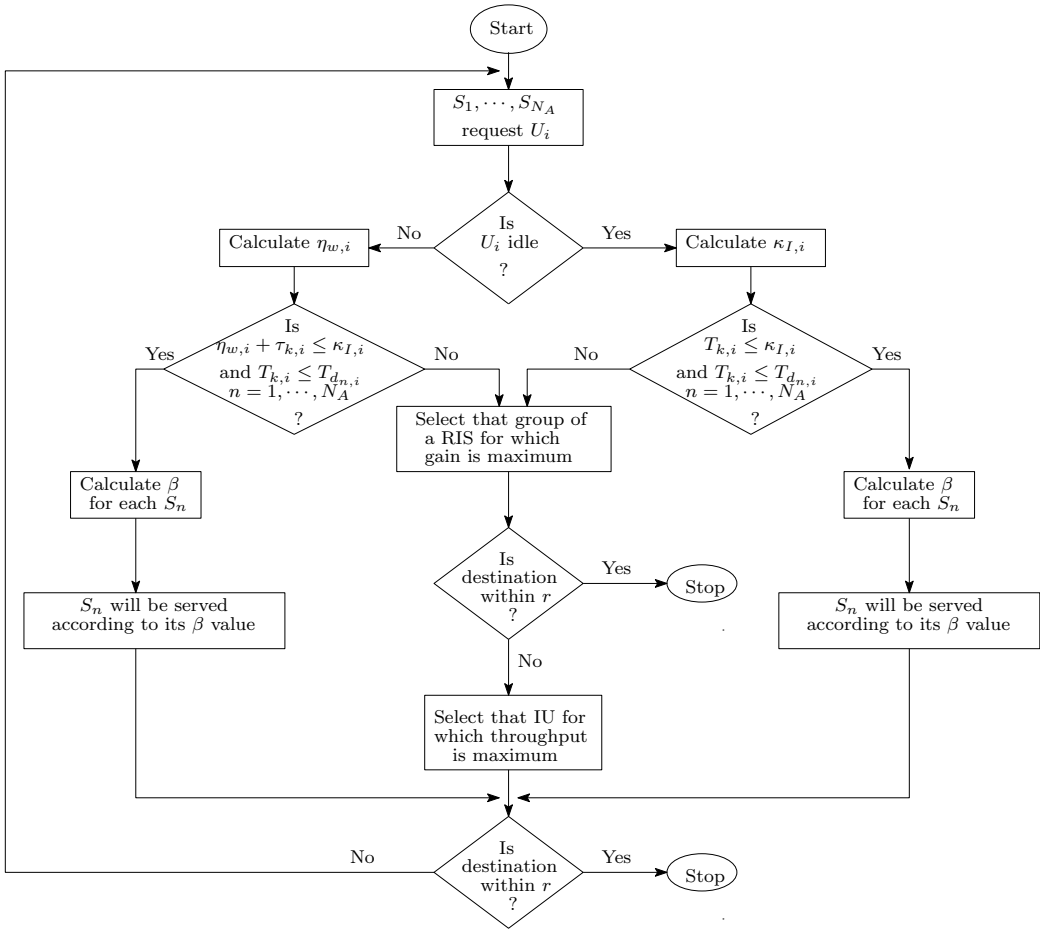

Figure 4.2: Flowchart of the proposed strategy.

and IU availability, we select that one as the next hop for which the achievable data rate is maximum. Accordingly, a particular algorithm is described in Fig. 4.2. However, we demonstrate the justification of our claim later in the result section.

4.4.6 Illustrative Example for Proposed Strategy

The entire proposed strategy is presented in Fig. 4.2 in the form of a concise flowchart, which is illustrated below with the help of an example. As demonstrated in Fig. 5.3, N sources $S_1, \cdots, S_N$ want to communicate with their respective destination $D_1, \cdots, D_N$ via IU U_1. The sources are prioritized based on their β values, i.e., acceptable delay limit and channel condition. We consider in this work that if U_1 is idle, it agrees to act as a relay, with the higher priority users being served first. In this figure, we assume S_1 to have the highest priority and hence, it is served prior to $S_2, \cdots, S_N$. Since there is no direct

$U_1 \rightarrow U_2$ or $U_1 \rightarrow U_3$ LoS link, U_1 sends the packets to U_2 or U_3 via the RIS $R_{1,1}$. Here, we consider that the concerned RIS R_1 is already partitioned into four non-overlapping surfaces, $R_{1,1}, R_{1,2}, R_{1,3}$ and $R_{1,4}$, respectively. For communication purposes, U_1 selects $R_{1,1}$ to connect to D_1 via U_2 or U_3. It is interesting to note, that although LRD from U_3 to D_1 is greater than that from U_2 to D_1, U_3 is selected as the next hop. The reason for is attributed to the higher effective throughput in the case of $U_1 \rightarrow R_1 \rightarrow U_3$ link as compared to $U_1 \rightarrow R_1 \rightarrow U_2$. Finally, U_3 forwards the information packets to U_4, which in turn forwards the same to D_1 and this completes the process.

4.5 Analysis of the Proposed Scheduling Strategy

As stated earlier in Section 4.4.3, here we investigate our proposed strategy in terms of delay-related metrics for information transfer from a source to a destination. The transmitted signals from a source reach their desired destination using IUs as well as RISs as hops. Now we go into more detail about the scenarios that are discussed in Section 4.4.3.

When the N_A sources place their request to U_i, depending on the considered value of c in (4.20), it calculates β for all of them. Accordingly, the βs are arranged in decreasing order and maintained in a queue, with the source corresponding to the maximum β getting service first. Therefore, the knowledge of c is useful for maintaining the queue of requested sources, i.e., which source will get service before or after the rest. With the arrival and the service rate of U_i being denoted by $\lambda_{i,a}$ and $\mu_{i,i+1}$, respectively, the sources receive non-preemptive service in decreasing order of β. This implies that a particular source, if selected by U_i for service, continues to receive the same, irrespective of the arrival of any other source (even with higher β). In case a source with higher β arrives, it receives service only after the ongoing work has been completed. This results in a queuing delay, which is estimated below.

Here we first analyse the delay bound for a single hop and then characterize the same for complete information transfer between intended $S - D$ pair.

4.5.1 U_i Status Aware Single Hop Delay Bound

Specifically, we consider two separate scenarios as follows.

1. U_i is presently idle

2. U_i is currently busy but the time after which it becomes idle can be estimated

4.3.1.1: U_i is presently idle

In this scenario, the source with maximum β gets immediate service, i.e., no queuing delay. Suppose $W_{k,i}$ be the waiting time of the k-th requesting source $\forall\ k = 1, \cdots, N_\kappa$ at U_i. Hence, as U_i is currently idle, for a source with highest β, we have $W_{1,i} = 0$. For a source with the second largest β, $W_{2,i}$ depends on the processing time of the former. In general, if we denote the processing time of the k-th source at U_i as $\tau_{k,i}(q_k)$, where q_k depends on the modulation employed (discussed in Section 4.4.4), we observe that $W_{k,i}$ is a function of $\tau_{2,i}(q_2), \cdots, \tau_{k-1,i}(q_{k-1})$, which in turn depends on the channel condition of the corresponding source-destination pairs. Accordingly, the data transfer rate for the chosen pair is based on the discussion in Section 4.4.4. Thereby, the processing time of k-th pair is

$$\tau_{k,i}(q_k) = \frac{\alpha_k \phi_k}{\mu_k}, \tag{4.24}$$

where the k-th source needs to transfer α_k packets of data with ϕ_k bits in each of them and μ_k is the channel-dependent service rate. Hence, we obtain the corresponding $W_{k,i}$ as

$$W_{k,i} = \sum_{j=1}^{k-1} \tau_{j,i}(q_j) = \sum_{j=1}^{k-1} \frac{\alpha_j \phi_j}{\mu_j} \tag{4.25}$$

Therefore, the total time required for the k-th pair at U_i is the sum of $W_{k,i}$ and its own processing time, i.e., the total time for the information transfer is

$$T_{k,i} = W_{k,i} + \frac{\alpha_k \phi_k}{\mu_k} = \sum_{j=1}^{k} \frac{\alpha_j \phi_j}{\mu_j}. \tag{4.26}$$

We assume that U_i shares the information about its current status as well as the list of other sources waiting to be served, with each of the incoming requesting pair. Accordingly, the k-th incoming source waits for service at U_i iff $T_{k,i} \leq \kappa_{I,i}$. Note that the requesting sources are serviced at U_i based on their corresponding β values, where the processing time depends on the channel conditions.

Hence, in the worst scenario, to guarantee a successful information transfer session, the entire process takes place with the minimum possible data rate, say binary phase shift keying (BPSK), with the service rate being $\mu_k = 1\ \forall\ k$. Therefore, in this case, we obtain

$$\tau_{k,i}(q_k) = \alpha_k \phi_k \text{ and } W_{k,i} = \sum_{j=1}^{k-1} \alpha_j \phi_j \tag{4.27}$$

from (4.24) and (4.25), respectively. Hence, from (4.26) we obtain

$$T_{k,i} = \sum_{j=1}^{k} \alpha_j \phi_j. \tag{4.28}$$

The best case scenario implies that it is possible to process the data at the maximum possible data rate. If $\mu_{\max}$ be the corresponding service rate, we obtain

$$W_{k,i} = \frac{1}{\mu_{\max}} \sum_{j=1}^{k-1} \alpha_j \phi_j \text{ and } T_{k,i} = \frac{1}{\mu_{\max}} \sum_{j=1}^{k} \alpha_j \phi_j. \tag{4.29}$$

Remark 11. *By considering the two extreme cases from* (4.28) *and* (4.29)*, we can state that*

$$\frac{1}{\mu_{\max}} \sum_{j=1}^{k} \alpha_j \phi_j \leq T_{k,i} \leq \sum_{j=1}^{k} \alpha_j \phi_j \ \forall \ c \in [0,1]. \tag{4.30}$$

Note that the application-specific nature of the quantity c is responsible in the calculation of β at an IU. It does not have any impact on the bound on $T_{k,i}$ as stated above.

4.3.1.2: U_i is currently busy but the time after which it becomes idle can be estimated

Here we first estimate the time interval $\eta_{w,i}$ from (4.21), after which a particular IU becomes idle, given that it is currently busy. Note that, while the requesting pair with maximum β was immediately getting service in the previous scenario, here it has to wait for time $\eta_{w,i}$, i.e., in this case, we have $W_{1,i} = \eta_{w,i}$ and not $W_{1,i} = 0$ as previously discussed. Apart from this, the entire approach of estimating $W_{k,i}$ remains the same. Therefore, from (4.25) and (4.26), we can aptly state that $\forall\ c \in [0,1]$, we have

$$W_{k,i} = \eta_{w,i} + \sum_{j=1}^{k-1} \frac{\alpha_j \phi_j}{\mu_j} \text{ and } T_{k,i} = W_{k,i} + \frac{\alpha_k \phi_k}{\mu_k}. \tag{4.31}$$

As a result, similar to Remark 11, in this case we obtain

$$\eta_{w,i} + \frac{1}{\mu_{\max}} \sum_{j=1}^{k} \alpha_j \phi_j \leq T_{k,i} \leq \eta_{w,i} + \sum_{j=1}^{k} \alpha_j \phi_j \ \forall \ c \in [0,1]. \tag{4.32}$$

Hence, we can summarize the complete subsection by generalizing the entire proposed framework as follows.

$$W_{k,i} = \begin{cases} a_i \eta_{w,i} + \dfrac{1}{\mu_{\max}} \displaystyle\sum_{j=1}^{k-1} \alpha_j \phi_j & \text{best scenario,} \\ a_i \eta_{w,i} + \displaystyle\sum_{j=1}^{k-1} \alpha_j \phi_j & \text{worst scenario.} \end{cases} \tag{4.33}$$

and

$$T_{k,i} = \begin{cases} a_i \eta_{w,i} + \dfrac{1}{\mu_{\max}} \displaystyle\sum_{j=1}^{k} \alpha_j \phi_j & \text{best scenario,} \\ a_i \eta_{w,i} + \displaystyle\sum_{j=1}^{k} \alpha_j \phi_j & \text{worst scenario.} \end{cases} \tag{4.34}$$

Here, $a_i = 0$ implies that U_i is idle and $a_i = 1$ otherwise.

4.5.2 Delay Bound for Complete Information Transfer for a Particular $S - D$ Pair

Let for an arbitrary $S_m - D_m$ pair, the information from S_m reaches D_m via n IUs $U_1, \cdots, U_n$. Hence, if the maximum acceptable waiting time and the actual waiting time at U_i is $T_{d_{m,i}}$ and $t_{d_{m,i}}$, respectively, $\forall\, i = 0, \cdots, n$, we must have

$$\sum_{i=0}^{n} T_{d_{m,i}} \leq T_{d_m}, \tag{4.35}$$

where T_{d_m} is the maximum acceptable delay for the entire process of information transfer from S_m to D_m. In the case of $t_{d_{m,i}} \leq T_{d_{m,i}}$ at U_i, the leftover waiting time $T_{d_{m,i}} - t_{d_{m,i}}$ is carried forward to U_{i+1}, i.e., the maximum acceptable waiting time $T_{d_{m,i+1}}$ at U_{i+1} is now updated as $T_{d_{m,i+1}} + (T_{d_{m,i}} - t_{d_{m,i}})$. This transfer of the 'left-over' time at a particular hop to the consecutive ones is based on the fact that we consider a scenario, where the IUs do not have a global knowledge of the system topology, i.e., they cannot communicate beyond a distance r. Therefore, U_i passes on $T_{d_{m,i}} - t_{d_{m,i}}$ to U_{i+1}, as it is unaware of exactly how many hops will be required for the complete information transfer.

Since the priority of $S_0 - D_0$ pair at U_i is inversely proportional to $T_{d_{0,i}}$, which in turn directly affects the calculation of β value at U_i, we can rightly state that the priority parameter is not identical at each of the n hops. For example, if the $S_0 - D_0$ pair is the k-th

candidate to be served at U_i (based on the calculation of the β values at U_i), this does not guarantee that it will also be the k-th candidate at $U_j \; \forall \; j \neq i$. We now provide a bound on the total time for information transfer corresponding to the $S_m - D_m$ pair, i.e., $\sum_{i=0}^{n} T_{d_{m,i}}$. From (4.31), we obtain the following.

$$\sum_{i=0}^{n} T_{d_{m,i}} = \sum_{i=0}^{n} a_i \eta_{w,i} + \sum_{i=0}^{n} \sum_{j=1}^{k_i} \frac{\alpha_m \phi_m}{\mu_j}, \tag{4.36}$$

where $a_i = 0$ implies that U_i is idle and $a_i = 1$, otherwise. Here, S_m intends to transfer α_m data packets of ϕ_m bits each to D_m and this $S - D$ pair is served at the k_i-th position at the i-th hop with the corresponding service rate μ_{k_i}. Note that, as discussed above, we do not guarantee $k_i \neq k_j \; \forall \; i \neq j$.

Remark 12. *If an arbitrary $S_m - D_m$ pair requires IUs $U_1, \cdots, U_n$ for complete information transfer, we have*

$$\frac{n\alpha_m \phi_m}{\mu_{\max}} \leq \sum_{i=0}^{n} T_{d_{m,i}} \leq \sum_{i=0}^{n} \eta_{w,i} + nk_{\max} \alpha_m \phi_m, \tag{4.37}$$

where $k_{\max}$ denotes the index of the last $S - D$ pair to be served by U_i $i = 1, \cdots, n$ such that (4.35) *holds. Note that the lower bound indicates the best case scenario, i.e., the $S_m - D_m$ pair finds all the IUs idle, gets served first among the competitors, and that also with the best channel condition. On the contrary, the upper bound implies that this $S - D$ pair has to wait at all the n hops, is always the last to be served by the IUs, and that too with the worst possible channel condition.*

Finally, Remark 12 holds for the scenario, where IUs are available for each hop and the RISs in the surroundings are not being used at all. In cases where the RISs are being used due to IU unavailability, the only difference will be that the service rate μ_j in (4.36) will get replaced by $\hat{T}^{r,b}_{j,j+1}$ from (4.17).

4.6 Numerical Results

In this section, we demonstrate the effectiveness of our proposed strategy and compare it with the existing benchmark schemes. Here we assume a Rician fading scenario, where the Rician factor is $K = 10$ dB. To simulate the results, we consider the IU transmission

Table 4.1: Transmission Modes for $P_b = 10^{-6}$.

SNR interval (dB)	Modulation	Rate (bits/sym.)
$(-\infty, 9.8554)$	No transmission	0
$[9.8554, 12.8657)$	BPSK	1
$[12.8657, 14.6266)$	QPSK	2
$[14.6266, 15.8760)$	8-QAM	3
$[15.8760, 16.8451)$	16-QAM	4
$[16.8451, 17.6369)$	32-QAM	5
$[17.6369, 18.3063)$	64-QAM	6
$[18.3063, 18.8863)$	128-QAM	7
$[18.8863, +\infty)$	256-QAM	8

power $P_{\text{tx}} = 30$ dBm, IU processing power $P_t = 10$ dBm, phase shift power consumption, i.e, the power required to shift the phase of a RIS patch is $P_{\text{ph}} = 5$ dBm [96], acceptable delay bound $T_d = 50$ ms [87], path loss at one meter distance $\rho_L = 10^{-3.53}$ [71], path loss exponent $\alpha = 4.2$ between two consecutive IUs and $\alpha = 2$ elsewhere, slot duration $T_s = 100\ \mu s$ [75] and wavelength $\lambda = 0.1$ m [19]. Moreover, a particular source S sends 10^6 data packets of unit length to its desired destination D and unless otherwise stated, we consider each RIS consisting of 400 individual reflecting patches. Furthermore, we employ the M-ary quadrature amplitude modulation (M-QAM) technique with a BER of $P_b = 10^{-6}$ as stated in Table 4.1. Finally, we compare our strategy with the existing approaches.

4.6.1 Impact of Grouping and Spatial Correlation

By accounting for the spatial correlation, here we demonstrate the advantage of grouping in terms of the achievable data rate. A particular RIS is sub-divided into groups with identical number of patches and patch spacing being $\lambda/8$ for the *correlated* scenario. Moreover, only one of these groups is used for the purpose of information transfer and the results corresponding to the *independent* channel scenario is obtained by setting the patch spacing to $\lambda/2$. Fig. 4.3 illustrates the achievable data rate versus the number of groups into which the RIS has been sub-divided and this depicts the importance of incorporating the aspect of spatial correlation. Intuitively, this gain in performance can be understood from (4.7), i.e., grouping essentially implies combination of channels corresponding to the adjacent patches. Hence, the combination is more likely to be constructive when the channels are correlated. We also observe, that the ideal group size is somewhere in between the two

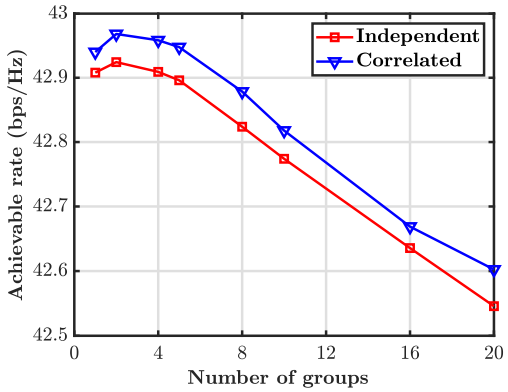

Figure 4.3: Impact of number of groups on achievable data rate.

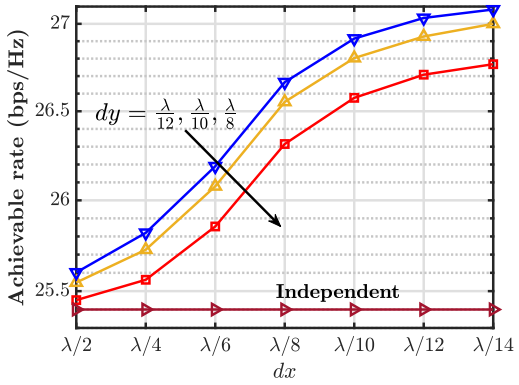

Figure 4.4: Impact of patch spacing on achievable data rate.

extreme scenarios of considering the group size to be unity or the total number of patches in the RIS. This further corroborates the trade-off investigated in [22] between the channel estimation overhead and the power gain offered by the group.

For a fixed number of patches in a group, Fig. 4.4 depicts the effect of the patch spacing on achievable data rate. In this context, we define the quantities dx and dy, which denote the horizontal and vertical distance between consecutive patches, respectively. We observe that for a fixed dx, the achievable rate increases with decreasing dy and vice-versa; for example, note the performance gap at $dx = \lambda/12$ between $dy = \lambda/12, \lambda/10$, and $\lambda/8$. This justifies the effect of spatial correlation in (4.6), which implies that the correlation is inversely proportional to the patch spacing. On the contrary, note that this aspect of patch distance does not have any impact in the *independent* scenario, i.e., when $dx = dy = \lambda/2$.

Fig. 4.5 shows the achievable data rate, defined in (4.17), as a function of the number of patches in a group. In this context, we consider groups with both *optimal* as well as *random* phases, where the optimal phase shift is calculated as in (4.4.2). Moreover, as proposed in

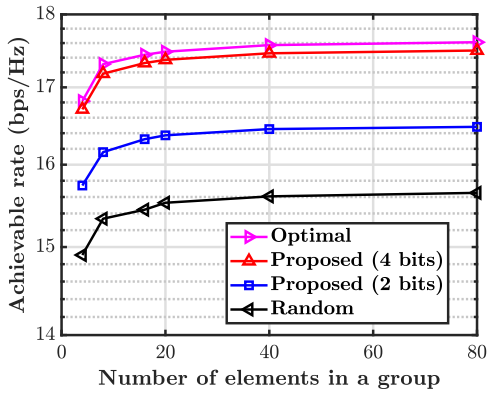

Figure 4.5: Impact of the number of patches in a group on achievable data rate.

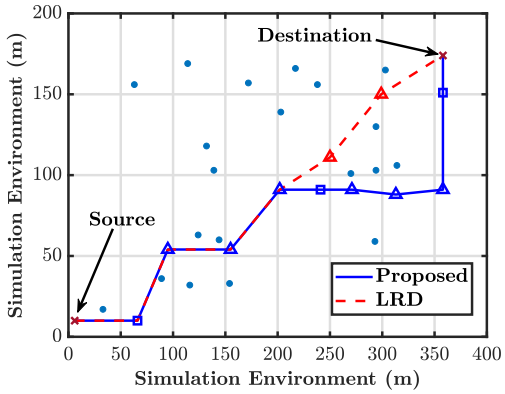

Figure 4.6: Trajectories for both the proposed framework and LRD-based approach; □ denotes RIS and Δ denotes IU.

Section 4.4.2, we also take into account the scenario when the optimal phase shift is not a continuous quantity but it is chosen from a finite set of predetermined values. Specifically, in our *proposed* approach, we consider the group to be 2 and 4 bit coded, i.e., we choose the phase shift that is closest to the optimal from a set of $4(=2^2)$ and $16(=2^4)$ predetermined values, respectively. The figure demonstrates that, irrespective of the scenario, the achievable rate increases with the number of patches while the performance is worst in the case of random phases. Moreover, with an increase in the number of coded bits, the performance approaches the optimal. As can be seen, the achievable data rate with 4 coded bits almost merges with its optimal counterpart.

4.6.2 Performance of Proposed Framework

An illustration of the proposed strategy based trajectory is presented in Fig. 4.6. Here, we consider a two-dimensional squared area of 400×400 m^2 where the RISs and IUs are

placed strategically and randomly, respectively. Moreover, we assume that an IU has a coverage of 60 meters, i,e., it cannot communicate beyond this distance. Furthermore, we consider a randomly selected $S - D$ pair in this grid, which is separated by a distance more than the coverage radius. Accordingly, a communication link is established both by the proposed strategy as well as the conventional LRD-based approach. The figure demonstrates that the proposed strategy requires more number of hops as compared to the other. However, in spite of this observation, to comment on the advantages of the former, we first define the following metrics.

4.6.2.1 Data throughput $\mathrm{D_T}$

We assume that the information transfer from S to D takes place by using $\aleph$ IUs and a certain number of RISs. Hence, S transfers the data packets in $\aleph + 1$ hops to D. Therefore, the data throughput is defined as

$$\mathrm{D_T} = \frac{1}{\sum\limits_{i=1}^{\aleph+1} \dfrac{1 - t_i}{(1 - P_b)\, m_{r_i}} + \dfrac{t_i}{T_i\,(\gamma_i)}}, \tag{4.38}$$

where

$$t_i = \begin{cases} 1, & \text{if } i\text{-th hop involves RIS,} \\ 0, & \text{else.} \end{cases}$$

Here P_b is the BER, m_{r_i} is the appropriate constellation size from Table 4.1, and T_i represents the achievable data rate from (4.8), when a RIS is chosen due to appropriate IU unavailability.

4.6.2.2 Energy Consumption $\mathrm{E_C}$

The system energy consumption for sending α_k packets of data with φ_k bits in each, where the $S - D$ pair connects in $\aleph + 1$ hops, is defined as

$$\begin{aligned} \mathrm{E_C} = \alpha\varphi \sum_{i=1}^{\aleph+1} \left(\frac{1 - t_i}{(1 - P_b)\, m_{r_i}} + \frac{t_i}{T_i\,(\gamma_i)} \right) \\ \times \left(P_{\mathrm{tx}} + s_i P_t + t_i P_{\mathrm{ph}} \right), \end{aligned} \tag{4.39}$$

where P_b, m_{r_i}, t_i and $T_i\,(\gamma_i)$ are already defined above and

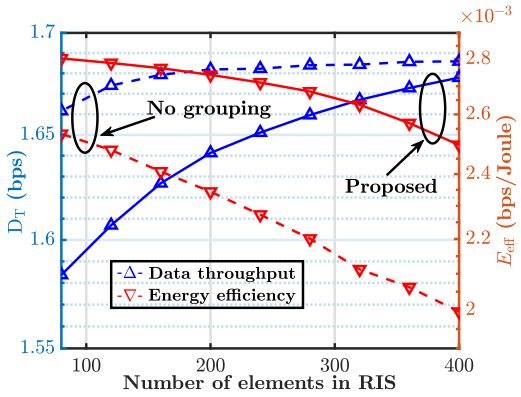

Figure 4.7: Performance trade-off investigation.

$$s_i = \begin{cases} 0, & \text{for } i = 1, \\ 1, & \text{else.} \end{cases}$$

Here, P_{tx}, P_t, and P_{ph} are the transmission, processing and phase shift power consumption, respectively. Note that, P_{ph} is considered only if a particular hop involves a RIS.

4.6.2.3 Energy Efficiency E_{eff}

Based on $\mathrm{D_T}$ and $\mathrm{E_C}$ from (4.38) and (4.39), respectively, the corresponding trajectory energy efficiency is obtained as

$$E_{\text{eff}} = \frac{\mathrm{D_T}}{\mathrm{E_C}}. \tag{4.40}$$

Based on these definitions, now we discuss the advantages of the proposed framework.

Fig. 4.7 illustrates the importance of RIS grouping on the performance indicators, i.e., $\mathrm{D_T}$ and $\mathrm{E_{eff}}$, as a function of the number of elements in a RIS. Namely, we investigate the impact of considering a no grouping-based scenario (nGBS) and a grouping-based scenario (nGBS), where the RIS to be subdivided into four groups of equal size and the total number of patches in the RIS is varied accordingly. We observe that in both cases, $\mathrm{D_T}$ $(\mathrm{E_{eff}})$ follows an increasing (decreasing) trend with the growing number of elements. This is because, growing number of patches supports better throughput. Note that, nGBS results in a higher data throughput as compared to GBS. This is intuitive as, unlike GBS, nGBS uses the entire RIS, which employs a fraction of the total number of patches in the RIS. Note that, nGBS limits the RIS usage to a single user, at any arbitrary point in time. On the contrary, GBS results in an enhanced energy efficiency performance. Hence, depending on the application at hand, for example, in a dense surrounding, we propose the usage of the GBS framework,

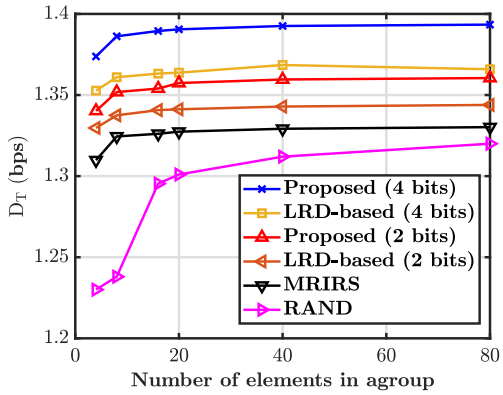

Figure 4.8: Comparison of Data throughput.

which leads to better E_{eff} performance and also, more users can be catered to by the RISs at the same time.

Hereafter, we briefly discuss the existing benchmark schemes, which will be employed for the purpose of performance comparison.

1. LRD [63]: A least remaining distance-based approach is considered, where factors such as wireless channel fluctuations are not taken into account. The sole objective here is to reduce the remaining distance to the destination in each hop.

2. MRIRS [54]: The work involves multihop route establishment between S and D, without considering factors such as user traffic characteristics or channel aware adaptive modulation (AM).

3. RAND [59]: The work investigates the impact of random phase shifts and its impact on the corresponding achievable data rate. It doesn't entail any multihop communication between S and D.

Fig. 4.8 depicts an overall increasing trend of D_T with number of RIS elements in a group, irrespective of the scheme considered. The reason behind this observation can be attributed to the fact that for hops involving a RIS, the achievable throughput is a function of the number of reflecting elements that are being used. As the proposed strategy is IU traffic aware, involves channel-dependent transmission techniques, and also considers the aspect of spatial correlation among the reflecting patches, it performs significantly better compared to its competitors. Moreover, the figure illustrates the fact that, as we are dealing with a delay-constrained scenario, an LRD-based approach is not always the best solution. It may result in a lesser number of hops (as observed in Fig. 4.6) but at the cost of reduced

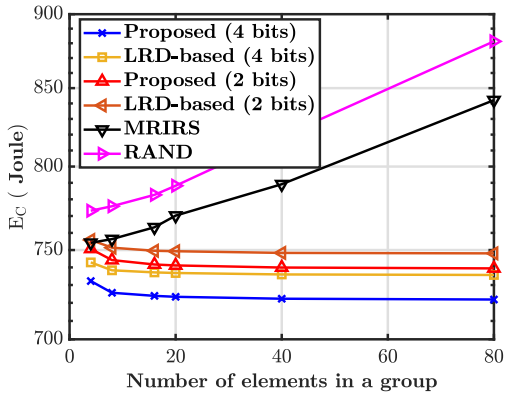

Figure 4.9: Performance comparison: Energy consumption.

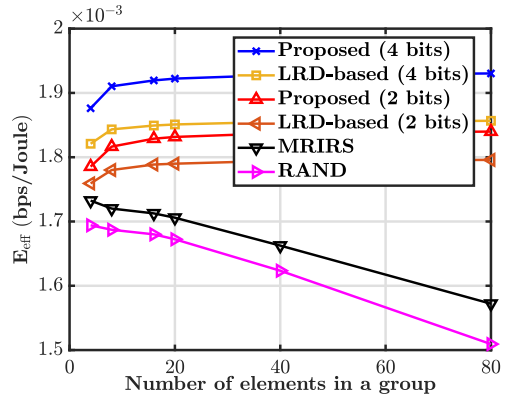

Figure 4.10: Performance comparison: Energy efficiency.

data rate due to factors such as wireless channel fluctuations. Furthermore, here also we observe the impact of having more number of coded bits in the RIS.

Fig. 4.9 investigates the aspect of energy consumption among the proposed strategy and the existing benchmarks. It is interesting to note that E_C, in the context of both our strategy and the LRD-based approach, decreases with an increasing number of elements in a RIS group. The reason behind this counter-intuitive observation is that, in both these scenarios, irrespective of the group size, a single phase shift is required for the entire group and the LRD becomes a criteria only when the next hop choice is concerned. Moreover, as observed from (4.8), the achievable data rate increases with the group size. Hence, when we combine both these factors, it leads to this interesting insight, which can also be noted from (4.39). On the contrary, both for MRIRS and RAND, as individual phase shifts are required at all the patches, the energy consumption increases linearly with increasing group size.

Finally, Fig. 4.10 shows the impact of the proposed strategy on the system energy efficiency. We observe that, while E_{eff} for MRIRS and RAND monotonically decreases

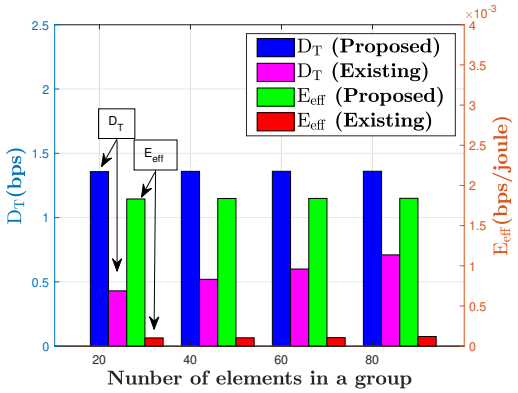

Figure 4.11: Impact of joint IU-RIS framework.

with the number of reflecting elements in a group, it follows an exact opposite trend in the context of our proposed strategy. The reason behind this observation is identical to the one as already described above in the discussion related to Fig. 4.9.

As discussed earlier, specifically the existing work in [58] investigates the aspect of energy efficiency maximization in the context of multihop RIS-assisted wireless networks. However, we argue, that there will be significant attenuation of the transmitted signal, if only RISs and no IUs are used to connect a transmitter to its intended receiver. Hence, we propose a novel joint IU-RIS framework, which also depends on the traffic characteristics of the IUs and the associated spatial correlation at the RIS. In this context, by varying the number of reflective elements in the group, Fig. 4.11 compares the D_T and E_{eff} performance of [58] and our proposed strategy. We observe here, that irrespective of the nature of variation of these performance metrics, our proposed strategy consistently and significantly outperforms [58]. This demonstrates the importance of incorporating the idle IUs to act as relays and not solely rely on the RISs deployed in the surroundings. Moreover, this also avoids unnecessary wastage of resources, i.e., dense RIS deployment.

4.6.3 Impact of IUs on System Performance

In the proposed framework, Fig. 4.12 investigates the aspect of data throughput as a function of the IU density. Here, we consider that each RIS consists of four identical groups with $\lambda/8$ spatial distance. We observe that, irrespective of the scheme, D_T increases with the growing number of IUs. This is also intuitive, as the growing number of IUs implies greater IU availability, which in turn, reduces the required number of hops for information transfer. As a result, fewer RISs are being used with increasing IU density. Moreover, it

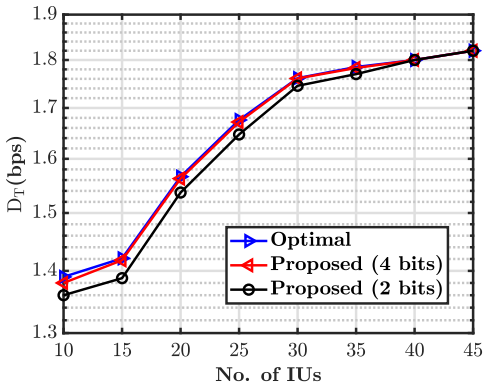

Figure 4.12: Impact of IUs: No. of IUs vs. data throughput.

is interesting to note that, the number of RIS used in establishing the desired multihop connection asymptotically reaches zero with increasing number of IUs in the surroundings. This explains the saturating trend of D_T with the number of IUs. Furthermore, with no RISs being used with higher number of IUs, the corresponding D_T of all the considered schemes merge together, i.e., when RISs are not being used, it does not matter, whether RIS grouping is considered or not.

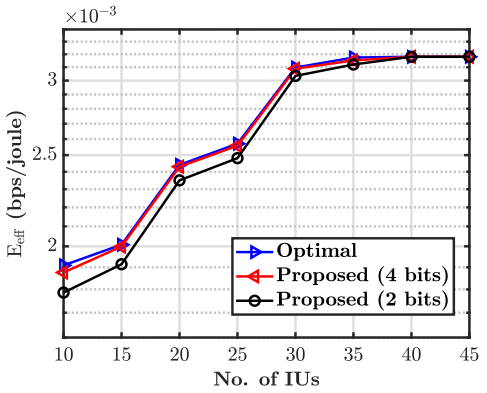

Figure 4.13: Impact of IUs: No. of IUs vs. energy efficiency.

In an identical setup as in Fig. 4.12, Fig. 4.13 demonstrates the impact of the IU density on the system energy efficiency E_{eff}. We observe that, for the scenarios as mentioned earlier, E_{eff} exhibits an increasing trend with the growing number of IUs. From (4.39), we note that, for a device pair to communicate via a RIS, an additional power consumption is incurred due to the required phase shift operation at the RIS. On the other hand, no such power consumption takes place if two devices communicate directly. As a result, a lesser amount of energy is required, i.e., a higher E_{eff}. Similar to the previous figure, here too, the RIS

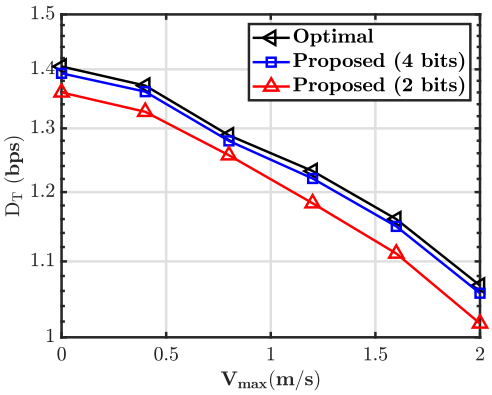

Figure 4.14: IU mobility vs. data throughput.

dependency reduces with the increasing number of IUs, which also explains the saturating nature of the curve.

User Mobility Model

As discussed earlier, here also a mobile scenario is considered, i.e., the IUs have a particular velocity in a certain direction. It is to be noted that this will have a significant effect on the performance of the proposed scheme, as the inter-IU distance changes during the process of information transfer. In this context, Fig. 4.14 illustrates the impact of IU mobility on the proposed framework, with the coverage being taken as 60 m and the mobility aspect being modeled by the standard RWP model [97]. Specifically, for this figure, we consider a pedestrian scenario [90], where we fix the maximum possible velocity $V_{\max}$ of the IUs, consider a random velocity chosen uniformly in $[0, V_{\max}]$ and observe its impact on the system data throughput. The figure illustrates that the performance deteriorates monotonically with increasing $V_{\max}$, which is intuitive. Such an observation is due to the mobility phenomenon, where a particular IU can move outside the coverage of another IU even during the communication process. This inevitably leads to outage, resulting in lesser data rate. Moreover, note that this figure with $V_{\max} = 0$ is a special case corresponding to the static scenario, i.e., Fig. 4.8. Furthermore, for a fixed $V_{\max}$, D_T decreases with the number of coded bits, which is also inline with the observation made in Fig. 4.8 as well.

4.7 Conclusion

In this paper, we proposed a novel priority-aware channel-dependent scheduling strategy for RIS-assisted multihop D2D communication, which also takes into account the aspect of element grouping at the RIS. The proposed strategy avoids resource wastage by exploiting the very structure of the RIS, the associated spatial correlation, and also the randomness in the wireless channel. Moreover, we also claim that, in this context of RIS-aided multihop routing, the LRD-approach does not always yield the best result in terms of system performance. Finally, numerical results demonstrate the advantages of the proposed framework in terms of higher data rate, lower energy consumption, and higher energy efficiency with respect to the existing benchmark schemes. An immediate extension of this work is to investigate scenarios, where even when idle, it depends on the IUs to decide whether to act as relays to its requesting neighbors or to prioritize its own sleep mode. Moreover, we intend to investigate the aspect of imperfect channel state and phase errors at the RISs on the proposed strategy. Finally, we also aim to comment on having various grouping criteria at the RISs and investigate its impact.

Chapter 5

Generalized Group Selection Strategies Using Self-sustainable RIS[1]

5.1 Introduction

In the preceding chapter, each device pair selects the most energy-efficient group, and if more than one pair chooses the same group, they are scheduled according to their priorities. However, the best group may lead to a large delay for some of the pairs. Moreover, the energy harvesting aspect is not considered there. Here, RIS-assisted grouping-based self-sustainable D2D communication with spatially correlated wireless channels is examined, along with different group selection techniques. The self-sustainable RIS's PS and TS configurations are specifically taken into account in order to assess system performance and suggest suitable limits on system parameter selection. The analysis considers both a realistic non-linear EH model and a simplified linear EH model. At the RIS, we suggest a number of group selection techniques based on the application requirements. Notably, each strategy schedules the k-th best available group at the RIS according to the energy harvested at a specific group of the RIS as well as the end-to-end SNR. Therefore, we derive analytical expressions for the outage probability of each selection strategy using tools from high-order statistics. Furthermore, we examine an asymptotic scenario in which the number of groups available for selection at a RIS approaches infinity by utilizing the tools from EVT. This approach yields nontrivial insights that are particularly useful in applications such as wireless communication aided by large intelligent surfaces. Finally, using metrics

[1]This chapter is based on the following publication:
L. Sau, P. Mukherjee, and S. C. Ghosh, "Generalized Group Selection Strategies for Self-sustainable RIS-aided Communication", **IEEE Transaction on Communications**, Vol. 74, pp. 6584-6598, DOI: 10.1109/T-COMM.2026.3675555

like data throughput and outage performance, the numerical results show the significance and advantages of the suggested approaches.

5.2 Chapter Organization

The chapter is organized as follows: System model and problem formulation are explained in Section 5.3, the system characterization is presented in Section 5.4, and the suggested group selection approaches are discussed in Section 5.5. The impact of the extreme value theorem on our proposed scheme is discussed in Section 5.6, numerical results are presented in Section 5.7, and Section 5.8 concludes the work.

5.3 System Model

Here, we discuss the considered system model and the related mathematical notations are summarized in Table I.

5.3.1 Network Model

As shown in Fig. 5.1, the considered topology consists of a single antenna source S and a single antenna destination D. Here, we assume that, due to the presence of obstacles, the direct LoS link does not exist between S and D. Therefore, an RIS, consisting of M reflecting elements, is employed to implement the entire communication process.

Notations: The probability distribution function (PDF) and cumulative distribution function (CDF) of a random variable X are denoted as $f_X(x)$ and $F_X(x)$, respectively. $E[\cdot]$ and $\mathrm{Var}(\cdot)$ denote the expectation and variance operators, respectively. Besides, $\Gamma(\cdot)$ and $\gamma(\cdot,\cdot)$ are the complete and the incomplete Gamma function, respectively. $B(\cdot,\cdot)$ is a Beta function, and $\mathcal{I}_\eta(a,b)$ is the incomplete normalized Beta function, which is defined by $\mathcal{I}_\eta(a,b) = \frac{1}{B(a,b)} \int_0^\eta y^{a-1}(1-y)^{b-1}$. Furthermore, $I_n(\cdot)$ is the first kind n-th order modified Bessel function [98].

5.3.2 RIS Characterization

As stated previously, we consider an RIS consisting of M reflecting elements. These reflecting elements are effectively controlled to adjust both the amplitude and phase of the

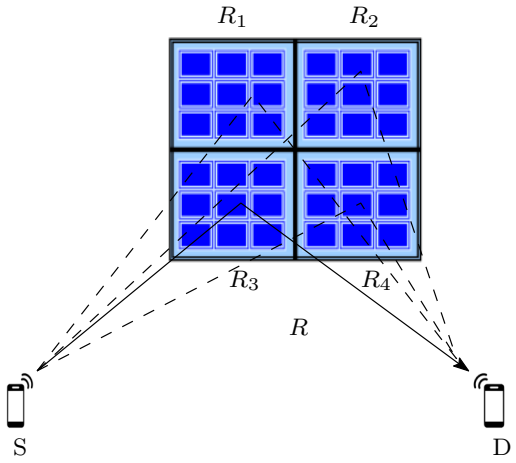

Figure 5.1: Considered system model.

incident waveform. However, we set the amplitude component to unity for mathematical tractability and simplicity. Moreover, we employ an RIS grouping strategy to reduce the channel estimation cost [22], where the RIS is partitioned into K_g non-overlapping sub-surfaces $R_i \; \forall \; i = 1, \ldots, K_g$ with M_g reflecting elements in each, i.e., $M = K_g \times M_g$. Note that the values of M and B are determined a-priori, a single group introduces a common phase shift, and at a particular instance, a group can serve only one request. In this scenario, each R_i has two possible states ON and OFF, and the phase of the incident signal can be changed to a desired direction while it is only in the ON state. Furthermore, a group R_i is configured in such a way, that the energy required for the phase shift operation is obtained by energy harvesting (EH) from the incident signals [38]. Additionally, we assume that the distance between two adjacent reflecting elements in a group is less than a half-wavelength, i.e., they are spatially correlated. In this context, we consider the following RIS configurations, namely, power splitting (PS) and time switching (TS).

5.3.2.1 PS Configuration

Here, the incident signals are designated as two separate streams, namely the information transmission (IT) stream and the EH stream [99, 100]. Specifically, the IT stream requires a sufficient amount of energy, which is provided by the EH stream. Also, the IT and EH stream division is controlled by the tunable power splitting factor ρ where $0 \leq \rho \leq 1$. We assume that only ρ portion of the received power is dedicated for EH and the remaining $1 - \rho$ portion for IT. Note that, here, EH and IT are simultaneously performed within R_i. Since $R_i \; \forall \; i = 1, ..., K_g$ introduces a common phase shift θ_i, where $\theta_i \in [-\pi, \pi]$, the

required amount of energy for information transfer via R_i is

$$\mathrm{E}_{\mathrm{req,PS}} = T_s(\mathcal{K}P_t + P_{ph}), \tag{5.1}$$

where T_s is the slot duration, P_t, $\mathcal{K}$ is the number of patches, and P_{ph} denotes the power consumption of each patch and controller power consumption of R_i for the desired phase shift operation [38].

5.3.2.2 TS Configuration

In this architecture, each patch of R_i is entirely devoted to EH or IT during a specific time slot. If T_s is the total time slot and $\zeta \in [0,1]$ fraction of it is required for EH to support the power consumption demand, the entire R_i operates in the EH mode during the interval $[0, \zeta T_s]$ and in the IT mode for the remaining $T_s(1-\zeta)$ time. Hence, in this case, the required amount of energy is given by

$$\mathrm{E}_{\mathrm{req,TS}} = T_s((1-\zeta)\mathcal{K}P_t + P_{ph}). \tag{5.2}$$

5.3.3 Channel Model

As discussed earlier, S communicates with D via an intermediate RIS R that is divided into K_g non-overlapping surfaces and each surface R_i consists of M_g reflecting elements. We denote the channel from S to R_i and R_i to D as $\mathbf{h} \in \mathbb{C}^{M_g \times 1}$ and $\mathbf{g} \in \mathbb{C}^{1 \times M_g}$, respectively. We assume that the wireless links suffer from both large-scale path-loss effect and small-scale block fading. Here, we consider that all the channels $h_j \in \mathbf{h}$ and $g_j \in \mathbf{g}\ \forall\ j = 1, ..., M_g$ experience Rician fading and their corresponding path-loss factor are $\rho_L d_{S,j}^{-\alpha/2}$ and $\rho_L d_{j,D}^{-\alpha/2}$, respectively, where ρ_L is the path loss at one meter distance, α is the path loss exponent, $d_{S,j}$ and $d_{j,D}$ denote the distance between S to j-th element of R_i, and j-th element of R_i to D, respectively. Note that both $|h_j|$ and $|g_j|$ follow the identical distribution as below.

$$\begin{aligned} f_{|h/g|}(\alpha, K_{h/g}) &= 2(1+K_{h/g})e^{-K_{h/g}} \\ &\times \alpha e^{-(1+K_{h/g})\alpha^2} I_0\left[2\alpha\sqrt{K_{h/g}(1+K_{h/g})}\right],\ \alpha \geq 0. \end{aligned} \tag{5.3}$$

Here $K_{h/g}$ is the Rician factor corresponding to the $S - R_i/R_i - D$ channel, respectively, and $I_0(\cdot)$ denotes the zero-order modified Bessel function of the first kind.

Since the inter-reflecting element distance of R_i is less than the half-wavelength, we cannot overlook the impact of spatial correlation on the wireless channels [101]. Therefore, the channels from S to R_i and R_i to D are defined as [102, 103]

$$\tilde{\mathbf{h}} = \sqrt{\beta}\mathbf{R}^{1/2}\mathbf{h} \qquad \text{and} \qquad \tilde{\mathbf{g}} = \sqrt{\beta}\mathbf{g}\mathbf{R}^{1/2}, \tag{5.4}$$

respectively, where β denotes the link gain and $\mathbf{R} \in \mathbb{R}^{M_g \times M_g}$ is the spatial correlation matrix. Note that, here we consider the *sinc* model [59] to characterize $\mathbf{R}_{p,q}\ \forall\ p,q = 1,\ldots,M_g$, i.e., $\mathbf{R}_{p,q} = \dfrac{\sin\left(\frac{2\pi}{\lambda}d_{p,q}\right)}{\frac{2\pi}{\lambda}d_{p,q}}$, where λ is the transmission wavelength and $d_{p,q}$ is the Euclidean distance between the p-th and q-th element of R_i [104]. Accordingly, the composite channel from S to R_i is defined as [22]

$$h_c = \sum_{i=1}^{M_g} \tilde{h}_i, \tag{5.5}$$

where $\tilde{h}_i \in \tilde{\mathbf{h}}$ and $|\tilde{h}_i|$ follows (5.3). Similarly, we obtain the composite channel g_c from R_i to D as

$$g_c = \sum_{i=1}^{M_g} \tilde{g}_i. \tag{5.6}$$

5.3.4 Energy Harvesting Model

As stated above, the signal from S reaches D via R_i which is self-sufficient in terms of energy. Here, every reflecting element of R_i is connected to an RF-to-DC converter, which can draw DC power from the incident signal [38]. To explain this phenomenon, several practical EH models have been proposed in the literature. Since the non-linear EH model suggested in [27] is more theoretically tractable, we consider it in our study. Therefore, the energy E_{harv}, as harvested by a reflecting element of R_i is expressed in terms of the received power P at the reflecting element as

$$E_{nl} = t\Big(\frac{aP|h|^2 + b}{P|h|^2 + c} - \frac{b}{c}\Big), \tag{5.7}$$

where $|h|^2$ is the power gain of the $S - R_i$ channel, t is the harvesting duration, and a, b, c are the circuit specific parameters. Moreover, as a benchmark, we also consider the linear

EH model, i.e.,

$$E_l = tP|h|^2. \tag{5.8}$$

Note that in (5.7) and (5.8), we will set the value of t according to the PS and TS configurations, which will be discussed in the following section.

5.3.5 Order-based Selection and Extreme Value Theory

Assume that x_i with $i \in \{1, \ldots, K_g\}$ represent K_g i.i.d random variables, which correspond to specific parameters that define the performance of R_i. Without loss of generality, we make the following ordering [105, 106]

$$x_1 \leq x_2 \leq \cdots \leq x_{K_g}, \tag{5.9}$$

in which training time is used to gain an understanding of this ordering. This ordering is based on the various selection schemes of our proposed framework (will be discussed later). On the basis of these schemes, the k-th best group is selected and accordingly, it reflects the incident signals in a desired direction by using its own harvested energy.

Let i^* denote the index of the k-th best group for each selection scheme. Therefore, the PDF of x_i^* is given by [105]

$$f_{x_i^*}(x) = k\binom{K_g}{k} f_{x_i}(x) F_{x_i}(x)^{K_g-k}(1 - F_{x_i}(x))^{k-1}, \tag{5.10}$$

where $F_{x_i}(x)$ and $f_{x_i}(x)$ are the CDF and PDF of x_i, respectively.

Furthermore, if R consists of a large number of reflecting elements, i.e., $M \to \infty$ [107], then we have $K_g \to \infty$ for a finite M_g, as $M = M_g \times K_g$. In this context, we use the tools of EVT to characterize the system performance. Now, based on the EVT, we get that x_{K_g} converges to one of the three limiting distributions: the Gumbel distribution, the Frechet distribution, or the Weibull distribution [108]. The complete overview of this scenario is analyzed in Section 5.6.

5.4 System Characterization

In the considered network topology, S communicates with D via R_i, where R_i harvests the energy E_{req} required for the phase shifting operation from the transmitted signal. As

stated in Section 5.3.2, the analytical characterization of this entire process depends on the configuration of the RIS, i.e., PS or TS. Hence, we characterize both the RIS configurations and their impact on the suitable choice of system parameters in the context of the considered network topology.

5.4.1 PS Configuration

According to Section 5.3.2.1, the RIS group R_i harvests energy by using a fraction ρ of the received power, while the remaining is allocated for IT. Therefore, in this case, the received signal at D is

$$y_{\text{PS}} = \rho_L \sqrt{(1-\rho) P_{\text{tx}} (d_{S,R_i} d_{R_i,D})^{-\alpha}} g_c h_c e^{j\phi_i} x + n, \tag{5.11}$$

where P_{tx} is the transmit power, x is the transmitted signal, ϕ_i is the associated phase shift provided at R_i, and n is the zero mean AWGN, with power σ_0^2.

Note that, in contrast to the traditional RIS-based method, we do not require a diagonal phase shift matrix of M non-zero elements. Here, the incoming signal receives a common phase shift from the components of R_i. Moreover, by rewriting the composite channels g_c and h_c as $|g_c|e^{-\phi_h}$ and $|h_c|e^{-\phi_g}$, respectively, we obtain the optimal phase shift ϕ_{R_i} corresponding to R_i as $\phi_{R_i} = \phi_h + \phi_g$ such that the maximum SNR can be achieved. Accordingly, the received signal at D is

$$y_{\text{PS}} = \rho_L \sqrt{(1-\rho) P_{\text{tx}} (d_{S,R_i} d_{R_i,D})^{-\alpha}} |g_c||h_c| x + n. \tag{5.12}$$

Next, in the following theorems, we investigate the performance bound on ρ, depending on the considered EH model.

Theorem 5.4.1. *By considering a linear EH model and assuming ρ to be equal for all the M reflecting elements of R_i, we have*

$$\frac{M_g P_t + P_{ph}}{\rho_L (d_{S,R_i})^{-\alpha} P_{\text{tx}} \sum_{i=1}^{M_g} |h_i|^2} \leq \rho \leq \frac{\eta}{2^{R_{\text{req}}} - 1 + \eta}, \tag{5.13}$$

where $\eta = \dfrac{\rho_L E_{l,PS} \times d_{R_i,D}^{-\alpha}}{T_s \sigma_0^2 \sum_{i=1}^{M_g} |\tilde{h}_i|^2} |g_c|^2 |h_c|^2$ and R_{req} is the application-specific minimum required data rate.

Proof. See Appendix A.

□

Although the linear EH model is analytically tractable, at times, it fails to capture the actual EH process. For such scenarios, we derive the bound on ρ by considering a nonlinear EH model. From (5.7), for M number of reflecting elements, the total harvested energy $E_{nl,PS}$ is given by

$$E_{nl,PS} = T_s \sum_{i=1}^{M_g} \Big(\frac{a\rho P_{\text{tx}} \rho_L (d_{S,R_i})^{-\alpha} |\tilde{h}_i|^2 + b}{\rho P_{\text{tx}} \rho_L (d_{S,R_i})^{-\alpha} |\tilde{h}_i|^2 + c} - \frac{b}{c} \Big). \tag{5.14}$$

Here, to find the bounds for ρ, we consider the worst and best channel conditions for EH. This is because, for a given $E_{\text{req,PS}}$, the worst channels require a larger ρ, while the best channels require a relatively lesser value of ρ. Therefore, with all other parameters remaining constant, we express $E_{nl,PS}$ as a function of the corresponding channel conditions, i.e.,

$$E_{nl,PS}^{\max} = E_{nl,PS}\left(|h_{\max}|\right) \text{ and } E_{nl,PS}^{\min} = E_{nl,PS}\left(|h_{\min}|\right), \tag{5.15}$$

where the worst and best channel conditions $|h_{\min}|$ and $|h_{\max}|$ are defined as

$$|h_{\min}| = \min\{|\tilde{h}_1|^2, \cdots, |\tilde{h}_{M_g}|^2\}. \tag{5.16}$$

and

$$|h_{\max}| = \max\{|\tilde{h}_1|^2, \cdots, |\tilde{h}_{M_g}|^2\}, \tag{5.17}$$

respectively. Accordingly, in the following theorem, we investigate the performance bound on ρ, depending on the considered non-linear EH model.

Theorem 5.4.2. *By considering a non-linear EH model and assuming ρ to be equal for all the M_g reflecting elements of R_i in the PS configuration, we obtain*

$$\begin{aligned} &\frac{c(M_g P_t + P_{ph})}{M_g \rho_L (d_{S,R_i})^{-\alpha} P_{\text{tx}} |h_{\max}|^2 \Big(a - \frac{M_g P_t + P_{ph}}{M_g} - \frac{b}{c} \Big)} \\ &\leq \rho \leq \frac{\kappa}{(2^{R_{\text{req}}} - 1) + \kappa}, \end{aligned} \tag{5.18}$$

where $\kappa = \dfrac{c E_{nl,PS}^{\min} \rho_L d_{R_i,D}^{-\alpha}}{M_g T_s |h_{\min}|^2 \left(a - \frac{E_{nl,PS}^{\min}}{M_g T_s} - \frac{b}{c} \right) \sigma_0^2} |g_c|^2 |h_c|^2.$

Proof. See Appendix B.

□

5.4.2 TS Configuration

In an arbitrary time slot, according to Section 5.3.2.2, R_i harvests the required energy from the received signal for time ζT_s while the remaining time, i.e., $(1-\zeta)T_s$ is dedicated for IT. Therefore, in this case, the received signal at D is

$$y_{\text{TS}} = \begin{cases} 0, & t \leq T_s\zeta \\ \Lambda g_c h_c e^{j\phi_i} x + n, & T_s\zeta < t \leq T_s, \end{cases} \tag{5.19}$$

where $\Lambda = \rho_L \sqrt{P_{\text{tx}}} \Big(d_{S,R_i} d_{R_i,D} \Big)^{-\alpha/2}$, ϕ_i is the associated phase shift at R_i, and n is defined earlier in (5.11). Accordingly, similar to (5.12), the received signal, corresponding to the maximum SNR that can be achieved, is

$$y_{\text{TS}} = \begin{cases} 0, & t \leq T_s\zeta \\ \Lambda |g_c||h_c| x + n, & T_s\zeta < t \leq T_s. \end{cases} \tag{5.20}$$

Here, we observe that ζ has a significant impact both on the EH and IT processes. In this context, we are looking for a compact bound of ζ that would allow the TS-configuration to perform smoothly. Now, based on our considered EH models, we investigate the performance bound of ζ for each case independently. In the following theorem, we investigate the performance bound on ζ for the linear EH model.

Theorem 5.4.3. *By considering a linear EH model and assuming ζ to be equal for all the M reflecting elements of R_i, we have*

$$\frac{M_g P_t + P_{ph}}{M_g P_t + P_{\text{tx}} \sum_{i=1}^{M_g} |h_i|^2} \leq \zeta \leq 1 - \frac{R_{\text{req}}}{R_{\text{arc}}}, \tag{5.21}$$

where $R_{\text{arc}} = \log_2(1+\gamma_{\text{TS}})$ is the achievable data rate and R_{req} is the application-specific minimum required data rate.

Proof. See Appendix C.

□

Table 5.1: Summary of results.

Cases	Linear EH model	Non-linear EH model
PS	$\frac{M_g P_t + P_{ph}}{\rho_L (d_{S,R_i})^{-\alpha} P_{\text{tx}} \sum_{i=1}^{M_g} \lvert h_i \rvert^2} \leq \rho \leq \frac{\eta}{2^{R_{\text{req}}} - 1 + \eta}$, where $\eta = \frac{\rho_L E_{l,PS} \times d_{R_i,D}^{-\alpha}}{T_s \sigma_0^2 \sum_{i=1}^{M_g} \lvert \tilde{h}_i \rvert^2} \lvert g_c \rvert^2 \lvert h_c \rvert^2$.	$\frac{c(M_g P_t + P_{ph})}{M_g \rho_L (d_{S,R_i})^{-\alpha} P_{\text{tx}} \lvert h_{\max} \rvert^2 \left(a - \frac{M_g P_t + P_{ph}}{M_g} - \frac{b}{c} \right)} \leq \rho \leq \frac{\kappa}{(2^{R_{\text{req}}} - 1) + \kappa}$, where $\kappa = \frac{c E_{nl,PS}^{\min} \rho_L d_{R_i,D}^{-\alpha}}{M_g T_s \lvert h_{\min} \rvert^2 \left(a - \frac{E_{nl,PS}^{\min}}{M_g T_s} - \frac{b}{c} \right) \sigma_0^2} \lvert g_c \rvert^2 \lvert h_c \rvert^2$.
TS	$\frac{M_g P_t + P_{ph}}{M_g P_t + P_{\text{tx}} \sum_{i=1}^{M_g} \lvert h_i \rvert^2} \leq \zeta \leq 1 - \frac{R_{\text{req}}}{R_{\text{arc}}}$.	$\frac{M_g P_t + P_{ph}}{M_g \left(P_t + \frac{a\varphi + b}{\varphi + c} - \frac{b}{c} \right)} \zeta \leq 1 - \frac{R_{\text{req}}}{R_{\text{arc}}^{\min}}$, where $\varphi = \rho_L d_{S,R_i}^{-\alpha} P_{\text{tx}} \lvert h_{\max} \rvert^2$.

Similar to the non-linear EH model-based PS configuration of the RIS, here, we investigate the performance bounds for ζ by taking into account both the best and worst-case scenarios of the channels. Specifically, we consider the cases $|\tilde{h}_i| = |h_{\min}|$ and $|\tilde{h}_i| = |h_{\max}| \ \forall \ i = 1, \cdots, M_g$, where $|h_{\min}|$ and $|h_{\max}|$ are obtained from (5.16) and (5.17), respectively. In the following theorem, we look at the performance bounds of ζ for the non-linear EH model.

Theorem 5.4.4. *By considering a non-linear EH model in TS configuration and assuming ζ to be equal for all the M reflecting elements of R_i, we obtain*

$$\frac{M_g P_t + P_{ph}}{M_g \left(P_t + \frac{a\varphi + b}{\varphi + c} - \frac{b}{c} \right)} \leq \zeta \leq 1 - \frac{R_{\text{req}}}{R_{\text{arc}}^{\min}}. \tag{5.22}$$

where $\varphi = \rho_L d_{S,R_i}^{-\alpha} P_{\text{tx}} |h_{\max}|^2$ and $R_{\text{arc}}^{\min}$ is the achievable data rate for the worst-case scenarios of the channels.

Proof. See Appendix D.

□

Finally, Table 5.1 presents a summary of the main analytical results derived in this section.

5.4.3 Composite Channel Characterization

From Section 5.3.3, we have the wireless channel from S to the i-th element of a group as $h_i \sim \mathcal{CN}\left(m_i, \sigma_i^2\right) \ \forall \ i = 1, \cdots, M_g$. Due to the impact of spatial correlation, from (5.4)

we obtain $\tilde{\mathbf{h}} = \sqrt{\beta}\mathbf{R}^{1/2}\mathbf{h}$, which can be rewritten as $\tilde{\mathbf{h}} = \mathbf{R}'\mathbf{h}$, where $\mathbf{R}' = \sqrt{\beta}\mathbf{R}^{1/2}$. In other words, we have

$$\begin{bmatrix} \tilde{h_1} \\ \tilde{h_2} \\ \vdots \\ \tilde{h_M} \end{bmatrix} = \begin{bmatrix} r_{11} & r_{12} & \cdots & r_{1M_g} \\ r_{21} & r_{22} & \cdots & r_{2M_g} \\ \vdots & \vdots & \vdots & \vdots \\ r_{K1} & r_{K2} & \cdots & r_{M_gM_g} \end{bmatrix} \begin{bmatrix} h_1 \\ h_2 \\ \vdots \\ h_{M_g} \end{bmatrix}. \tag{5.23}$$

Hence, from (5.23), we get $\tilde{h_i} = \sum_{j=1}^{M_g} r_{ij}h_j$.

Here, $\tilde{h_i}$ is expressed as a linear combination of $h_j \; \forall \; j = 1, \cdots, M_g$. Therefore, the mean and variance of $\tilde{h_i}$ are obtained as

$$\begin{aligned} \mathbb{E}\left[\tilde{h_i}\right] &= \mathbb{E}\left[\sum_{j=1}^{M_g} h_j r_{ij}\right] = \sum_{j=1}^{M_g} r_{ij}\mathbb{E}[h_j] = \sum_{j=1}^{M_g} r_{ij}m_j \text{ and} \\ \text{Var}\left(\tilde{h_i}\right) &= \sum_{j=1}^{M_g} \text{Var}\left(h_j\right) r_{ij}^2 = \sum_{j=1}^{M_g} \sigma_j^2 r_{ij}^2, \end{aligned} \tag{5.24}$$

respectively. Since m_i and $\sigma_i \; \forall \; i = 1, \cdots, M_g$ are finite, by using the Central Limit Theorem [83], we get

$$\tilde{h_i} \sim \mathcal{CN}\left(\sum_{j=i}^{M_g} m_j r_{ij}, \sum_{j=i}^{M_g} \sigma_j^2 r_{ij}^2\right). \tag{5.25}$$

As a result, by using (5.25) in (5.5), we obtain

$$h_c = \sum_{i=1}^{M_g} \tilde{h_i} \sim \mathcal{CN}\left(\sum_{i=1}^{M_g}\sum_{j=1}^{M_g} m_j r_{ij}, \sum_{i=1}^{M_g}\sum_{j=1}^{M_g} \sigma_j^2 r_{ij}^2\right). \tag{5.26}$$

Since h_c has a non-zero mean, $|h_c|$ follows the Rician PDF. Therefore, $|h_c|^2$ follows a non-central χ^2 distribution with the density function [83]

$$f_{|h_c|^2}(\mu) = \frac{1}{2}\left(\frac{\mu}{\Delta_h^2}\right)^{\frac{1}{4}(k_h-2)} e^{-\frac{1}{2}(\mu+\Delta_h^2)} I_{\frac{1}{2}(k_h-2)}(\Delta_h\sqrt{\mu}), \tag{5.27}$$

where Δ_h is the non-centrality parameter, k_h is the degree of freedom, and $I_n(\cdot)$ is the

modified Bessel function of the first kind. Similarly, the density function of $|g_c|^2$ is

$$f_{|g_c|^2}(\mu) = \frac{1}{2}\left(\frac{\mu}{\Delta_g^2}\right)^{\frac{1}{4}(k_g-2)} e^{-\frac{1}{2}(\mu+\Delta_g^2)} I_{\frac{1}{2}(k_g-2)}(\Delta_g\sqrt{\mu}). \tag{5.28}$$

From the previous discussion, we know that the received SNR at D is a function of $Z = |g_c|^2|h_c|^2$. However, the product of two non-central χ^2 distributions does not have a closed-form. Hence, we approximate the resulting distribution by the moment matching technique [109, 110]. We propose using the Gamma distribution for approximation as it is a Type-III Pearson distribution [111], which is widely used in fitting distributions for positive RVs by matching the first and second moments. Specifically, we approximate the product $Z \sim \mathcal{F}(\delta, \beta)$ as Gamma-distributed random variable with the shape and scaling parameters δ and β, respectively. Moreover, the PDF and CDF of Z is given as [109]

$$f_Z(x) = \frac{\beta^{-}\delta}{\Gamma(\delta)} x^{\delta-1} \exp\left(\frac{-x}{\beta}\right), \qquad x > 0 \quad \text{and} \tag{5.29}$$

$$F_Z(x) = \frac{\gamma\left(\alpha, \frac{x}{\delta}\right)}{\Gamma(\alpha)}, \tag{5.30}$$

respectively, where $\gamma(\alpha, x)$ and $\Gamma(\cdot)$ denote the incomplete and complete Gamma function, respectively.

5.5 Proposed Group Selection Strategies

In this section, we propose various group selection strategies for the considered framework, where R is partitioned into K_g non-overlapping subgroups R_i $i = 1, \ldots, K_g$. Specifically, we propose strategies to select one of the R_i, corresponding to various performance metrics, as discussed below. Here, the implementation of these strategies is characterized in terms of their respective data and energy outage probabilities. In this context, by using the definition of γ_{PS} and γ_{TS} from (5.61) and (5.81), respectively, the outage probability, corresponding to a predetermined required data rate R_{req}, is defined as

$$\mathcal{O}_{\text{PS/TS}} = \mathbb{P}\left(\mathbf{f}(\zeta)\log_2(1+\gamma_{\text{PS/TS}}) < R_{\text{req}}\right), \tag{5.31}$$

where

$$\mathbf{f}(\zeta) = \begin{cases} 1, & \text{for PS configuration} \\ 1-\zeta, & \text{for TS configuration.} \end{cases} \tag{5.32}$$

Similarly, by using (5.7) and (5.8), the energy outage probability [112] is defined as

$$\mathbb{O}_{\mathrm{PS/TS}} = \mathbb{P}\left(E_{l/nl} \leq E_{\mathrm{req}}\right), \tag{5.33}$$

where E_{req} is a predefined energy threshold. Hereafter, depending on the outage probability, the group selection mechanisms are described below.

5.5.1 Random Group Selection (RGS)

In this group selection technique, a subgroup is randomly chosen from among those that are accessible to share the information. Here, we define a set $\mathcal{S}$ of all subgroups that can provide the minimum required data rate at D, i.e.,

$$\begin{aligned} S = \{R_i \; &: R_{i,\mathrm{PS/TS}} \geq R_{\mathrm{req}} \\ &\& \; E_{i,\mathrm{req,PS/TS}} \leq E_{i,\mathrm{PS/TS}}, \; i = 1, \cdots, K_g\}, \end{aligned} \tag{5.34}$$

where $R_{i,\mathrm{PS/TS}}$ denotes the achievable data rate at D, $E_{i,\mathrm{req}}$ and E_i are the minimum required and harvested energy corresponding to the PS or TS configuration of R_i, respectively. Note that all $R_i \in S$ can harvest the required amount of energy E_{req}. Therefore, without loss of generality, if an arbitrary $R_i \in S$ is randomly selected, the resulting outage performance is characterized by the following theorem.

Theorem 5.5.1. *The outage probability for the RGS scheme is obtained as*

$$\begin{aligned} i) \quad \mathcal{O}_{\mathrm{PS}}^{RGS} &= \frac{\gamma\left(\alpha, \frac{2^{R_{\mathrm{req}}}-1}{\delta\left(1-\rho\right)\Psi}\right)}{\Gamma(\alpha)} \\ ii) \quad \mathcal{O}_{\mathrm{TS}}^{RGS} &= \frac{\gamma\left(\alpha, \frac{2^{\frac{R_{\mathrm{req}}}{1-\zeta}}-1}{\delta\Psi}\right)}{\Gamma(\alpha)}. \end{aligned} \tag{5.35}$$

Proof. From (5.31), we have $\mathcal{O}_{\mathrm{PS/TS}}^{RGS} = \mathbb{P}\left(\gamma_{\mathrm{PS/TS}} \leq 2^{\frac{R_{\mathrm{req}}}{f(\zeta)}} - 1\right)$. Hence, by using (5.61)

and (5.32), we obtain

$$\begin{aligned}
&\mathcal{O}_{\mathrm{PS}}^{RGS} \\
&= \mathbb{P}\left(\frac{\left(1-\rho\right)P_{\mathrm{tx}}\rho_L^2\left(d_{S,R_i}d_{R_i,D}\right)^{-\alpha}}{\sigma_0^2}|g_c|^2|h_c|^2 \leq 2^{R_{\mathrm{req}}}-1\right) \\
&= \mathbb{P}\left(|g_c|^2|h_c|^2 \leq \frac{2^{R_{\mathrm{req}}}-1}{\left(1-\rho\right)\Psi}\right), \qquad (5.36)
\end{aligned}$$

where $\Psi = \frac{P_{\mathrm{tx}}\rho_L^2\left(d_{S,R_i}d_{R_i,D}\right)^{-\alpha}}{\sigma_0^2}$. From (5.29), we know that the quantity $Z = |g_c|^2|h_c|^2$ is approximated by a Gamma random variable. Therefore, by using its CDF, we have

$$\mathcal{O}_{\mathrm{PS}}^{RGS} = \int_0^{\frac{2^{R_{\mathrm{req}}}-1}{\left(1-\rho\right)\Psi}} f_Z(y)dy = \frac{\gamma\left(\alpha, \frac{2^{R_{\mathrm{req}}}-1}{\delta\left(1-\rho\right)\Psi}\right)}{\Gamma(\alpha)}. \qquad (5.37)$$

Similarly, by using (5.81) and (5.31), we obtain

$$\mathcal{O}_{\mathrm{TS}}^{RGS} = \mathbb{P}\left(|g_c|^2|h_c|^2 \leq \frac{2^{\frac{R_{\mathrm{req}}}{1-\zeta}}-1}{\Psi}\right) = \frac{\gamma\left(\alpha, \frac{2^{\frac{R_{\mathrm{req}}}{1-\zeta}}-1}{\delta\Psi}\right)}{\Gamma(\alpha)}.$$

□

However, in most practical scenarios, the best subgroup may not be always available. In that case, we have to go for the second-best group selection. Generalizing, we concentrate on how the outage probability for the various selection schemes is affected by the k-th best group selection. Accordingly, the outage probability for the k-th best group selection scheme is

$$\mathcal{O}_{k,\mathrm{PS/TS}} = \mathbb{P}\left(\mathbf{f}(\zeta)\log_2(1+\gamma_{\mathrm{PS/TS}}^*) < R_{\mathrm{req}}\right), \qquad (5.38)$$

where $\gamma_{\mathrm{PS/TS}}^*$ is the received SNR at D for the k-th best group. Therefore, the k-th best group selection schemes, based on different system parameters, are presented below.

5.5.2 SNR-Based Group Selection (SBGS)

Here, we investigate a group selection strategy based on the achievable SNR. In this context, we consider the channel state information (CSI) to be known a priori. Specifically, in this scheme, the group that attains the k-th highest SNR at D is the k-th best group, and we select that one accordingly. Note that all the available groups constitute the set $\mathcal{S}$ as defined in (5.34). Consequently, let us consider that $X_1 \leq X_2 \leq \cdots \leq X_{|\mathcal{S}|}$ be the ordering of the received SNR and the index of the group corresponding to the k-th best SNR is i^*. That is,

$$i^* = \underset{i \in \{1,\ldots,|\mathcal{S}|\}}{\overset{(k)}{\operatorname{argmax}}} \{X_1, \ldots, X_{|\mathcal{S}|}\}. \tag{5.39}$$

Therefore, from (5.10), we obtain the PDF of X_{i^*} as

$$f_{X_{i^*}}(x) = k\binom{|\mathcal{S}|}{k} f_{X_i}(x) F_{X_i}(x)^{|\mathcal{S}|-k} (1 - F_{X_i}(x))^{k-1}, \tag{5.40}$$

where $f_{X_i}(x)$ and $F_{X_i}(x)$ are provided in (5.29) and (5.30), respectively. In the following, the outage performance for the SBGS scheme is characterized by the following theorem.

Theorem 5.5.2. *The outage probability for the SBGS scheme, where the k-th best group is selected, is determined by*

$$\mathcal{O}_{k,\mathrm{PS/TS}}^{SBGS} = \mathcal{I}_{F_{X_i}(x)} \left(|\mathcal{S}| - k + 1, k\right), \tag{5.41}$$

Proof. In Section 5.4.3, we approximate $|g_c|^2|h_c|^2$ by a Gamma distribution. Therefore, from (5.36), the SNR $\left(1-\rho\right)\Psi|g_c|^2|h_c|^2$ is a scaled Gamma random variable. Hence, the outage probability for the SBGS scheme, in the PS configuration, is

$$\mathbb{P}\left(\log_2(1 + X_{i^*}) < R_{\mathrm{req}}\right) = \mathbb{P}\left(X_{i^*} \leq x\right), \tag{5.42}$$

where $x = 2^{R_{req}} - 1$. Also, from (5.40) and (5.42), the CDF of X_{i^*} is obtained as

$$\begin{aligned} \mathcal{O}_{k,\mathrm{PS}}^{SBGS} &= \int_0^x f_{X_{i^*}}(z) dz \\ &= k\binom{|\mathcal{S}|}{k} \int_0^x f_{X_i}(z) F_{X_i}(z)^{|\mathcal{S}|-k} (1 - F_{X_i}(z))^{k-1} dz \end{aligned} \tag{5.43}$$

In (5.43), by substituting $y = F_{X_i}(x)$ and using the definition of normalized incomplete

Beta function [98], we obtain

$$\mathcal{O}_{k,\mathrm{PS}}^{SBGS} = \mathcal{I}_{F_{X_i}(x)}\left(|\mathcal{S}| - k + 1, k\right). \tag{5.44}$$

Similarly, now we obtain the outage of the k-th best group selection in the TS configuration. Note that in TS configuration, the outage is obtained by (5.44) itself, where the only difference is that in this case, we have $\rho = 0$ and $x = 2^{\frac{R_{\mathrm{req}}}{1-\zeta}} - 1$.

□

According to the system configuration considered, the residual harvested energy has a significant impact on data communication. Therefore, we will discuss the energy-based group selection scheme in detail below.

5.5.3 Energy-Based Group Selection (EBGS)

In this scheme, each R_i $i = 1, \ldots, B$ harvests the required energy from the incident signals. Note that the EH process depends on the RIS characterization, the considered EH models, and also the correlated wireless channels from S to R, i.e., on $\tilde{h}_i,\ i = 1, \ldots, M_g$. Here, we consider the linear as well as the nonlinear EH models for both the PS and TS configurations of the considered framework. We define the set of groups that are able to harvest the minimum required energy and support the minimum data rate as

$$\begin{aligned}\mathcal{A} = \{E_i \ :\ & E_{i,\mathrm{req,PS/TS}} \leq E_{i,\mathrm{PS/TS}}, \\ & \& \ R_{i,\mathrm{PS/TS}} \geq R_{\mathrm{req}} \ \ i = 1, \cdots, K_g\},\end{aligned} \tag{5.45}$$

where E_i is the energy harvested by the i-th group.

In this scheme, the group that harvests the k-th highest energy is defined as the k-th best group, and we select that one accordingly. Consequently, let us consider that $E_1 \leq E_2 \leq \cdots \leq E_{|\mathcal{A}|}$ be the ordering of the harvested energy and the index of the group corresponding to the k-th best harvested energy is i^*, i.e.,

$$i^* = \underset{i \in \{1,\ldots,|\mathcal{S}|\}}{\overset{(k)}{\operatorname{argmax}}} \{E_1, \ldots, E_{|\mathcal{A}|}\}. \tag{5.46}$$

Therefore, from (5.10), we obtain the PDF of E_{i^*} as

$$f_{E_{i^*}}(x) = k\binom{|\mathcal{A}|}{k} f_{E_i}(x) F_{E_i}(x)^{|\mathcal{A}|-k}(1-F_{E_i}(x))^{k-1}, \tag{5.47}$$

where $f_{E_i}(x)$ and $F_{E_i}(x)$ are the PDF and CDF of E_i, respectively. Accordingly, the energy outage for the proposed EBGS scheme is characterized by the following theorem.

Theorem 5.5.3. *The energy outage probability for the EBGS scheme in both the PS and TS configurations for the k-th best group is evaluated as*

$$\mathcal{O}_{k,\mathrm{PS/TS}}^{EBGS} = \mathcal{I}_{F_{E_i}(x)}\left(|\mathcal{A}|-k+1,k\right). \tag{5.48}$$

Proof. From (5.64), we observe that a group is able to transfer information if it harvests the minimum required energy. Therefore, for the PS configuration, the outage of the k-th best group in the EBGS scheme is

$$\mathbb{P}\left(E_{i^*} \leq E_{\mathrm{req,PS}}\right), \tag{5.49}$$

where $E_{\mathrm{req,PS}}$ is the minimum required energy in PS configuration. Hence, from (5.47), the outage of the k-th best group is obtained as

$$\begin{aligned}\mathcal{O}_{\mathrm{PS/TS}}^{EBGS} &= \int_0^x f_{E_{i^*}}(z)dz \\ &= k\binom{|\mathcal{A}|}{k}\int_0^x f_{E_i}(z)F_{E_i}(z)^{|\mathcal{A}|-k}(1-F_{E_i}(z))^{k-1}dz \\ &= \mathcal{I}_{F_{E_i}(x)}\left(|\mathcal{A}|-k+1,k\right),\end{aligned} \tag{5.50}$$

where $f_{E_{i^*}}(z)$ denotes the PDF of the k-th best group.

For the linear EH model, by using (5.8) we have $E_i = \nu \sum_{j=1}^{M_g} |\tilde{h_j}|^2$, where $\nu = T_s\rho P_{\mathrm{tx}}\rho_L d_{S,R_i}^{-\alpha}$. Therefore, with all the other parameters remaining constant, E_i is a function of $\sum_{j=1}^{M_g} |\tilde{h_j}|^2$. Since $|\tilde{h_j}|^2$ follows the non-central χ^2 distribution, we approximate E_i as a Gamma random variable [113]. Now, for the non-linear EH model, by using (5.7), which followed by trivial algebraic manipulations, results in

$$\frac{aP_{\mathrm{tx}}|h|^2+b}{P_{\mathrm{tx}}|h|^2+c} - \frac{b}{c} = \frac{ac-b}{c} + (b-ac)\times\frac{1}{P_{\mathrm{tx}}|h|^2+c}. \tag{5.51}$$

Accordingly, by using (5.51), the harvested energy is

$$E_i = T_s \sum_{j=1}^{M_g} \left(\frac{a P_{\text{tx}} \rho_L (d_{S,R_i})^{-\alpha} |\tilde{h}_j|^2 + b}{P_{\text{tx}} \rho_L (d_{S,R_i})^{-\alpha} |\tilde{h}_j|^2 + c} - \frac{b}{c} \right)$$
$$= T_s \left(\frac{M_g(ac-b)}{c} + \sum_{j=1}^{M_g} \frac{b - ac}{\rho_L (d_{S,R_i})^{-\alpha} P_{\text{tx}} |\tilde{h}_j|^2 + c} \right). \tag{5.52}$$

Here, (5.51) can be approximated to an inverse Gamma approximation [114]. Therefore, (5.52) can also be approximated to a scaled inverse Gamma random variable.

Lastly, note that if we set ρ as unity in (5.8), and substitute $E_{\text{req,PS}}$ by $E_{\text{req,TS}}$ in (5.49), in a similar way, we obtain the outage performance corresponding to the TS configuration for both the linear and non-linear cases. □

Remark: Note that, both SBGS and EBGS consider a perfect CSI scenario. We assume that, for all i, the $S - R_i$ and $R_i - D$ channels remain constant during a channel coherence block of length T_c and that this satisfies $T_p < T_c$, where T_p is the pilot length [115]. Then the estimate for the channels is obtained in [116], which exists iff $T_p \geq M + 1$. This very condition implies that the channel estimation overhead T_p scales at least linearly with M [22]. Moreover, by considering alternative assumptions, such as models involving sparsity, more efficient channel estimation methods may also be employed. In such cases, the overhead may be even lesser. Furthermore, the work in [117] investigates the aspect of imperfect wireless channel estimation for RIS-aided systems. Therefore, based on the framework proposed here and by using [117], we can extend the present work and propose an intelligent channel estimation strategy-based generalized group selection framework for a self-sustainable RIS-aided set-up.

5.6 EVT-Based Performance Analysis

Here, we investigate the asymptotic performance of the proposed selection strategies in terms of the number of groups, i.e., when $K_g \to \infty$. Specifically, to analyze the performance of the proposed k-th best selection schemes, we derive the limiting distribution of the k-th best group and use EVT tools to assess the asymptotic outage probability. In this context, as mentioned in Section 5.3.5, let us assume that X_{K_g} denotes the largest order statistic of B i.i.d. random variables and the corresponding PDF and CDF are denoted as $F_{X_{K_g}}(x)$ and

$f_{X_{K_g}}(x)$, respectively. Note that the random variable of interest for the EBGS scheme in PS configuration corresponding to the linear and nonlinear EH model is obtained by using (5.59) and (5.14), respectively. Similarly, (5.61) and (5.74) are used to obtain the random variable of interest for the SBGS scheme in PS configuration corresponding to the linear and nonlinear EH model, respectively. Accordingly, the value of ρ and ζ will be set to obtain the random variables in the TS configuration as stated earlier in Section 5.4.2.

Now we consider that $H(x)$ is the limiting CDF of $\frac{X_{K_g}-\kappa}{\tau}$, where κ and τ are normalizing constants. In our proposed group selection schemes, it can be shown that

$$\lim_{x\to\infty} \frac{1-F_{X_i}(x)}{f_{X_i}(x)} = l,\ 0 < l\ \forall\ i = 1,\dots K_g. \tag{5.53}$$

As a result, the limiting distribution of the k-th best group follows the Gumbel distribution [118] with CDF

$$H(x) = \exp(-\exp(-x)),\ -\infty < x < \infty. \tag{5.54}$$

Therefore, for a large B, the limiting CDF of the k-th best group is defined as [118]

$$H^{(k)}(x) = \frac{1}{(k-1)!}\int_{\psi(x)}^{\infty} e^{-t}t^{k-1}dt = H(x)\sum_{j=0}^{k-1}\frac{(\Psi(x))^j}{j!}, \tag{5.55}$$

where $\Psi(x) = -\log H(x)$. By using (5.54) and (5.55), we obtain

$$H^{(k)}(x) = \exp\left(-\exp\left(-x\right)\right)\sum_{j=0}^{k-1}\frac{\exp\left(-jx\right)}{j!}. \tag{5.56}$$

Hence, the outage probability for the k-th best group is

$$\begin{aligned}\mathcal{O}_k^{EVT}(x) &= P\{X_{K_g-k+1} \le x\}\\ &= P\left\{\frac{X_{K_g-k+1}-\kappa}{\tau} \le \frac{x-\kappa}{\tau}\right\} = H^k\left(\frac{x-\kappa}{\tau}\right).\end{aligned} \tag{5.57}$$

Next, we discuss the impact of EVT-based performance on both the SBGS and EBGS schemes. In the SBGS (EBGS) system, the asymptotic outage probability of the k-th best group selection is expressed as

$$\mathcal{O}_k^{EVT}(x) = \exp\left(-\exp\left(-\frac{x-\kappa_l}{\tau_l}\right)\right)\sum_{j=0}^{k-1}\frac{\exp\left(-j\frac{x-\kappa_l}{\tau_l}\right)}{j!}, \tag{5.58}$$

where $l \in \{SBGS, EBGS\}$ and the corresponding constants κ_l and τ_l are derived from the PDF of the k-th best group selection scheme according to the SBGS (EBGS) scheme.

5.7 Simulation Results

In this section, we now validate the derived analytical results. We consider a Rician fading scenario with the following system parameters: transmission power $P_{\text{tx}} = 30$ dBm [96], path loss factor ρ_L at a distance of one meter is $\rho_L = 10^{-3.53}$, slot duration $T_s = 100$ μs [75], wavelength $\lambda = 0.1$ m [19], and noise power $\sigma_0^2 = -104$ dBm [119]. Moreover, we consider that the total number of patches of an RIS is 400, i.e., $N = 400$, and the inter-patch distance is $\lambda/8$. Furthermore, the normalizing constants for the considered non-linear EH model are $a = 2.463$, $b = 1.635$, and $c = 0.826$ [120]. Finally, we compare our proposed approach with an existing benchmark scheme.

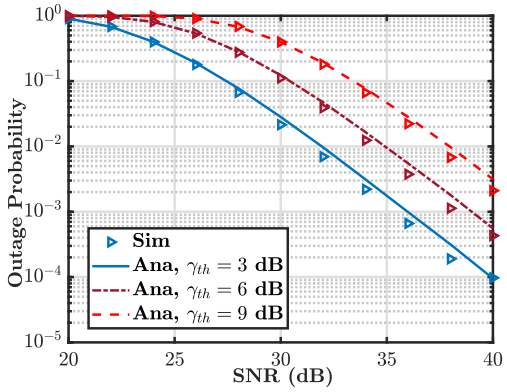

Figure 5.2: Validation of concept for different SNR thresholds. Variation of outage with SNR.

Fig. 5.2 compares the analytically obtained outage probability in Section 5.5 with the extensive Monte Carlo simulations performed. For this, we consider that $R_i \; \forall \, i = 1, \cdots, 20$ consists of 20 patches, the inter-patch distance is $\lambda/8$, and the Rician fading factor $K = 1$. Here, by considering the correlated channels, we perform the procedure 10^6 times in the Monte Carlo simulation, figuring out the optimal phase shift each time. Therefore, we observe from the figure that, irrespective of the SNR threshold γ_{th}, the outage probability

exhibits a decreasing trend with respect to the SNR, which is the function of distance, pathloss, transmit power, and noise. This is quite intuitive because the data rate increases with the SNR, leading to a downward trend in the outage probability. Moreover, for a particular SNR, we also observe an increased outage probability with increasing γ_{th}; for example, observe the performance gap at SNR $= 30$ dB between $\gamma_{th} = 3$ dB, $\gamma_{th} = 6$ dB, and $\gamma_{th} = 9$ dB. It can be observed that the analytical results closely resemble the simulation results, which validates our analytical framework.

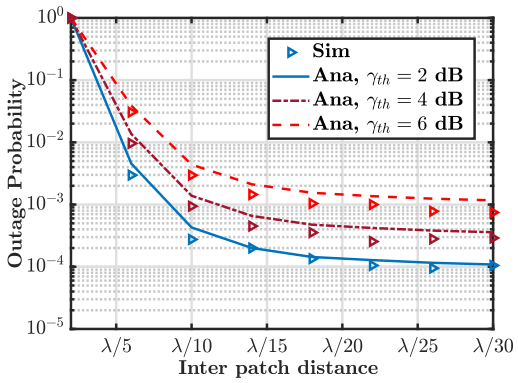

Figure 5.3: Validation of proposed strategy for different SNR thresholds and Variation of outage with inter-patch distance.

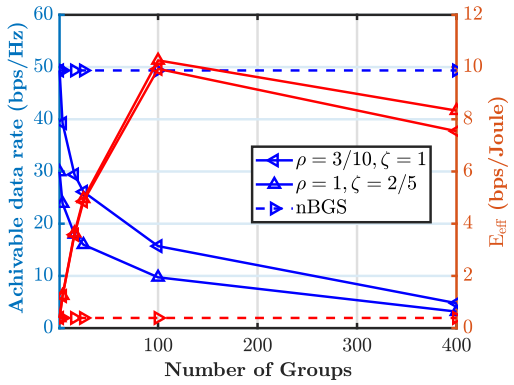

Figure 5.4: Data rate and E_{eff} performance trade-off investigation.

With identical system parameters as in Fig. 5.2 and also considering a transmit power $P_{\text{tx}} = 30$ dBm, Fig. 5.3 investigates the impact of the inter-patch distance on the outage probability. Thereafter, we match the analytical results obtained with the corresponding Monte Carlo simulation, which further verifies our analytical framework. We observe that the outage probability for $\gamma_{th} = 2$ dB, $\gamma_{th} = 4$ dB, and $\gamma_{th} = 6$ dB exhibits a decreasing

trend with the decreasing inter-patch distance. This is because a decreasing inter-patch distance enhances the channel correlation, which results in more gain on the received SNR. Moreover, as observed in Fig. 5.2, here also we notice that the outage probability corresponding to a smaller SNR threshold is less than its higher counterpart.

Based on (5.1), (5.2), and the discussion in Section 5.4, the energy-efficiency of a particular group is defined as

$$\mathrm{E_{eff}} = \frac{\mathrm{R_{arc}}}{\mathrm{E_{req,o}}} \quad \mathrm{o} \in \{\mathrm{PS}, \mathrm{TS}\},$$

where R_{arc}, and $E_{\mathrm{req,o}}$ are the achievable data rate and energy consumption of a group, respectively. Fig. 5.4 illustrates the importance of RIS grouping on the achievable data rate and $\mathrm{E_{eff}}$, as a function of the number of groups of a RIS, which consists of 400 patches. Specifically, we investigate the consequences of adopting a GBS and a nGBS. The effect of both the PS and TS configurations in GBS is investigated by considering $(\rho = 3/10, \zeta = 1)$ and $(\rho = 1, \zeta = 2/5)$, respectively. We observe that, in both cases, the achievable data rate exhibits a downward trend with increasing number of groups. This is because an increasing number of groups implies a decreasing number of elements per group, which results in a lower data rate. Conversely, it is interesting to observe that $\mathrm{E_{eff}}$ increases up to a certain group size and then decreases thereafter. The reason for this is attributed to the fact that, $\mathrm{E_{eff}}$ is defined as the ratio of R_{arc}, which is a logarithmic function of a positive quantity, to the required energy, $E_{\mathrm{req,o}}$, which is a linear function of the same. Consequently, beyond a certain point, the linear growth in energy consumption dominates, leading to a reduction in $\mathrm{E_{eff}}$. On the contrary, as the entire RIS is being used in nGBS and the required number of phase shifts equals to the total number of reflecting elements, the aspect of grouping does not have any impact on the achievable data rate and $\mathrm{E_{eff}}$. Hence, we suggest using the GBS framework depending on the application, such as in a dense environment, which improves $\mathrm{E_{eff}}$ performance and allows the RISs to serve more users at a time.

Fig. 5.5 shows the impact of the considered nonlinear EH model parameters on the derived analytical bounds for ρ and ζ corresponding to both the PS and TS configurations of the considered RIS. In this case, we consider the Rician factor $K = 2$, a group consists of 100 patches, and the received power is a function of transmit power, path-loss factor, and the distance from the S to the group. We obtain the lower bound for both the PS and TS configurations by utilizing two distinct sets of parameters $\{a = 2.463, b = 1.635, c = 0.826\}$ and $\{a = 0.392, b = 0.0167, c = 0.044\}$ in (5.18) and (5.22) as suggested in [27].

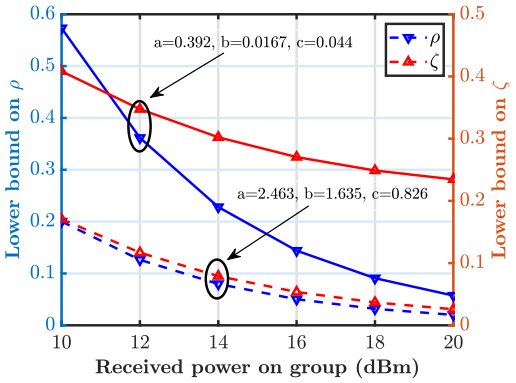

Figure 5.5: Impact of received power on the lower bound of PS and TS.

Irrespective of the parameters, the figure demonstrates an overall decreasing trend of both the lower bounds of ρ and ζ with the received power in a group. The reason for this observation is justified by the fact that, for a fixed energy requirement, an increase in the received power leads to a decrease in both ρ and ζ.

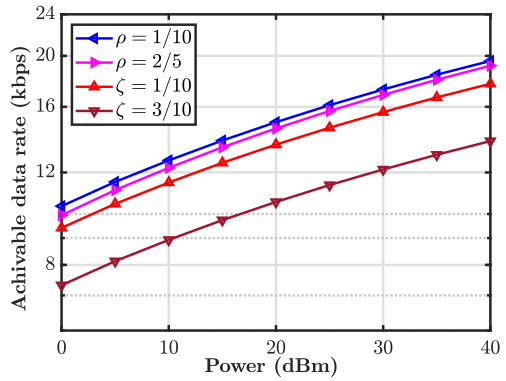

Figure 5.6: Impact of ρ and ζ on data rate.

Fig. 5.6, for both the PS and TS configurations, demonstrates an overall increasing trend of the achievable data rate with increasing transmitted power. Here, to obtain the achievable data rate from (5.11) and (5.20), we consider $K = 1$, the distance from S to R_i and R_i to D is 15 m and 20 m, respectively. It is observed that the achievable data rate for a smaller ρ (ζ), outperforms the performance for a higher value of ρ (ζ). This is because, according to the PS configuration, the higher ρ helps to harvest more energy at the RIS, which leads to a lower data rate at D. In contrast, for a smaller ζ, the energy harvesting time is small, resulting in a higher data rate at D. Note that in both the PS and TS configurations, we choose the value of ρ and ζ in such a way that they are able to harvest the minimum required

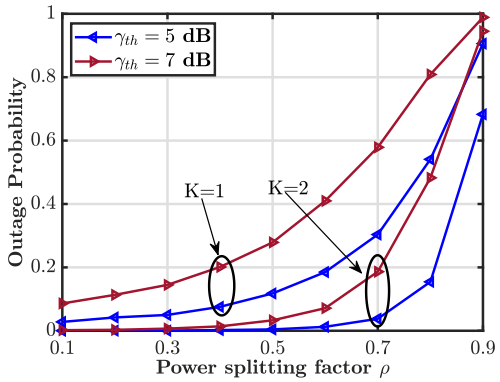

Figure 5.7: Variation of ρ with outage performance for different Rician K-factor values.

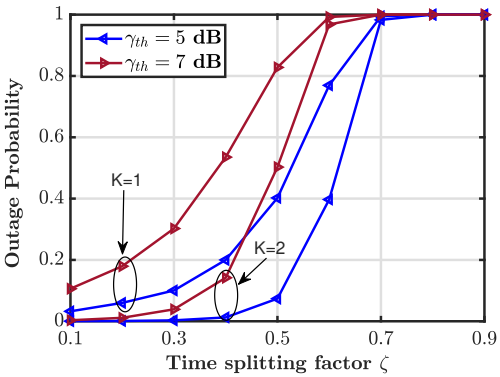

Figure 5.8: Variation of ζ with outage performance for different Rician values.

energy for IT as well as satisfy the minimum data required conditions as shown in Table 5.1.

We observe that the outage probability exhibits an increasing trend with increasing ρ and ζ in Fig. 5.7 and Fig. 5.8, respectively. In this case, simulations are performed for two distinct Rician factors $K = 1$ and $K = 2$, as well as two different SNR thresholds $\gamma_{th} = 5$ dB and $\gamma_{th} = 7$ dB. Here, the other system parameters are considered as in Fig. 5.2. Fig. 5.7 depicts that the outage probability as obtained in (5.31), in PS configuration, for all predefined SNR thresholds, exhibits an increasing trend with increasing power splitting factor. This is because, as mentioned earlier, a higher ρ aids in harvesting of more energy, which lowers the data rate and causes more outages. Similarly, for TS configuration, Fig. 5.8 shows that the data outage exhibits an increasing trend with increasing ζ. In both cases, we also observe that for a particular K, the outage probability for $\gamma_{th} = 7$ dB is more than $\gamma_{th} = 5$ dB. Moreover, as a higher K implies a higher data rate, the outage probability for $K = 1$ outperforms the outage probability for $K = 2$.

Fig. 5.9 illustrates the impact of the SNR on data outage for the proposed group

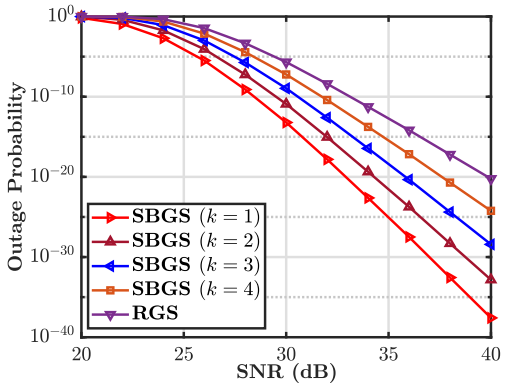

Figure 5.9: Impact of the SBGS's k-th selection.

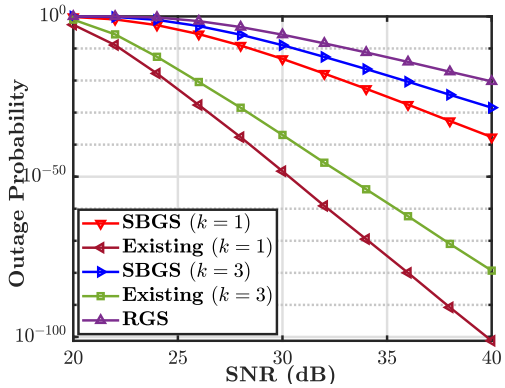

Figure 5.10: Comparison of the proposed and an existing scheme.

selection strategies. Specifically, from (5.35) and (5.41), we evaluate how the SBGS and RGS schemes perform in terms of data outages for k-th best selection for different k values. Note that the necessary energy is harvested according to the linear or nonlinear EH model of the PS or TS configuration, and their effects on the received SNR are preserved. Here, we consider a simulation setup of each group consisting of 10 patches and 10 groups are available to aid communication. We observe that the outage probability for all the cases of SBGS and RGS exhibits a decreasing trend with increasing SNR values. This is due to the fact that rising SNR raises the achievable data rate, which causes the outage probability to decrease. Moreover, we observe that the outage performance of RGS is inferior to SBGS implying that a strategic selection is always better than the random selection. Furthermore, the performance of the k-th best group selection is superior to the $(k+1)$-th best group selection. This is because, in this case, we are choosing the optimal group as compared to having a sub-optimal choice.

Fig. 5.10 demonstrates the role of spatial correlation at the RIS on the outage probability

by using the inter-patch distance as $\lambda/8$. By considering the system parameters as in Fig. 5.9, we compare our method with an existing framework [23] that groups the RISs without taking spatial correlation into account. The figure shows that the curves are in a decreasing trend with respect to the increasing SNR values, and the outage for uncorrelated scenario is less than that of its correlated counterpart. This is because, in an uncorrelated scenario, one channel being unusable for communication does not necessarily affect its neighboring channels, which is not the case in a correlated scenario. This may give us an impression that it is unwise to take spatial correlation into account. However, in the uncorrelated scenario, the inter-patch distance in an RIS of finite dimension cannot be reduced below $\lambda/2$, which severely limits the number of available patches and thus the data rate. On the other hand, from (5.11) and (5.20), we observe that SNR is a function of h_c and g_c, which are the sum of correlated channels. This indicates that with reduced inter-patch distance, more patches are accessible for the correlated case, which eventually raises the data rate. Lastly, as also observed previously, the outage corresponding to the RGS scheme results in the worst outage performance. Note that the diversity order may be possible to derive by studying the asymptotic outage probability in the high SNR regime. But finding the closed-form expression might be cumbersome.

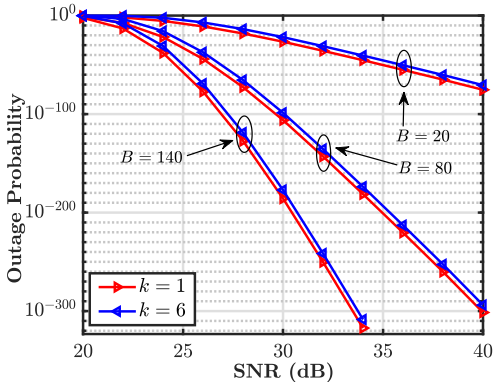

Figure 5.11: Impact of EVT in SBGS.

The effect of EVT on the SBGS selection scheme, as evident in (5.58), is shown in Fig. 5.11, where we consider $M_g = 10$, Rician factor $K = 1$, required SNR threshold $\gamma_{th} = 5$ dB, and the number of groups $K_g = 20, 80$ and 140, respectively. In this figure, we perform a k-th best selection scheme for $k = 1, 6$. Note that, regardless of the value of K_g, the outage performance demonstrates a decreasing trend, which has also been previously observed. Moreover, for a given SNR, the outage performance sharply improves with increasing K_g.

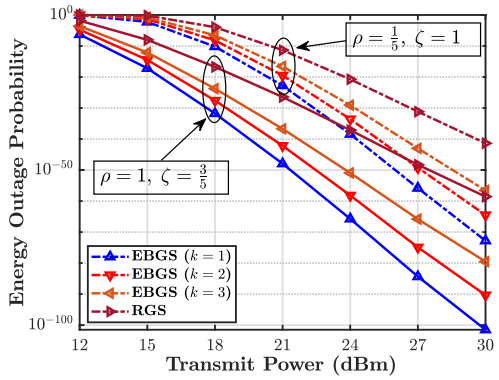

Figure 5.12: Variation of P_{tx} with energy outage in a linear EH model.

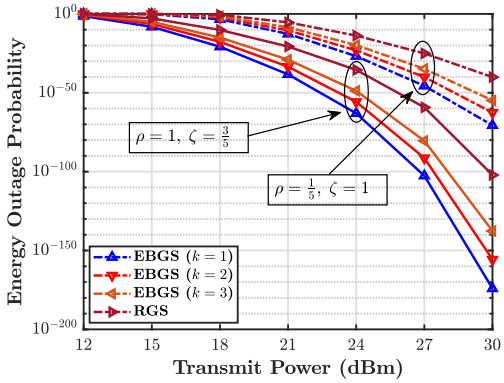

Figure 5.13: Variation of P_{tx} with energy outage in a nonlinear EH model.

The reason for this is attributed to the fact that as K_g increases, the 'chance of the best group being available' also increases, which improves the outage performance.

Fig. 5.12 and Fig. 5.13 illustrate the impact of transmit power on the energy outage as computed in (5.48) for the k-th best group selection in a linear and non-linear EH scenario, respectively. Here, we consider both the PS and TS configurations by using $(\zeta = 1, 0 < \rho < 1)$ and $(\rho = 1, 0 < \zeta < 1)$, respectively. We consider that each group has 10 patches and 40 groups are accessible to facilitate communication, distance from S to R_i is 15 m, $P_{ph} = 5$ dBm, and $P_t = 5$ dBm. In both the figures, we observe that, irrespective of k, the energy outage exhibits a decreasing trend with increasing transmit power, which is intuitive. This is supported by the fact that the suggested selection schemes perform better as the transmit power increases. Moreover, we notice that the energy outage for the 1st best group is lesser than the 2nd best, which in turn, is lesser than the 3rd best. Consequently, as also observed earlier, we find that the RGS scheme performs the worst.

Fig. 5.14 illustrates the impact of RIS configuration on the achievable data rate for

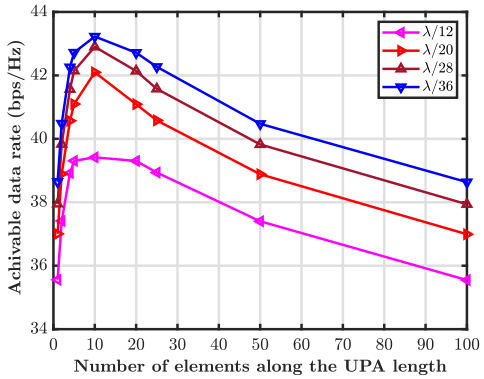

Figure 5.14: Impact of RIS configuration on achievable data rate.

various inter-patch distance; here we consider the Rician $K = 2$, power splitting factor $\rho = 0.2$, and the number of elements in each group $M = 100$. Specifically, for a fixed inter-patch distance, we arrange these M elements in various uniform planar array (UPA)-based configurations. Therefore, the configuration $(N_x, N_y) \in \{(1,100), (2,50), (4,25), (5,20), (10,10), (20,5), (25,4), (50,2), (100,1)\}$, where N_x and N_y represent the number of elements along the UPA length and width, respectively. We observe that, irrespective of the UPA configuration, the data rate increases with decreasing inter-patch distance. Moreover, with all other system parameters remaining constant, the maximum data rate is achieved for the square configuration, i.e., $N_x = N_y = 10$. The reason for this is attributed to the fact that, among all the possible configurations, $N_x = N_y$ results in the most compact shape with minimum distance among any pair of farthest located reflecting elements in the group. Hence, in scenarios, where it is not possible to have $N_x = N_y$, the best result is obtained by choosing N_x, N_y very close to each other.

5.8 Conclusion

In this chapter, we proposed novel order statistics-based generalized group selection strategies for a self-sustainable RIS-assisted D2D communication set-up in a Rician fading scenario, which takes into account the aspect of correlated channels. These strategies are based on the performance metrics like the end-to-end SNR and the energy harvested at the RIS group. Here, we considered both the PS and the TS configurations of the RIS and provided performance bounds for the system parameters of concern. We demonstrated the importance of spatial correlation at the RIS (in terms of the inter-patch spacing) on

the system performance by analytically characterizing both the data outage and the energy outage. Moreover, by using EVT, we further looked into the asymptotic scenario of having a large number of groups available at the RIS for selection. Thereafter, we observed that the outage performance, in this case, monotonically improves with increasing number of groups. As an immediate extension of this work, we intend to investigate the aspect of considering an adaptive selection of number of elements in the group for self-sustainable RIS-aided communication scenario.

Appendices

A. Proof of Theorem 5.4.1

As ρ is equal for all the M_g reflecting elements of R_i, from (5.8), we obtain the harvested energy

$$E_{l,PS} = T_s \rho P_{\text{tx}} \rho_L d_{S,R_i}^{-\alpha} \sum_{i=1}^{M_g} |\tilde{h}_i|^2. \tag{5.59}$$

By rewriting (5.59), we obtain

$$P_{\text{tx}} = \frac{E_{l,PS}}{T_s \rho \rho_L d_{S,R_i}^{-\alpha} \sum_{i=1}^{M_g} |\tilde{h}_i|^2}. \tag{5.60}$$

Accordingly, the received SNR γ_{PS} at D is

$$\gamma_{\text{PS}} = \frac{\left(1-\rho\right) P_{\text{tx}} \rho_L^2 \left(d_{S,R_i} d_{R_i,D}\right)^{-\alpha}}{\sigma_0^2} |g_c|^2 |h_c|^2. \tag{5.61}$$

By using (5.60) in (5.61), we have

$$\gamma_{\text{PS}} = \left(\frac{1}{\rho} - 1\right) \frac{\rho_L E_{l,PS} \times d_{R_i,D}^{-\alpha}}{T_s \sigma_0^2 \sum_{i=1}^{M_g} |\tilde{h}_i|^2} |g_c|^2 |h_c|^2 \tag{5.62}$$

and the resultant achievable data rate is

$$R_{\text{PS}} = \log_2\left(1 + \gamma_{\text{PS}}\right). \tag{5.63}$$

Here, we observe that the power splitting factor ρ has a significant impact on both the EH and IT performances. Therefore, we now investigate the performance bounds on ρ, which will allow the PS configuration to function flawlessly.

According to Section 5.3.2.1, the R_i will not be able to transfer the incoming signal in the desired direction if $E_{l,PS} < E_{\text{req,PS}}$. As a result, for proper functioning of R_i, we require

$$E_{l,PS} \geq E_{\text{req,PS}} = T_s\Big(M_g P_t + P_{ph}\Big). \tag{5.64}$$

Hence, by using (5.1) and (5.59), we obtain

$$T_s \rho P_{\text{tx}} \rho_L d_{S,R_i}^{-\alpha} \sum_{i=1}^{M_g} |\tilde{h}_i|^2 \geq T_s\Big(M_g P_t + P_{ph}\Big), \tag{5.65}$$

which finally results in

$$\frac{M_g P_t + P_{ph}}{P_{\text{tx}} \rho_L d_{S,R_i}^{-\alpha} \sum_{i=1}^{M_g} |\tilde{h}_i|^2} \leq \rho. \tag{5.66}$$

Therefore, if the application-specific minimum required data rate is R_{req}, we must have

$$R_{\text{req}} \leq R_{\text{PS}} = \log_2(1 + \gamma_{\text{PS}}). \tag{5.67}$$

As a result, from (5.62) and (5.67), we obtain

$$2^{R_{\text{req}}} - 1 \leq \gamma_{\text{PS}} = \left(\frac{1}{\rho} - 1\right)\eta, \tag{5.68}$$

where $\eta = \frac{\rho_L E_{l,PS} \times d_{R_i,D}^{-\alpha}}{T_s \sigma_0^2 \sum_{i=1}^{M_g} |\tilde{h}_i|^2} |g_c|^2 |h_c|^2$. This, after trivial algebraic manipulations, results in

$$\frac{2^{R_{\text{req}}} - 1}{\eta} + 1 \leq \frac{1}{\rho} \implies \rho \leq \frac{\eta}{2^{R_{\text{req}}} - 1 + \eta}. \tag{5.69}$$

Hence, by combining (5.66) and (5.69), we obtain (5.13).

B. Proof of Theorem 5.4.2

Note that, for the proper functioning of R_i, we require $E_{nl,PS} \geq E_{\text{req,PS}}$, i.e., we must have

$$E_{nl,PS}^{\max} \geq E_{\text{req,PS}} \text{ and } E_{nl,PS}^{\min} \geq E_{\text{req,PS}}. \tag{5.70}$$

Hence, if we consider the best-case scenario, i.e., $|\tilde{h}_i| = |h_{\max}| \; \forall \; i = 1, \cdots, M$, by using (5.1) and (5.14), we obtain

$$M_g T_s \Big(\frac{a\rho P_{\text{tx}} \rho_L (d_{S,R_i})^{-\alpha} |h_{\max}|^2 + b}{\rho P_{\text{tx}} \rho_L (d_{S,R_i})^{-\alpha} |h_{\max}|^2 + c} - \frac{b}{c} \Big) \geq E_{\text{req,PS}}. \tag{5.71}$$

On further simplification and by using (5.1), we obtain

$$\frac{c(M_g P_t + P_{ph})}{M_g \rho_L (d_{S,R_i})^{-\alpha} P_{\text{tx}} |h_{\max}|^2 \Big(a - \frac{M_g P_t + P_{ph}}{M_g} - \frac{b}{c} \Big)} \leq \rho. \tag{5.72}$$

Similarly, now we consider the worst-case scenario, i.e., $|\tilde{h}_i| = |h_{\min}| \; \forall \; i = 1, \cdots, M_g$ and from (5.14), we have

$$P_{\text{tx}} = \frac{\frac{c E_{nl,PS}^{\min}}{M_g T_s}}{\rho \rho_L (d_{S,R_i})^{-\alpha} |h_{\min}|^2 \left(a - \frac{E_{nl,PS}^{\min}}{M_g T_s} - \frac{b}{c} \right)}. \tag{5.73}$$

Accordingly, the received SNR γ_{PS} at D is

$$\begin{aligned} \gamma_{\text{PS}} &= \frac{(1-\rho) P_{\text{tx}} \rho_L^2 \left(d_{S,R_i} d_{R_i,D} \right)^{-\alpha}}{\sigma_0^2} |g_c|^2 |h_c|^2 \\ &= \left(\frac{1}{\rho} - 1 \right) \frac{c E_{nl,PS}^{\min} \rho_L d_{R_i,D}^{-\alpha}}{M_g T_s |h_{\min}|^2 \left(a - \frac{E_{nl,PS}^{\min}}{M_g T_s} - \frac{b}{c} \right) \sigma_0^2} |g_c|^2 |h_c|^2. \end{aligned} \tag{5.74}$$

Note that, irrespective of the channel conditions, the data rate needs to be above the threshold R_{req}, i.e., (5.67) results in

$$R_{\text{req}} \leq R_{\text{PS}} \implies 2^{R_{\text{req}}} - 1 \leq \gamma_{PS} = \left(\frac{1}{\rho} - 1 \right) \kappa, \tag{5.75}$$

where

$$\kappa = \frac{cE_{nl,PS}^{\min}\rho_L d_{R_i,D}^{-\alpha}}{M_g T_s |h_{\min}|^2 \left(a - \frac{E_{nl,PS}^{\min}}{M_g T_s} - \frac{b}{c}\right)\sigma_0^2}|g_c|^2|h_c|^2. \tag{5.76}$$

Thereafter, further simplifications result in

$$\rho \leq \frac{\kappa}{(2^{R_{\text{req}}}-1)+\kappa}. \tag{5.77}$$

Finally, by combining (5.72) and (5.77), we have (5.18).

C. Proof of Theorem 5.4.3

The harvested energy, in a slot, is obtained from (5.8) as

$$E_{l,TS} = \zeta T_s P_{\text{tx}} \rho_L d_{S,R_i}^{-\alpha} \sum_{i=1}^{M_g} |\tilde{h}_i|^2. \tag{5.78}$$

For proper RIS functioning, we must have $E_{l,TS} \geq E_{\text{req,TS}}$, i.e., by using (5.2) and (5.78), we get

$$\begin{aligned} E_{l,TS} \geq E_{\text{req,TS}} &= T_s\Big(M_g P_t(1-\zeta) + P_{ph}\Big) \\ \implies \zeta T_s P_{\text{tx}} \rho_L d_{S,R_i}^{-\alpha} \sum_{i=1}^{M_g} |\tilde{h}_i|^2 &\geq T_s\Big(M_g P_t(1-\zeta) + P_{ph}\Big), \end{aligned}$$

which finally results in

$$\frac{M_g P_t + P_{ph}}{M_g P_t + P_{\text{tx}} \rho_L d_{S,R_i}^{-\alpha} \sum_{i=1}^{M_g} |\tilde{h}_i|^2} \leq \zeta. \tag{5.79}$$

Similar to the PS configuration, if the application-specific minimum required data rate is R_{req}, we have

$$R_{\text{req}} \leq R_{\text{TS}} = (1-\zeta)\log_2(1+\gamma_{\text{TS}}) = (1-\zeta)R_{\text{arc}}, \tag{5.80}$$

where $R_{\text{arc}} = \log_2(1+\gamma_{\text{TS}})$ is the achievable data rate and

$$\gamma_{\text{TS}} = \frac{P_{\text{tx}}\rho_L^2\left(d_{S,R_i}d_{R_i,D}\right)^{-\alpha}}{\sigma_0^2}|g_c|^2|h_c|^2. \tag{5.81}$$

Further simplification of the above results in

$$\zeta \leq 1 - \frac{R_{\text{req}}}{R_{\text{arc}}}. \tag{5.82}$$

Thus, by combining (5.79) and (5.82), we obtain (5.21).

D. Proof of Theorem 5.4.4

If $E_{nl,TS}^{\max}$ is the harvested energy by considering $|\tilde{h_i}| = |h_{\max}| \ \forall\ i = 1, \cdots, M$, from the proper functioning condition of R_i, we have, $E_{nl,TS}^{\max} \geq E_{\text{req,Ts}}$. Hence, by using (5.2) and (5.7), we obtain

$$\zeta T_s M_g\Big(\frac{a\rho P_{\text{tx}}\rho_L(d_{S,R_i})^{-\alpha}|h_{\max}|^2+b}{\rho P_{\text{tx}}\rho_L(d_{S,R_i})^{-\alpha}|h_{\max}|^2+c} - \frac{b}{c}\Big) \geq E_{\text{req,TS}}. \tag{5.83}$$

The above equation can be rewritten as

$$\zeta M_g\left(\frac{a\varphi+b}{\varphi+c} - \frac{b}{c}\right) \geq (1-\zeta)M_g P_t + P_{ph}, \tag{5.84}$$

where $\varphi = \rho_L d_{S,R_i}^{-\alpha} P_{\text{tx}}|h_{\max}|^2$. Thereafter, further simplification results in

$$\frac{M_g P_t + P_{ph}}{M_g\left(P_t + \frac{a\varphi+b}{\varphi+c} - \frac{b}{c}\right)} \leq \zeta. \tag{5.85}$$

Note that, during the EH process, we are concerned only with the $S - R_i$ link; hence, the role of g_c is irrelevant. Moreover, from (5.5), we have $h_c = \sum_{i=1}^{M_g} \tilde{h_i}$, which results in $|h_c|^2 = M_g^2|h_{\min}|^2$ for the considered worst-case scenario. Thus, the resultant SNR at D is

$$\gamma_{\text{TS}}^{\min} = \frac{M_g^2 P_{\text{tx}}\rho_L^2\left(d_{S,R_i}d_{R_i,D}\right)^{-\alpha}}{\sigma_0^2}|g_c|^2|h_{\min}|^2 \tag{5.86}$$

and the resultant achievable data rate is

$$R_{\mathrm{TS}} = \big(1-\zeta\big)\log_2(1+\gamma_{\mathrm{TS}}^{\min}). \tag{5.87}$$

Regardless of the channel conditions, the data rate must exceed the specified threshold R_{req}, i.e.,

$$R_{\mathrm{req}} \leq R_{\mathrm{TS}} = (1-\zeta)\log_2(1+\gamma_{\mathrm{TS}}^{\min}) = (1-\zeta)R_{\mathrm{arc}}^{\min},$$

where we define $R_{\mathrm{arc}}^{\min} = \log_2(1+\gamma_{\mathrm{TS}}^{\min})$. Further simplification of the above results in

$$\zeta \leq 1 - \frac{R_{\mathrm{req}}}{R_{\mathrm{arc}}^{\min}}. \tag{5.88}$$

Hence, by combining (5.85) and (5.88), we obtain (5.22).

Chapter 6

Conclusion and Future Research Direction

6.1 Concluding Remarks

This thesis discusses various strategies to get around some of the difficulties that arise when utilizing RISs for D2D communication at 5G and beyond mmWave communication. RIS can be used to improve D2D communication performance by increasing wireless network connectivity, throughput, spectral efficiency, and reliability by properly tuning the phases and providing an indirect LoS link between two proximate users. In this context, the following aspects have been addressed:

In Chapter 2, we proposed a novel RIS deployment strategy by allowing single as well as double reflections to provide an indirect LoS link between two obstructed device pairs. Additionally, to prevent resource wastage, we proposed an energy-efficient group selection strategy for a device pair to complete their successful communication. Furthermore, we proved that sometimes double reflections are more energy-efficient than single reflection, which is non-intuitive. In Chapter 3, by assuming that the RISs are already deployed in the surroundings, we proposed a novel double-RIS assisted adaptive modulation-based cooperative multihop routing scheme. This cooperative routing scheme makes use of both the IUs and RISs. It is to be noted that a particular RIS can handle only a single request in a particular time instance. Moreover, multiple requesting device pairs may demand the same RIS for their seamless communication. In this context, in chapter 4, we proposed a priority-aware channel-dependent user scheduling strategy for RIS-assisted multihop D2D communication, which also takes into account the aspect of element grouping at the RIS. Furthermore, we demonstrated that the least remaing distance based approach does not

always yield the best result in terms of system performance. In addition, in RIS-assisted D2D communication scenarios, a group that provides the best data rate may not always be available to serve as a relay node. In these cases, a request may have to wait until the desired RIS is available. In this context, in Chapter 5, we proposed a novel order statistics-based generalized group selection strategy for a self-sustainable RIS-assisted D2D communication setup in a Rician fading scenario, which takes into account the aspect of correlated channels. Note that, due to the low-power communication scenario, here, we used the self-sustainable RISs, which can harvest energy from the incoming signals. Additionally, by using EVT, we further looked into the asymptotic scenario of having a large number of groups available at the RIS for group selection.

6.2 Future Work Directions

In this thesis, we have addressed various aspects of RIS-aided mmWave D2D communication scenarios. However, we believe that there will be a lot of opportunities for future RIS-assisted mmWave D2D communications research owing to our techniques and experimental findings. This work opens up several promising avenues for future research, some of which are outlined below.

- **RIS deployment in continuous domain:** In Chapters 2, we proposed a novel RIS deployment strategy in the double RIS-assisted D2D wireless communication scenario. In this work, the RISs are deployed in the discrete domain by discretizing the entire environment into a specific resolution of a grid. In this setup, we considered that a grid is either fully occupied by an obstacle or not. However, in practice, each cell of a grid may not be fully blocked, which results in a bad approximation. In this context, we should propose a RIS deployment strategy in the continuous domain. Note that the continuous domain refers to the domain in which the precise position can be found.

- **Scheduling strategy for non-cooperative scenarios:** In Chapter 3, we proposed a novel double-RIS assisted adaptive modulation-based multihop routing scheme for D2D wireless networks, which takes into account the aspect of multi-RIS secondary reflection. An immediate extension of this work is to investigate a non-cooperative scenario, where the users are independent in deciding whether they would like to act as a relay or not. If they do, then for which corresponding $S - D$ pair they will be agreed and in that case what incentives can be provided.

- **Scheduling strategy for imperfect CSI:** In Chapter 4, we proposed a novel priority-aware channel-dependent scheduling strategy for RIS-assisted multihop D2D communication, which also takes into account the aspect of element grouping at the RIS. An immediate extension of this work is to investigate scenarios, where even when idle, it depends on the IUs to decide whether to act as relays to its requesting neighbors or to prioritize its own sleep mode. Moreover, we intend to investigate the aspect of imperfect channel state and phase errors at the RISs on the proposed strategy. Finally, we also aim to comment on having various adaptive grouping criteria at the RISs and investigate its impact.

- **Element splitting-based RIS design:** In Chapter 5, we proposed novel order statistics-based generalized group selection strategies for a self-sustainable RIS-assisted D2D communication set-up in a Rician fading scenario, which takes into account the aspect of correlated channels. Specifically, here, we design a RIS architecture for two specific EH models where the elements of a group take part either for EH or information transfer. As an immediate extension of this work, we aim to investigate the aspect of considering an element splitting-based self-sustainable RIS-aided communication scenario. The scenario of incorporating the aspect of spatial correlation in such a case can also be considered. Furthermore, in this chapter, we assumed a single antenna transceivers. Therefore, an immediate extension of this work is to investigate the generalized group selection criteria for multi-user multi-antenna communication scenarios.

Bibliography

[1] Ericsson Mobility Report, June 2025. [Online]. Available: https://www.ericsson.com/en/mobility-report/reports/june-2023.

[2] Arash Asadi, Qing Wang, and Vincenzo Mancuso. A survey on device-to-device communication in cellular networks. *IEEE Commun. Surv. Tutorials*, 16(4):1801–1819, Apr. 2014.

[3] Nikolaos Giatsoglou, Konstantinos Ntontin, Elli Kartsakli, Angelos Antonopoulos, and Christos Verikoukis. D2D-aware device caching in mmWave-cellular networks. *IEEE J. Sel. Areas Commun.*, 35(9):2025–2037, Sep. 2017.

[4] Akhil Gupta and Rakesh Kumar Jha. A survey of 5G network: Architecture and emerging technologies. *IEEE Access*, 3:1206–1232, Aug. 2015.

[5] Mamta Agiwal, Abhishek Roy, and Navrati Saxena. Next Generation 5G Wireless Networks: A Comprehensive Survey. *IEEE Commun. Surv. Tutorials*, 18(3):1617–1655, 2016.

[6] Marco Mezzavilla, Menglei Zhang, Michele Polese, Russell Ford, Sourjya Dutta, Sundeep Rangan, and Michele Zorzi. End-to-end simulation of $5g\ mmwave$ networks. *IEEE Commun. Surv. Tutorials*, 20(3):2237–2263, Mar. 2018.

[7] Xiong Wang, Linghe Kong, Fanxin Kong, Fudong Qiu, Mingyu Xia, Shlomi Arnon, and Guihai Chen. Millimeter wave communication: A comprehensive survey. *IEEE Commun. Surv. Tutorials*, 20(3):1616–1653, 2018.

[8] Ertugrul Basar, Marco Di Renzo, Julien De Rosny, Merouane Debbah, Mohamed-Slim Alouini, and Rui Zhang. Wireless communications through reconfigurable intelligent surfaces. *IEEE Access*, 7:116753–116773, Aug. 2019.

[9] Cunhua Pan, Gui Zhou, Kangda Zhi, Sheng Hong, Tuo Wu, Yijin Pan, Hong Ren, Marco Di Renzo, A Lee Swindlehurst, Rui Zhang, et al. An overview of signal processing techniques for RIS/IRS-aided wireless systems. *IEEE J. Sel. Areas Commun.*, 16(5):883–917, May 2022.

[10] Majid H Khoshafa, Omar Maraqa, Jules M Moualeu, Sylvester Aboagye, Telex MN Ngatched, Mohamed H Ahmed, Yasser Gadallah, and Marco Di Renzo. RIS-assisted physical layer security in emerging RF and optical wireless communication systems: A comprehensive survey. *IEEE Commun. Surv. Tutorials*, 2024.

[11] Manzoor Ahmed, Abdul Wahid, Sayed Shariq Laique, Wali Ullah Khan, Asim Ihsan, Fang Xu, Symeon Chatzinotas, and Zhu Han. A survey on STAR-RIS: Use cases, recent advances, and future research challenges. *IEEE Internet Things J.*, 10(16):14689–14711, 2023.

[12] Zhengquan Zhang, Yue Xiao, Zheng Ma, Ming Xiao, Zhiguo Ding, Xianfu Lei, George K. Karagiannidis, and Pingzhi Fan. 6G wireless networks: Vision, requirements, architecture, and key technologies. *IEEE Veh. Tech. Mag.*, 14(3):28–41, Sep. 2019.

[13] Simon Tewes, Markus Heinrichs, Rainer Kronberger, and Aydin Sezgin. IRS-enabled breath tracking with colocated commodity WiFi transceivers. *IEEE Internet Things J.*, 10(8):6870–6886, Apr. 2023.

[14] Chongwen Huang, Zhaohui Yang, George C Alexandropoulos, Kai Xiong, Li Wei, Chau Yuen, Zhaoyang Zhang, and Mérouane Debbah. Multi-hop RIS-empowered terahertz communications: A DRL-based hybrid beamforming design. *IEEE J. Sel. Areas Commun.*, 39(6):1663–1677, Jun. 2021.

[15] Beixiong Zheng, Changsheng You, and Rui Zhang. Double-IRS assisted multi-user MIMO: Cooperative passive beamforming design. *IEEE Trans. Wireless Commun.*, 20(7):4513–4526, July 2021.

[16] Jaya Prakash Champati, Hussein Al-Zubaidy, and James Gross. Transient analysis for multihop wireless networks under static routing. *IEEE/ACM Trans. Networking*, 28(2):722–735, Apr. 2020.

[17] Georgy Levin and Sergey Loyka. Amplify-and-forward versus decode-and-forward relaying: Which is better? In *Proc. 22nd Int. Zurich Seminar Commun. (IZS)*, Zürich, Switzerland, 2012.

[18] Jaya Goel and J Harshan. One-Hop listening based ARQs for low-latency communication in multihop networks. *IEEE Trans. Wireless Commun.*, 22(2):1044–1059, Feb. 2023.

[19] Zan Li, Neel Kanth Kundu, Junhui Rao, Shanpu Shen, Matthew R. McKay, and Ross Murch. Performance analysis of RIS-assisted communications with element grouping and spatial correlation. *IEEE Wireless Commun. Lett.*, 12(4):630–634, Apr. 2023.

[20] Krisma Asmoro and Soo Young Shin. RIS grouping based index modulation for 6G telecommunications. *IEEE Wireless Commun. Lett.*, 11(11):2410–2414, 2022.

[21] Ying Gao, Qingqing Wu, Wen Chen, Yang Liu, Ming Li, and Daniel Benevides Da Costa. IRS-aided overloaded multi-antenna systems: Joint user grouping and resource allocation. *IEEE Trans. Wireless Commun.*, 23(8):8297–8313, Aug. 2024.

[22] Yifei Yang, Beixiong Zheng, Shuowen Zhang, and Rui Zhang. Intelligent reflecting surface meets OFDM: Protocol design and rate maximization. *IEEE Trans. Commun.*, 68(7):4522–4535, Jul. 2020.

[23] Neel Kanth Kundu, Zan Li, Junhui Rao, Shanpu Shen, Matthew R McKay, and Ross Murch. Optimal grouping strategy for reconfigurable intelligent surface assisted wireless communications. *IEEE Wireless Commun. Lett.*, 11(5):1082–1086, May 2022.

[24] Emil Björnson and Luca Sanguinetti. Rayleigh fading modeling and channel hardening for reconfigurable intelligent surfaces. *IEEE Wireless Commun. Lett.*, 10(4):830–834, Apr. 2020.

[25] Cunhua Pan, Gui Zhou, Kangda Zhi, Sheng Hong, Tuo Wu, Yijin Pan, Hong Ren, Marco Di Renzo, A Lee Swindlehurst, Rui Zhang, et al. An overview of signal processing techniques for RIS/IRS-aided wireless systems. *IEEE J. Sel. Top. Signal Process.*, 16(5):883–917, Aug. 2022.

[26] Zhiguo Ding, Caijun Zhong, Derrick Wing Kwan Ng, Mugen Peng, Himal A Suraweera, Robert Schober, and H Vincent Poor. Application of smart antenna technologies in simultaneous wireless information and power transfer. *IEEE Commun. Mag.*, 53(4):86–93, Apr. 2015.

[27] Yunfei Chen, Nan Zhao, and Mohamed-Slim Alouini. Wireless energy harvesting using signals from multiple fading channels. *IEEE Trans. Commun.*, 65(11):5027–5039, Nov. 2017.

[28] Eduard E Bahingayi, Nemanja Stefan Perović, and Le-Nam Tran. Weighted Sum-Rate Maximization for Large-Scale RIS-Assisted Multi-User MISO Systems. In *2025 IEEE Wireless Commun. Networking Conf. (WCNC)*, pages 1–6. IEEE, 2025.

[29] Huayan Guo, Ying-Chang Liang, Jie Chen, and Erik G Larsson. Weighted sum-rate maximization for intelligent reflecting surface enhanced wireless networks. In *2019 IEEE Global Commun. Conf. (GLOBECOM)*, pages 1–6. IEEE, 2019.

[30] Qingqing Wu, Beixiong Zheng, Changsheng You, Lipeng Zhu, Kaiming Shen, Xiaodan Shao, Weidong Mei, Boya Di, Hongliang Zhang, Ertugrul Basar, et al. Intelligent surfaces empowered wireless network: Recent advances and the road to 6G. *Proceedings of the IEEE*, 112(7):724–763, 2024.

[31] T. Weiss, J. Hillenbrand, A. Krohn, and F.K. Jondral. Mutual interference in OFDM-based spectrum pooling systems. In *2004 IEEE 59th Veh. Technol. Conf.*, volume 4, pages 1873–1877, 2004.

[32] Ramin Hashemi, Samad Ali, Nurul Huda Mahmood, and Matti Latva-aho. Average rate and error probability analysis in short packet communications over RIS-aided URLLC systems. *IEEE Trans. Vehi. Technol.*, 70(10):10320–10334, Oct. 2021.

[33] Fabio Saggese, Federico Chiariotti, Kimmo Kansanen, and Petar Popovski. Efficient URLLC with a reconfigurable intelligent surface and imperfect device tracking. In *ICC 2023-IEEE Inter. Conf. Commun.*, pages 2722–2728. IEEE, 2023.

[34] Bhagawat Adhikari, Muhammad Jaseemuddin, and Alagan Anpalagan. Resource allocation for co-existence of embb and urllc services in 6g wireless networks: A survey. *IEEE Access*, 12:552–581, 2023.

[35] Lakshmikanta Sau and Sasthi C Ghosh. A geometry-based strategic placement of RISs in millimeter wave device to device communication. In *Proc. 3rd Int. Conf. Comput. Commun. Engineering. (CCCE)*, pages 1–13, Mar. 2023.

[36] Souvik Deb and Sasthi C Ghosh. An RIS deployment strategy to overcome static obstacles in millimeter wave D2D communication. In *Proc. IEEE 20th Int. Symp. Netw. Comput. Appl. (NCA)*, pages 1–8, Nov. 2021.

[37] Shuhao Zeng, Hongliang Zhang, Boya Di, Zhu Han, and Lingyang Song. Reconfigurable intelligent surface (RIS) assisted wireless coverage extension: RIS orientation and location optimization. *IEEE Commun. Lett.*, 25(1):269–273, Jan. 2021.

[38] Dimitrios Tyrovolas, Sotiris A. Tegos, Vasilis K. Papanikolaou, Yue Xiao, Prodromos-Vasileios Mekikis, Panagiotis D. Diamantoulakis, Sotiris Ioannidis, Christos K. Liaskos, and George K. Karagiannidis. Zero-Energy Reconfigurable Intelligent Surfaces (zeRIS). *IEEE Trans. Wireless Commun.*, 23(7):7013–7026, July 2024.

[39] Zhenyao He et al. Joint training and reflection pattern optimization for non-ideal RIS-aided multiuser systems. *IEEE Trans. Commun.*, 72(9):5735–5751, Sep. 2024.

[40] Shuaiqi Jia, Xiaojun Yuan, and Ying-Chang Liang. Reconfigurable intelligent surfaces for energy efficiency in D2D communication network. *IEEE Wireless Commun. Lett.*, 10(3):683–687, 2020.

[41] Jindan Xu, Wei Xu, and Chau Yuen. On performance of distributed RIS-aided communication in random networks. *IEEE Trans. Wireless Commun.*, 23(12):18254–18270, Dec. 2024.

[42] Shuaiqi Jia, Xiaojun Yuan, and Ying-Chang Liang. Reconfigurable intelligent surfaces for energy efficiency in D2D communication network. *IEEE Wireless Commun. Lett.*, 10(3):683–687, Mar. 2021.

[43] Yali Chen, Bo Ai, Hongliang Zhang, Yong Niu, Lingyang Song, Zhu Han, and H. Vincent Poor. Reconfigurable intelligent surface assisted device-to-device communications. *IEEE Trans. Wireless Commun.*, 20(5):2792–2804, May 2021.

[44] Kayhan Zrar Ghafoor, Linghe Kong, Sherali Zeadally, Ali Safaa Sadiq, Gregory Epiphaniou, Mohammad Hammoudeh, Ali Kashif Bashir, and Shahid Mumtaz.

Millimeter-wave communication for Internet of Vehicles: Status, challenges, and perspectives. *IEEE Internet Things J.*, 7(9):8525–8546, Sep. 2020.

[45] Jiguang He, Henk Wymeersch, and Markku Juntti. Channel estimation for RIS-aided mmWave MIMO systems via atomic norm minimization. *IEEE Trans.Wireless Commun.*, 20(9):5786–5797, 2021.

[46] Mustafa A Kishk and Mohamed-Slim Alouini. Exploiting randomly located blockages for large-scale deployment of intelligent surfaces. *IEEE J. Sel. Areas Commun.*, 39(4):1043–1056, Apr. 2020.

[47] Tu V. Nguyen, Diep N. Nguyen, Marco Di Renzo, and Rui Zhang. Leveraging secondary reflections and mitigating interference in Multi-IRS/RIS aided wireless networks. *IEEE Trans. Wireless Commun.*, 22(1):502–517, Jan. 2023.

[48] Zhenyu Kang, Changsheng You, and Rui Zhang. Double-Active-IRS aided wireless communication: Deployment optimization and capacity scaling. *IEEE Wireless Commun. Lett.*, 12(11):1821–1825, Nov. 2023.

[49] Yitao Han, Shuowen Zhang, Lingjie Duan, and Rui Zhang. Cooperative double-IRS aided communication: Beamforming design and power scaling. *IEEE Wireless Commun. Lett.*, 9(8):1206–1210, Aug. 2020.

[50] Monowar Hasan, Ekram Hossain, and Dong In Kim. Resource allocation under channel uncertainties for relay-aided device-to-device communication underlaying LTE-A cellular networks. *IEEE Trans. Wireless Commun.*, 13(4):2322–2338, Apr. 2014.

[51] Peng Yang, Zhihao Zhang, Jing Yang, and Xiong Wang. Incorporating user willingness in contract-based incentive mechanism for D2D cooperative data forwarding. *IEEE Access*, 6:54927–54937, 2018.

[52] Chunsheng Tian, Zhihong Qian, Xue Wang, and Liangshuai Hu. Analysis of joint relay selection and resource allocation scheme for relay-aided D2D communication networks. *IEEE Access*, 7:142715–142725, 2019.

[53] Durgesh Singh and Sasthi C Ghosh. Mobility-aware relay selection in 5G D2D communication using stochastic model. *IEEE Trans. Veh. Technol.*, 68(3):2837–2849, 2019.

[54] Zhaleh Sadreddini, Erkan Güler, Mohsen Khalily, and Halim Yanikomeroglu. MRIRS: Mobile ad hoc routing assisted with intelligent reflecting surfaces. *IEEE Trans. Cognit. Commun. Networking*, 7(4):1333–1346, Dec. 2021.

[55] Marsa Rayani, Amin Ebrahimzadeh, Roch H. Glitho, and Halima Elbiaze. Ensuring profit and QoS when dynamically embedding delay-constrained ICN and IP slices for content delivery. *IEEE Trans. Network Sci. Eng.*, 9(2):769–782, Mar. 2022.

[56] Zhongyuan Zhao, Gunjan Verma, Chirag Rao, Ananthram Swami, and Santiago Segarra. Link scheduling using graph neural networks. *IEEE Trans. Wireless Commun.*, 22(6):3997–4012, June 2022.

[57] Mengyuan Lee, Guanding Yu, and Geoffrey Ye Li. Graph embedding-based wireless link scheduling with few training samples. *IEEE Trans. Wireless Commun.*, 20(4):2282–2294, Apr. 2020.

[58] Renjie Liang and Jiancun Fan. Energy-efficient mmwave IoT communications with multihop IRS-assisted systems. *IEEE Internet Things J.*, 10(21):19344–19355, Nov. 2023.

[59] Emil Björnson and Luca Sanguinetti. Rayleigh fading modeling and channel hardening for reconfigurable intelligent surfaces. *IEEE Wireless Commun. Lett.*, 10(4):830–834, Apr. 2021.

[60] Dan Yang, Jindan Xu, Wei Xu, Yongming Huang, and Zhaohua Lu. Secure communication for spatially correlated RIS-aided multiuser massive MIMO systems: Analysis and optimization. *IEEE Commun. Lett.*, 27(3):797–801, Mar. 2023.

[61] Hongliang Zhang, Boya Di, Lingyang Song, and Zhu Han. Reconfigurable intelligent surfaces assisted communications with limited phase shifts: How many phase shifts are enough? *IEEE Trans. Veh. Technol.*, 69(4):4498–4502, Apr. 2020.

[62] Swades De. On hop count and Euclidean distance in greedy forwarding in wireless ad hoc networks. *IEEE Commun. Lett.*, 9(11):1000–1002, Nov. 2005.

[63] Sen Du, Junjie Hou, Shijin Song, Yuefeng Song, and Yongxin Zhu. A geographical hierarchy greedy routing strategy for vehicular big data communications over millimeter wave. *Phys. Commun.*, 40:101065, 2020.

[64] Priyadarshi Mukherjee, Constantinos Psomas, and Ioannis Krikidis. DCSK-based waveform design for self-sustainable RIS-aided noncoherent SWIPT. *IEEE Trans. Commun.*, 73(9):8435–8450, Sept. 2025.

[65] Andreas Nicolaides, Constantinos Psomas, Ghassan M. Kraidy, Sheng Yang, and Ioannis Krikidis. Outage and DMT analysis of partition-based schemes for RIS-aided MIMO fading channels. *IEEE J. Sel. Areas Commun.*, 41(8):2336 – 2349, Aug. 2023.

[66] Minchae Jung, Walid Saad, Mérouane Debbah, and Choong Seon Hong. On the optimality of reconfigurable intelligent surfaces (RISs): Passive beamforming, modulation, and resource allocation. *IEEE Trans. Wireless Commun.*, 20(7):4347–4363, July 2021.

[67] Vijay V Vazirani. *Approximation algorithms*, volume 1. Springer, 2001.

[68] Akram Al-Hourani et al. Path loss study for millimeter wave device-to-device communications in urban environment. In *2014 IEEE Int. Conf. on Commun. Workshops (ICC)*, pages 102–107, 2014.

[69] Chongwen Huang et al. Reconfigurable intelligent surfaces for energy efficiency in wireless communication. *IEEE Trans. Wireless Commun.*, 18(8):4157–4170, Aug. 2019.

[70] P. Mukherjee, D. Mishra, and S. De. Gaussian mixture based context-aware short-term characterization of wireless channels. *IEEE Trans. Veh. Technol.*, 69(1):26–40, Jan. 2020.

[71] Zhaohui Yang, Mingzhe Chen, Walid Saad, Wei Xu, Mohammad Shikh-Bahaei, H Vincent Poor, and Shuguang Cui. Energy-efficient wireless communications with distributed reconfigurable intelligent surfaces. *IEEE Trans. Wireless Commun.*, 21(1):665–679, Jan. 2021.

[72] Qingqing Wu, Shuowen Zhang, Beixiong Zheng, Changsheng You, and Rui Zhang. Intelligent reflecting surface-aided wireless communications: A tutorial. *IEEE Trans. Commun.*, 69(5):3313–3351, May 2021.

[73] Beixiong Zheng, Changsheng You, and Rui Zhang. Double-IRS assisted multi-user MIMO: Cooperative passive beamforming design. *IEEE Trans. Wireless Commun.*, 20(7):4513–4526, July 2021.

[74] Steven Kisseleff, Symeon Chatzinotas, and Björn Ottersten. Random access-based reliable uplink communication and power transfer using dynamic power splitting. *IEEE Trans. Wireless Commun.*, 19(6):4307–4320, June 2020.

[75] Priyadarshi Mukherjee and Swades De. A system state aware switched-multichannel protocol for energy harvesting CRNs. *IEEE Trans. Cognit. Commun. Networking*, 6(2):669–682, June 2020.

[76] Chao ZHANG, Guanghui ZHOU, Jiacheng XIAO, Tianyu QIN, and Yaguang ZHOU. Multi-dimensional and multi-scale modeling and edge-cloud collaborative configuration method for digital twin manufacturing cell. *Computer Integrated Manufacturing System*, 29(2):355, 2023.

[77] Qurrat-Ul-Ain Nadeem, Abla Kammoun, Anas Chaaban, Mérouane Debbah, and Mohamed-Slim Alouini. Asymptotic Max-Min SINR analysis of reconfigurable intelligent surface assisted MISO systems. *IEEE Trans. Wireless Commun.*, 19(12):7748–7764, Dec. 2020.

[78] Jun Huang, Yide Zhou, Zhaolong Ning, and Hamid Gharavi. Wireless power transfer and energy harvesting: Current status and future prospects. *IEEE Wireless Commun.*, 26(4):163–169, Aug. 2019.

[79] E. Boshkovska, D. W. K. Ng, N. Zlatanov, and R. Schober. Practical non-linear energy harvesting model and resource allocation for SWIPT systems. *IEEE Commun. Lett.*, 19(12):2082–2085, Dec. 2015.

[80] C. E. Shannon. A mathematical theory of communication. *Bell Syst. Tech. J.*, 27(3):379–423, July 1948.

[81] Yury Polyanskiy, H. Vincent Poor, and Sergio Verdu. Channel coding rate in the finite blocklength regime. *IEEE Trans. Inf. Theory*, 56(5):2307–2359, May 2010.

[82] Linqing Gui, Fu Xiao, Yang Zhou, Feng Shu, and Thierry Val. Connectivity based DV-Hop localization for Internet of Things. *IEEE Trans. Veh. Technol.*, 69(8):8949–8958, Aug. 2020.

[83] Athanasios Papoulis and S. Unnikrishna Pillai. *Probability, Random Variables, and Stochastic Processes*. McGraw-Hill Higher Education, Fourth edition, 2002.

[84] Andrea Goldsmith. *Wireless Communications*. Cambridge Univ. Press, 2005.

[85] Chandan Kumar and Salil Kashyap. On the power transfer efficiency and feasibility of wireless energy transfer using double IRS. *IEEE Trans. Veh. Technol.*, 2023. early access.

[86] Zhaohui Yang, Mingzhe Chen, Walid Saad, Wei Xu, Mohammad Shikh-Bahaei, H. Vincent Poor, and Shuguang Cui. Energy-efficient wireless communications with distributed reconfigurable intelligent surfaces. *IEEE Trans. Wireless Commun.*, 21(1):665–679, Jan. 2022.

[87] Koushik A.M., Fei Hu, and Sunil Kumar. Intelligent spectrum management based on transfer actor-critic learning for rateless transmissions in cognitive radio networks. *IEEE Trans. Mobile Comput.*, 17(5):1204–1215, May 2018.

[88] Jiapin Guo and Xinen Zhu. An improved analytical model for RF-DC conversion efficiency in microwave rectifiers. In *Proc. IEEE MTT-S Int. Microw. Symp. Dig.*, pages 1–3, Montreal, QC, Canada, June 2012.

[89] Yury Polyanskiy, H. Vincent Poor, and Sergio Verdu. Channel coding rate in the finite blocklength regime. *IEEE Trans. Inf. Theory*, 56(5):2307–2359, May 2010.

[90] Suresh Kumaar Jayaraman, Lionel P Robert, X Jessie Yang, and Dawn M Tilbury. Multimodal hybrid pedestrian: A hybrid automaton model of urban pedestrian behavior for automated driving applications. *IEEE Access*, 9:27708–27722, 2021.

[91] Norman C. Beaulieu and Kasun T. Hemachandra. Novel simple representations for Gaussian class multivariate distributions with generalized correlation. *IEEE Trans. Inf. Theory*, 57(12):8072–8083, Dec. 2011.

[92] Andreas Nicolaides, Constantinos Psomas, and Ioannis Krikidis. A Markov chain approach for myopic multi-hop relaying: Outage and diversity analysis. *IEEE J. Sel. Top. Signal Process.*, 16(1):56–69, Jan. 2022.

[93] Xuelin Cao, Bo Yang, Chongwen Huang, Chau Yuen, Marco Di Renzo, Dusit Niyato, and Zhu Han. Reconfigurable intelligent surface-assisted aerial-terrestrial communications via multi-task learning. *IEEE J. Sel. Areas Commun.*, 39(10):3035–3050, Oct. 2021.

[94] Priyadarshi Mukherjee and Swades De. Reduced-feedback scheduling policies for energy-efficient MAC. In *Proc. IEEE ICC Workshops*, pages 1–6, Montreal, QC, Canada, June 2021.

[95] Andrea Goldsmith. *Wireless communications*. Cambridge University Press, 2005.

[96] Chongwen Huang, Alessio Zappone, George C Alexandropoulos, Mérouane Debbah, and Chau Yuen. Reconfigurable intelligent surfaces for energy efficiency in wireless communication. *IEEE Trans. Wireless Commun.*, 18(8):4157–4170, Jun. 2019.

[97] C. Bettstetter, G. Resta, and P. Santi. The node distribution of the random waypoint mobility model for wireless ad hoc networks. *IEEE Trans. Mob. Comput.*, 2(3):257–269, July-Sept. 2003.

[98] I. S. Gradshteyn and I. M. Ryzhik. *Table of Integrals, Series, and Products*. Elsevier, 2007.

[99] Liang Liu, Rui Zhang, and Kee-Chaing Chua. Wireless information and power transfer: A dynamic power splitting approach. *IEEE Trans. Commun.*, 61(9):3990–4001, Sep. 2013.

[100] Kui Xu, Zhexian Shen, Yurong Wang, Xiaochen Xia, and Dongmei Zhang. Hybrid time-switching and power splitting SWIPT for full-duplex massive MIMO systems: A beam-domain approach. *IEEE Trans. Veh. Technol.*, 67(8):7257–7274, Aug. 2018.

[101] Renjith Ravindran Unnithan Jalaja, Vetrivel Chelian Thirumavalavan, Periakarupan Gurusamy Sivabalan Velmurugan, and Sundarrajan Jayaraman Thiruvengadam. Spatially correlated dual hop RIS aided next generation wireless systems: An outage perspective. *IEEE Access*, 9:56127–56139, 2021.

[102] Ikram Singh, Peter J Smith, and Pawel A Dmochowski. Optimal SNR analysis for single-user RIS systems in Ricean and Rayleigh environments. *IEEE Trans. Wireless Commun.*, 21(11):9834–9849, Nov. 2022.

[103] Arathi P Ajayan, Soumya P Dash, and Barathram Ramkumar. Performance analysis of an IRS-aided wireless communication system with spatially correlated channels. *IEEE Wireless Commun. Lett.*, 11(3):563–567, Mar. 2021.

[104] Ikram Singh, Peter J Smith, and Pawel A Dmochowski. Optimal SNR analysis for single-user RIS systems in Ricean and Rayleigh environments. *IEEE Trans. Wireless Commun.*, 21(11):9834–9849, Nov. 2022.

[105] Hong-Chuan Yang and Mohamed-Slim Alouini. *Order Statistics in Wireless Communications: Diversity, Adaptation, and Scheduling in MIMO and OFDM Systems*. U.K.: Cambridge Univ. Press, 2011.

[106] Samuel Stanley Wilks. Order statistics. *Bulletin of the American Mathematical Society*, 54(1):6–50, 1948.

[107] Mihai-Alin Badiu and Justin P. Coon. Communication through a Large Reflecting Surface with phase errors. *IEEE Wireless Commun. Lett.*, 9(2):184–188, Feb. 2020.

[108] CD Lai, Min Xie, and DNP Murthy. A modified weibull distribution. *IEEE Trans. reliab.*, 52(1):33–37, Jan. 2003.

[109] Saad Al-Ahmadi and Halim Yanikomeroglu. On the approximation of the generalized-K distribution by a gamma distribution for modeling composite fading channels. *IEEE Trans. Wireless Commun.*, 9(2):706–713, Feb. 2010.

[110] Saad Al-Ahmadi and Halim Yanikomeroglu. On the approximation of the generalized-K PDF by a Gamma PDF using the moment matching method. In *2009 IEEE Wireless Commun. Networking Conf.*, pages 1–6. IEEE, 2009.

[111] Melvin D. Springer. *The Algebra of Random Variables*. John Wiley & Sons, 1979.

[112] Constantinos Psomas and Ioannis Krikidis. Energy beamforming in wireless powered mmwave sensor networks. *IEEE J. Sel. Areas Commun.*, 37(2):424–438, Feb. 2019.

[113] Samer Hanna and Danijela Cabric. Distributed transmit beamforming: Design and demonstration from the lab to UAVs. *IEEE Trans. Wireless Commun.*, 22(2):778–792, Feb. 2022.

[114] Stefan M Moser. Expectations of a noncentral Chi-square distribution with application to IID MIMO Gaussian fading. In *Proc. Int. Conf. Symp. Inf. Theory Appl.*, pages 1–6. IEEE, 2008.

[115] Neel Kanth Kundu and Matthew R Mckay. Large Intelligent Surfaces with channel estimation overhead: Achievable rate and optimal configuration. *IEEE Wireless Commun. Lett.*, 10(5):986–990, May 2021.

[116] Tobias Lindstrøm Jensen and Elisabeth De Carvalho. An optimal channel estimation scheme for Intelligent Reflecting Surfaces based on a minimum variance unbiased estimator. In *Proc. IEEE Int. Conf. Acoust. Speech Signal Process. (ICASSP)*, pages 5000–5004, Barcelona, Spain, May 2020.

[117] Paulo RB Gomes, Gilderlan Tavares de Araújo, Bruno Sokal, André LF de Almeida, Behrooz Makki, and Gábor Fodor. Channel estimation in RIS-assisted MIMO systems operating under imperfections. *IEEE Trans. Veh. Technol.*, 72(11):14200–14213, Nov. 2023.

[118] Herbert A David and Haikady N Nagaraja. *Order statistics*. John Wiley & Sons, 2004.

[119] Sultangali Arzykulov, Abdulkadir Celik, Galymzhan Nauryzbayev, and Ahmed M Eltawil. Artificial noise and RIS-aided physical layer security: Optimal RIS partitioning and power control. *IEEE Wireless Commun. Lett.*, 12(6):992–996, June 2023.

[120] Yunfei Chen, Nan Zhao, and Mohamed-Slim Alouini. Wireless energy harvesting using signals from multiple fading channels. *IEEE Trans. Commun.*, 65(11):5027–5039, Nov. 2017.